ISTANBUL TECHNICAL UNIVERSITY ★ GRADUATE SCHOOL

THE EFFECTS OF THE DOUBLE-WAVELENGHT LEADING EDGE SERRATIONS ON AERODYNAMIC PERFORMANCE OF THE WING

M.Sc. THESIS

Zehra Nur KAPLAN

Department of Aeronautics and Astronautics Engineering

Aeronautics and Astronautics Engineering Graduate Programme

OCTOBER 2023

ISTANBUL TECHNICAL UNIVERSITY ★ GRADUATE SCHOOL

THE EFFECTS OF THE DOUBLE-WAVELENGHT LEADING EDGE SERRATIONS ON AERODYNAMIC PERFORMANCE OF THE WING

M.Sc. THESIS

Zehra Nur KAPLAN
(511201146)

Department of Aeronautics and Astronautics Engineering

Aeronautics and Astronautics Engineering Graduate Programme

Thesis Advisor: Dr. Duygu ERDEM

OCTOBER 2023

ISTANBUL TEKNİK ÜNİVERSİTESİ ★ LİSANSÜSTÜ EĞİTİM ENSTİTÜSÜ

ÇİFT DALGA BOYLU HÜCUM KENARI ÇENTİKLERİNİN KANADIN AERODİNAMİK PERFORMANSI ÜZERİNDEKİ ETKİLERİ

YÜKSEK LİSANS TEZİ

Zehra Nur KAPLAN
(511201146)

Uçak ve Uzay Mühendisliği Anabilim Dalı

Uçak ve Uzay Mühendisliği Yüksek Lisans Programı

Tez Danışmanı: Dr. Duygu ERDEM

EKİM 2023

Zehra Nur Kaplan, a M.Sc. student of İTU Graduate School student ID 511201146, successfully defended the thesis/dissertation entitled "THE EFFECTS OF THE DOUBLE-WAVELENGHT LEADING EDGE SERRATIONS ON AERODYNAMIC PERFORMANCE OF THE WING", which she prepared after fulfilling the requirements specified in the associated legislations, before the jury whose signatures are below.

Thesis Advisor : **Dr. Duygu ERDEM** ....
Istanbul Technical University

Jury Members : **Doç. Dr. Sertaç ÇADIRCI** ....
Istanbul Technical University

Dr. Şule KAPKIN ....
Istanbul University

Date of Submission : 21 September 2023
Date of Defense : 12 October 2023

To my husband and parents,

FOREWORD

First of all, I would like to express my sincere thanks to my advisor Dr. Duygu Erdem, because she constantly supported me during my master's thesis and enlightened my path with her knowledge in the field, and I always felt her sincerity and interest.

Additionally, this study was supported by Istanbul Technical University (ITU) Scientific Research Projects Coordination Unit (Project ID: 43746). I would like to express my gratitude for their support in making the project possible.

And the last, I would like to express my endless thanks to my mother, Ayşe and father, Ahmet. I wouldn't be able to be at where I am without their love, effort and guidance on my life journey. And of course I'm thanksful to my lovely spouse, Muhammet Kaplan, for supporting me in every respect. With his belief in me, his endless support, patience and understanding, this process has become much more meaningful and easier for me.

June 2023 Zehra Nur KAPLAN

TABLE OF CONTENTS

Page

ABBREVIATIONS

AIN : Aerofoil Interaction Noise
ASN : Aerofoil Self Noise
TE : Trailing Edge
LE : Leading Edge
TBL : Turbulent Boundary Layer
LBL : Laminar Boundary Layer
AFC : Active Flow Control
PFC : Passive Flow Control
rms : Root mean squared
SW : Single Wavelength
DW : Double Wavelength
NR : Noise reduction
aoa : Angle of attack
PWL : Sound Power Level

SYMBOLS

h	: Amplitude
λ	: Wavelength
c_0	: Mean chord
ϕ	: Phase difference
$c(r)$	: Chord length according to spanwise direction
$2a$	: Total amplitude
C_L	: Lift coefficient
C_D	: Drag coefficient
C_P	: Pressure coefficient
C_{Pl}	: Pressure coefficient's contribution to lift
C_{Pd}	: Pressure coefficient's contribution to drag
ω	: Frequency
U	: Freestream velocity

LIST OF TABLES

<u>Page</u>

LIST OF FIGURES

Page

THE EFFECTS OF THE DOUBLE-WAVELENGHT LEADING EDGE SERRATIONS ON AERODYNAMIC PERFORMANCE OF THE WING

SUMMARY

The negative effects of noise on the environment and living things are known to everyone. One of the sources of noise is aviation. So, noise reduction is a very important issue in aviation.

Due to the effects of noise, there are many studies on noise reduction methods. Recent studies have focused especially on double-wavelength leading edge profiles designed as a combination of sine wave functions. When the studies in progress were examined, it was observed that the experiments were at a certain angle of attack and focused only on noise. In other words, the issue of how the aerodynamic performance of wings with such a design is affected in the majority of studies is not discussed, which is a situation considered to be missing in the literature.

In this thesis, it is aimed to experimentally investigate how will be affected the aerodynamic performance of wings with double wavelength leading edge serrations, whose noise effect has been examined in the literature.

In this context, an introduction has been made in the first part of the thesis that primarily focuses on why noise reduction is important. Then, where and how the noise occurs on the wings is explained. Following the examination of the noise source, the methods used from past to present to reduce the noise on the wings are imparted in detail. It is mentioned that the recent studies are serrations applied to the leading or trailing edges, and the studies on this subject are detailed. After providing detailed information about the study used as a reference in the content of the thesis, the motivation of the thesis is mentioned.

In the second part of the thesis, the wing designs used in the experiments are mentioned. In this context, firstly, the two-dimensional shapes of the double wavelength leading edge serrations depending on the amplitude change are shown with the help of drawings and the design parameters are given as a table. Then, the three-dimensional designs of the wings created using the NACA 65-(12)10 airfoil were mentioned. At the same time, the situations that were taken into consideration during the wing drawings and that the wing was designed in two parts, front and rear, and that these parts could slide inside each other were mentioned. Three-dimensional drawings of the wings were made with the help of Solidworks program. By the way, it was also mentioned that due to the size limit in production, the wing was produced by dividing it into equal parts in the spanwise direction. The drawings prepared with the help of the program and then produced with a 3D printer and the surface roughness was eliminated. In addition to the double wavelength designs with two different amplitudes, a straight leading edge wing was also produced for comparison. So, in total there are 3 different wings.

In the third part of the thesis, information about the experimental setup is given. Experiments in terms of aerodynamics were provided by the subsonic, open circuit

wind tunnel in the Trisonic Research Laboratory within Istanbul Technical University. The speed at which the experiments were carried out, the placement of the wings in the tunnel and the angle of attack adjustment mechanism are also mentioned in this section. In addition, pressure measurement and flow visualization methods were mentioned. The placement of pressure taps on the wing for pressure measurement is explained visually. Additionally, brief information is given about the device used in the measurements. The tuft method was used during the flow visualization experiments, its features were briefly mentioned, and its application on the wings produced within the scope of the thesis was visually demonstrated. During the application of these methods, the angle of attack was also increased from low to high, and the effect of angle of attack was also examined.

The experimental results are mentioned in the fourth chapter of the thesis. First, photographs obtained from flow imaging experiments were shown for each wing separately. Explanations were made with the help of images about the flow, whose behavior on the wing changes as the angle of attack changes. Following the results of the flow visualization experiments, the data obtained from the pressure measurements were presented graphically. Also shown is the comparison graph for the baseline wing. The graphs are non-dimensional and the pressure coefficient is used instead of pressure. To compare the wings with each other, the components perpendicular to the flow and parallel to the flow were calculated using the pressure coefficients obtained from the upper surface of the wing. The component perpendicular to the flow is called Cpl, and the component parallel to the flow is called Cpd. Using these data expressed in graphics, a comment was made about the aerodynamic performance of the wings relative to each other.

In the conclusion part, the thesis was concluded by summarizing the data obtained from the experiments. According to the results of the experimental study conducted in this thesis, the pressure coefficients obtained from the upper surface of the wing and their perpendicular and parallel components to the flow have shown that the designed wings have better resistance to high angles of attack than the baseline wing. Among these two wings with double wavelength notched leading edges, it has been observed that this strength is better in the wing where the $2a$ value, expressed as the total amplitude, is smaller.

ÇİFT DALGA BOYLU HÜCUM KENARI ÇENTİKLERİNİN KANADIN AERODİNAMİK PERFORMANSI ÜZERİNDEKİ ETKİLERİ

ÖZET

Gürültünün çevre ve canlılar üzerindeki negatif etkileri herkes tarafından bilinen bir durumdur. Gürültü kaynaklarından biri de havacılıktır. Bu yüzden, gürültü seviyelerinin azaltılması havacılık açısından oldukça önemli bir konu haline gelmiştir.

Bu etkilerden dolayı havacılıkta gürültü azaltma metodları üzerine pek çok çalışma bulunmaktadır. Özellikle son zamanlarda üzerine odaklanılan çalışmalar pasif kontrol yöntemlerinden biri olan çift dalga boylu hücum kenarı çentiklerinin kanatlar üzerine uygulanmasıdır. Bu çift dalga boyuna sahip tasarımlar temelde iki sinüs dalgasının birbirine eklenmesi sonucu elde edilmektedirler. Yapılmakta olan çalışmalar incelendiğinde, deneylerin belirli bir hücum açısı değerinde ve sadece gürültü odaklı olduğu gözlemlenmiştir. Yani büyük bir çoğunluğunda böyle bir tasarıma sahip kanatların aerodinamik performansının nasıl etkilendiği konusu ele alınmamıştır ki bu da literatürde eksik olduğu düşünülen bir durumdur.

Bu tezde, literatürde gürültü etkisi incelenmiş çift dalga boylu hücum kenarı çentiklerine sahip kanatların aerodinamik açıdan performanslarının nasıl etkileneceğinin deneysel olarak araştırılması amaçlanmıştır.

Bu kapsamda tezin ilk bölümünde öncelikli olarak neden gürültü azaltılmasının önemli olduğuna değinen bir giriş yapılmıştır. Ardından kanatlar üzerinde gürültünün nerelerde ve nasıl meydana geldiği açıklanmıştır. Gürültü kaynağının incelenmesinin ardından, kanatlarda meydana gelen gürültünün azaltılması hususunda geçmişten günümüze hangi yöntemlerin kullanıldığı detaylı olarak belirtilmiştir. Son zamanlardaki çalışmaların hücum ya da firar kenarlarına uygulanan çentikler olduğundan bahsedilerek bu konu üzerine yapılan çalışmalar detaylandırılmıştır. Tez içeriğinde referans olarak kullanılan çalışma hakkında detaylı bir bilgi sağlandıktan sonra tezin motivasyonunun neler olduğuna değinilmiştir.

Tezin ikinci kısmında, deneylerde kullanılan kanat tasarımlarından bahsedilmiştir. Bu kapsamda ilk olarak genlik değişimine bağlı çift dalga boylu hücum kenarı çentiklerinin iki boyutlu şekilleri çizimler yardmıyla gösterilmiş ve tasarım parametreleri tablo olarak verilmiştir. Ardından NACA 65-(12)10 kanat profilini kullanılarak oluşturulan kanatların üç boyutlu tasarımlarından bahsedilmiştir. Kanatların tasarımları için nelere dikkat edilmiş olduğu özetlenmiştir.Deneyler ve üretim sırasında kolaylık sağlaması için kanat arka ve ön olarak iki parça halinde üretilmiştir ve bu parçalar birbiri içerisinden kayarak geçebilmektedir. Bu sayede arka parçaların sabit kalması planlanmıştır. Kanatların üç boyutlu çizimleri Solidworks programı yardımıyla yapılmıştır. Program yardımıyla hazırlanan çizimler, sonrasında 3B yazıcı ile üretilmiş ve yüzey pürüzleri elimine edilmiştir. 3B yazıcının boyutlarından dolayı üretilen parçaların boyutları konusunda da bir sınır bulunmkatadır.Bu sınıra uygun üretim yapılabilmesi için kanat genişliği doğrultusun-

-da kanat eşit parçalara ayrılarak düşünülmüştür. Yani toplamda beş eşit parçanın bir araya gelmesi ile kanat tasarlanan kanat genişliğine ulaşmaktadır. İki farklı genliğe sahip çift dalga boylu tasarımlara ek olarak kıyaslama yapılabilmesi için düz hücum kenarına sahip bir kanat da üretilmiştir. Yani toplamda 3 farklı kanat bulunmaktadır. Üretilen bu kanatlar görselleriyle birlikte açıklanmıştır.

Tezin üçüncü bölümünde ise deney düzeneği hakkında bilgi verilmiştir. Aerodinamik açıdan yapılan deneyler İstanbul Teknik Üniversitesi bünyesinde yer alan Trisonik Araştırma Laboratuvarı'ndaki sesaltı, açık devre rüzgar tüneli ile sağlanmıştır. Deneyler tek bir hız değerinde gerçekleştirilmiştir. Parçalar halinde üretilen kanatlar bir araya getirilerek deney odasına yerleştirilmiştir. Kanatların deney odasındaki yerleşimi görsel olarak sunulmuştur. Ayrıca deneyler sırasında hücum açısı da değiştiği için hücum açısının ayarlandığı basit bir mekanizma da yapılmıştır. Hücum açısının bu mekanizma sayesinde nasıl ayarlandığı örnek bir görselle de ifade edilmiştir.Basınç ölçüm ve akım görüntüleme yöntemlerinin nasıl olduğundan da bahsedilmiştir. Basınç ölçümlerini yapabilmek için kanat yüzeyinde delikler açılarak basınç hortumlarının yerleştirilmesi gerekmektedir. Yüzeyin teğetine dik olacak şekilde konumu belirlenen bu delikler yine Solidworks programı aracılığıyla yapılmış olup doğrudan delikli olarak üretilmiştir.Sonrasında bu kısımlardan basınç hortumları yerleştirilmiştir. Kanadın arka parçası için yüzeyde bir kapak tasarlanmıştır ve bu sayede basınç hortumlarının yerleşimi kolaylıkla yapılabilmiştir. Hem basınç deliklerinin kanat üzerindeki duruşu hem de basınç hortımların yerleştirilmiş hali fotoğraflar yardımıyla daha net olarak anlatılmıştır.Bunun yanı sıra basınç ölçümleri sırasından kullanılmış olan cihaz hakkında da özet bilgi verilmiştir. Akım görüntüleme deneyleri içinse 'iplikçik' metodunun kullanılması planlanmıştır. İplikçik yöntemi ile görüntülemenin nasıl yapıldığı, kullanılan malzemeler, iplik boyutları gibi bu yönteme dair temel bilgilerden bahsedilmiştir. Sonrasında ise tez kapsamında yapılan deneylerde kullanılan kanatlar üzerindeki iplikçik metodu uygulaması görsel ile özetlenmiştir. Tüm bu yöntemlerin uygulanması sırasında hücum açısı da düşük değerden yüksek değere doğru arttırılarak hücum açısı etkisi de incelenmiştir.

Deney sonuçlarından tezin dördüncü bölümünde bahsedilmiştir. İlk olarak akım görüntüleme deneylerine ait sonuçlar verilmiştir. Her bir kanat için ayrı ayrı fotoğraflar olup kanatlar içerisinde de ölçülen her bir açı değeri için de ayrı görseller verilmiştir. Bu sayede açı geçişlerinde kanat üzerindeki akışın davranışının nasıl değiştiği de daha net olarak gözlemlenmiştir. Akım görüntüleme sonuçlarının verilmesinin ardından, deneylerden elde edilen basınç ölçümlerinden bahsedilmiştir. Basınç değerlerine başlanmadan önce ölçümler hakkında bilgi verilmiştir. Çift dalga boyu çentikli kanatların tasarımlarından dolayı ölçülmesi gereken iki farklı kesit bulunmaktadır. Kesit olarak ifade edilen yerlerin nereye denk geldiği yine çizim görselleri yardımıyla açıklanmıştır. Bu kesit durumlarından dolayı ölçüm yapılacak basınç noktaları da hem konum olarak hem sayı olarak farklılık göstermiştir.Bu kapsamda yapılan deneyler sırasında hangi kanadın hangi kesitinde ne kadar basınç noktası olduğu belirtilmiştir. Ölçülen basınç değerleri boyutsuzlaştırılarak daha anlamlı hale getirilmiştir. Yani tünelden alınan toplam ve statik basınçlar kullanılarak, ölçülen basınçlar basınç katsayısı olarak ifade edilmiştir. Bu katsayıya ait formül de bölüm içerisinde verilmiştir. Grafikler oluşturulurken x noktaları da ortalama veter ile boyutsuzlaştırılarak kullanılmıştır. Ardından, akım görüntülemede de olduğu gibi her bir kanat ayrı ayrı grafikler incelenmiştir. İlk olarak referans kanat ile başlanmıştır.Referans kanatta kendi deneysel verilerimizle literatürden elde edilmiş olan bu kanada ait deneysel veriler de ayrıca kıyaslanmıştır. Kanatta ayrılmanın olabi-

-leceği açılar belirlenmiştir. Sonrasında sırasıyla DW1 ve DW2 olarak adlandırılmış olan iki farklı genlikli kanatların basınç katsayısı grafikleri verilmiştir. Bu kanatlar için de ayrılmanın tam olarak gözlemlenildiği düşünülen açılar belirlenmiştir. Her bir kanada ait basınç verilerinin ayrı ayrı incelenmesinin ardından kanatların birbirleriyle olan durumu hakkında kıyaslama yapılmıştır. Kıyaslama yapılırken, basınç katsayıları kullanılarak kanat üzerindeki akışa dik ve akışa paralel bileşenler hesaplanmıştır. Akışa dik bileşen Cpl, akışa paralel bileşen ise Cpd olarak isimlendirilmiştir. Bu bileşenlerin grafikleri doğrultusunda kanatların aerodinamik performanslarının birbirlerine göre olan durumu hakkında yorumda bulunulmuştur.

Sonuç bölümünde yapılan çalışmalardan elde edilen veriler özetlenerek tez sonlandırılmıştır. Bu tezde yapılmış olan deneysel çalışmanın sonuçlarına göre, kanadın üst yüzeyinden elde edilen basınç katsayıları ve bunların akışa dik ve paralel bileşenleri, tasarlanan kanatların referans düz kanada göre yüksek hücum açılarına dayanımının daha iyi olduğunu göstermiştir. Bu iki, çift dalga boyu çentikli hücum kenarına sahip kanatlar arasında ise toplam genlik olarak ifade edilen $2a$ değerinin daha küçük olduğu kanatta bu dayanımın daha iyi olduğu gözlemlenmiştir.

1. INTRODUCTION

Aviation is an important sector both socially and economically and it is developing day by day in order to meet the increasing demands. These developments bring along various environmental problems such as noise. It is a known fact that noise has negative effects on the health of both humans and other living things. In addition to visible health problems, the occurance of factors affecting the quality of life such as sleep problems, reading diffuculties and distraction in school age children [1] shows that noise poses a great threat. From an aviation point of view, broadband noise, especially from engine blades and wind turbine blades, is seen as the main source of noise. According to Flightpath 2050 published by the National Civil Aviation Organization (ICAO), reducing noise emissions by 65% is among the future targets [2].

1.1 Source of Noise on Wing

Noise generation on wing structures can be divided into two as ‘aerofoil/turbulence interaction noise (AIN)’ and ‘aerofoil self noise (ASN)’. In fact, these two noises can be considered as the dominant noise sources that occur at the leading and trailing edge of the wing, respectively [3].

The upstream turbulent flows impinging on the leading edge of an aerofoil is believed to be the dominant source mechanism of broandband noise for aerofoil interaction noise. Its visualized version is given in Figure 1.1.

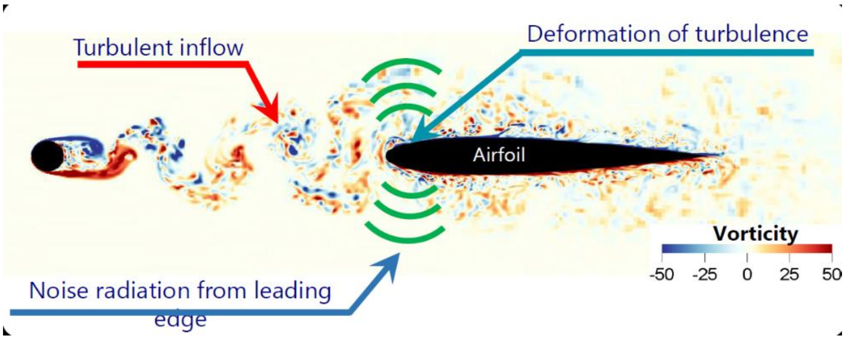

Figure 1.1 : Aerofoil / turbulence interaction noise [4].

Otherwise, the aerofoil self noise can occur in four ways [5]. These are; turbulent boundary layer - trailing edge noise (TBL-TE), laminar boundary layer – trailing edge noise (LBL-TE), blunt trailing edge noise and wing tip noise [6]. In generally, TBL-TE noise is the noise generated as a result of the turbulent boundary layer encountering the wake or flow separations at the trailing edge. LBL-TE is the noise generated as a result of the laminar boundary layer encountering vortex shedding at the trailing edge. Tip noise, on the other hand, is the noise that occurs as a result of the encounter of the tip vortex which arise from the pressure difference at the top and bottom of the wing with the trailing edge. Finally, blunt TE noise is the noise as a result of Von Karman vortex that produced by blunt edge. However among these, the most dominant noise source is the TBL-TE noise [7]. All types of aerofoil self noise are shown in Figure 1.2. In order to reduce these noises on the wings, flow control methods are used.

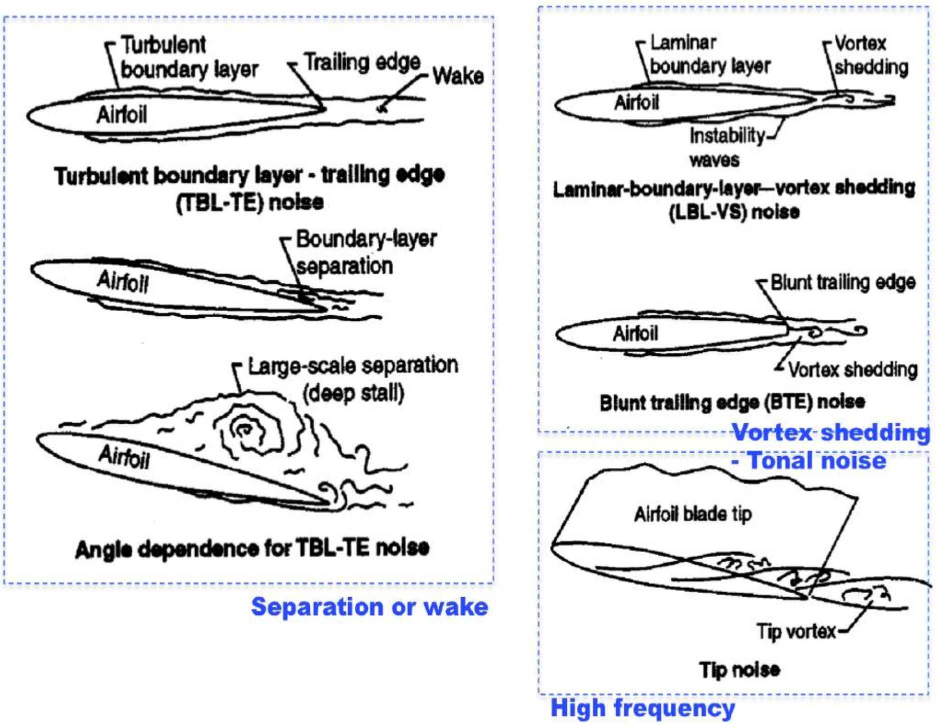

Figure 1.2 : Aerofoil self noise [8].

1.2 Flow Control Methods for Aerodynamic Noise Reduction

Many methods have been researched until now and are still researching to reduce noise on wing. These flow control methods [9] are divided into two as active (AFC) and passive (PFC) [4,10]. In generally, the aim is a reduction of turbulent velocity fluctuations in the boundary layer and hence a decrease of the surface pressure fluctuations [3]. The reduction of these fluctuations on the surface also allows noise reduction.

1.2.1 Active flow control methods

Active flow control methods can be applied to reduce trailing edge noise [11]. In active methods, external energy is used to bring the desired properties to the flow [12]. Therefore, the energy consumed is also taken into account when determining the effectiveness of the control mechanism. Meanwhile, AFC is mostly used in motor technology [13,14], especially in rotating devices such as compressors [15] and fans [16]. There are two methods that have been researched in the literature for noise reduction. These are blowing/suction and morphing.

1.2.1.1 Suction/blowing

In the blowing (or suction) method, air is supplied to the surface (or air is taken from the surface) by means of jet actuator [17]. The main purpose of suction is to reduce the boundary layer thickness. Because, in this way the magnitude of the turbulent eddies inside the boundary layer decreases and hence noise decreases [18]. By the way, according to [19], it has been observed that it is more reasonable to use the blowing method because of the thought that the substances that can be taken from outside by suction can cause pollution over time. Blowing leads to uplift of near-wall vortices and so the turbulence fluctuations in the TE region and hence the noise reduces [20,21]. According to the study in [22] the noise reduction was achieved with the blowing method used just before the flow separation observed. This is due to the fact that eddies containing energy near the wall are pushed away from the wall, thus reducing their effect on surface pressure fluctuations. However, as these eddies move farther near the trailing edge, they increase the energy level, leading to the formation of large structures, which means that the noise level increases. Therefore, the blowing application should be as close to the trailing edge as possible.

1.2.1.2 Morphing

It defines as structures that can change shape of trailing edge according to the flight conditions [23]. Morphing TE actively changes shape through structural deformation rather than rigid body motion and ın this way, it also presents a continuous smooth surface [24]. With this change, the behavior of the boundary layer is significantly affected and hence noise reduction on wing can be ensure. Studies have shown that these structures have good aerodynamic performances as well as noise reduction.

1.2.2 Passive flow control methods

When we look at the recent studies, it has been seen that passive methods are used more frequently because they do not need an external energy requirement whereas active methods need it and are easier to apply [25]. As in many engineering applications studies inspired by the nature are the majority in these methods, such as owls or humpack whale [3,4,6,8]. Passive methods can be used in either LE or TE, depending on the source of the noise to be reduced. Among the passive methods, the application of rough / porous surface the use of brush structure and serrated edge structures are the most common methods.

1.2.2.1 Porous material

The presence of porous material the boundary layer around the aerofoil is affected. Studies are showing that the root mean squared (rms) velocity fluctuations of the profile are reduced due to the treatments, hence noise reduces. However, it has been observed that is valid only in the low frequency range. Conversely, in the high frequency range, there is an increase in noise level due to the surface roughness. Therefore, this method is rarely used [26-28].The appearance of the porous material and its use on the wing are given in Figure 1.3 and Figure 1.4, respectively.

Figure 1.3 : Porous material [25].

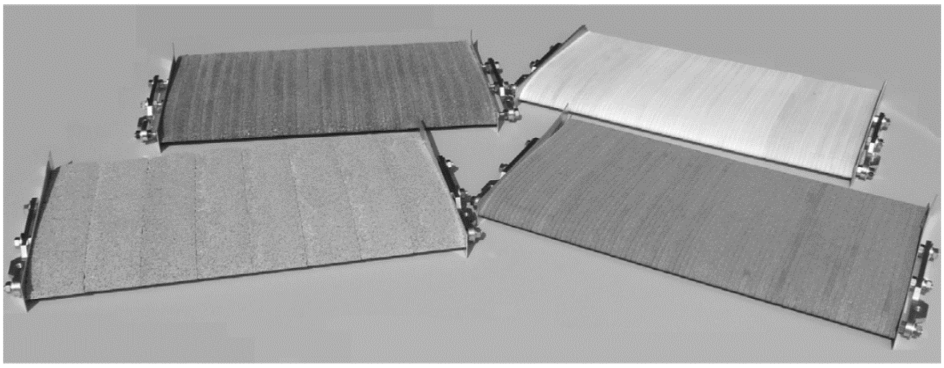

Figure 1.4 : Wing designed with porpus material [28].

1.2.2.2 Brushes

It is a method based on the silent flight characteristics of owls [29]. The noise reduction mechanism of this method can be explained with the help of nature of turbulence. According to the [30] study, space -time correlation analysis showed that the time and the spanwise length scales are both reduced by the brush fibers. This means that smaller structures with shorter lifetimes are formed. In other words, they can disparse without emitting sound to the environment and thus noise is reduced. [31]. Usage examples of brushes structure are given in Figure 1.5.

Figure 1.5 : Brushes [30,31].

1.2.2.3 Serrations

In particular, owls known with their quiet flight are a major source of inspiration for serrated edge profiles [32-35]. Serration structures have been known and used for a long time, but new types are constantly being developed to increase efficiency [36-38]. In addition, studies show that the use of serrated structures is much more effective than other methods [39-41]. In generally, serration leading (or trailing) edge causes a instantaneous phase variation of the pressure fluctuations along the LE/TE as compared to the straight LE/TE. This phase difference leads to additional far field noise reductions. Serration structures used to reduce LE noise is related to the correlation function (hence integral lenght scale) of incoming turbulent flow [42]. The TE serrations [43-50] retard the growth of vortices and the velocity fluctuations near the TE region reduces [51]. Hence the strenght of the pressure fluctuations near the TE reduced. As a result, noise reduction occurs. By the way, serrations are the most studied method and so there is a wide range of serration structures [52,53]. Depending on the amplitude and wavelenght of the structure used, the effect on the noise also changes. Briefly, these structures are sharp sawtooth serration(classic serration) [54-56], slitted root serration [57,58], chopped peak serration, single wavelenght serration (SW) and double wavelenght serration (DW). By the way, depending on the type of noise to be controlled (AIN or ASN), these serration structures can be applied either in LE or TE. These structures searched for serration are shown in Table 1.1.

Table 1.1 : All types of serration structures.

Serration Types	Sketch of Serration Types
Sharp Sawtooth Serration [43]	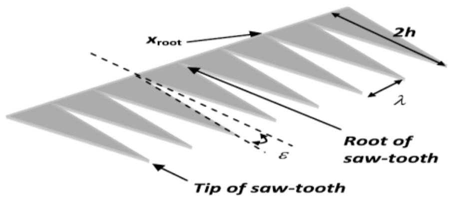
Slitted Root Serration [53]	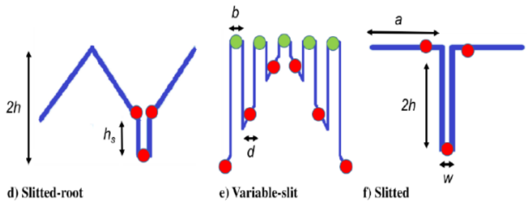
Chopped Peak Serration [53]	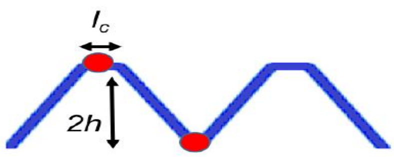
Single Wavelength Serration [53]	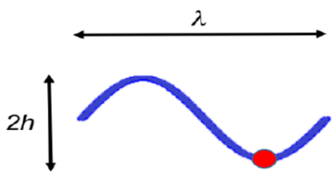
Double Wavelength Serration [53]	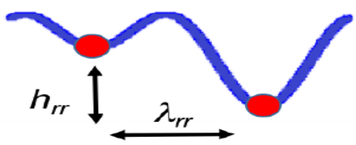

In order to make these structures even more efficient, wave-shaped serrated edge profiles have recently been created inspired by the tubercles of humpback whales [8]. Because these tubercle structures affect aerodynamic performance as well as noise. Humpback whale tubercles and their application on the wing are indicated in Figure 1.6.

Figure 1.6 : Tubercles of humpback whale (left) and an application to wind turbine blade(right) [59].

In this context, wing designs with single wavelength form have been studied by many researchers and are still being studied. In paper of Johari et al. [60], which is the one of the older studies, water tunnel tests were performed using the NACA 63_4-021 airfoil in order to examine effect of LE protuberance (wavelength serration) on airfoil performance. According to the results of this study, while the lift decreases and drag increases before the stall angle of the reference straight wing, it is seen that the lift increases and the drag becomes independent of the LE shape in the post-stall condition. That is, with the use of LE wavelength serration, the lift-drag ratio can increase in the post-stall condition. In addition, according to the force measurements obtained in the study, while the effect of wavelength is very small, it has been seen that amplitude is very effective on these forces and also, in regard to the data obtained after flow visualization, it has been observed that the flow adheres better to the wavy wing surface even at higher angles of attack than in the reference straight wing. In study of Hansen et al. [61], an experimental study was carried out using the NACA 0021 airfoil with LE tubercles and both aerodynamic and acoustic measurements were made. Acoustic measurements were carried out in a wind tunnel with an anechoic design, and a total of two microphones were used for measurements, one positioned perpendicular to the TE and one positioned near the atmospheric reference nick at the downstream end. According to the results obtained from the study, it has been seen that the wing design with a combination of higher amplitude and lower wavelength is more efficient in terms of noise reduction (NR). Similarly, as regards the aerodynamic force measurements, it has been observed that the wing with the lower wavelength in the LE design has the highest efficiency in terms of aerodynamic performance. Looking at the study of Clair et al. [62], NACA65-(12)10 airfoil is based on which commonly used in turbofans. A wind tunnel in an anechoic chamber was used for aeroacoustic measurements, and unlike the previous study, a circularly positioned microphone series at a certain distance from the wing was used for measurements. The purpose of the study is also to predict numerically the aerofoil interaction noise occurring in sinusoidal LE, as well as experimental measurements. In a similar numerical study of Skillen et al. [63], NACA 0021 airfoil was used for the design of wing that has single wavelength leading edge. Only one LE design was used and numerical studies were performed at 20°, which corresponds to the post-stall situation with respect to the baseline wing. As a result of numerical studies carried out under these conditions, an increase of 58% in average lift and a decrease of 59% in average drag were observed. In addition, according to the numerically obtained flow separation images, the separations in the modified wing were significantly reduced compared to the baseline wing. Afterwards, studies on the efficiency of wavelength-formed LE have become increasingly detailed. For example, in the study of Narayanan et al. [64], LE with sinusoidal profile were created on the flat plate. In addition to the experiments using the flat plate, experiments were also carried out on the wing using the NACA-65 airfoil and compared in terms of noise levels. The purpose of using flat plate is to reduce the studies completely to two dimensions and to observe the changes in noise reduction depending on amplitude and wavelength more clearly. Already, the comparison of the real wing (NACA-65 airfoil) and flat plate data has shown that the noise reduction levels are similar, however in the flat plate is higher. In the content of the study, experiments were carried out on twenty different serrated aerofoils, at different speed values, and the results were also compared with the flat shaped reference aerofoil. According to the results of the article, above a certain frequency value, there is a significant reduction in noise levels of wings with sinusoidal LE serration compared to straight wing. Besides, as in previous studies, it has been observed that amplitude has a greater effect rather than wavelength, and it is said that the entire noise reduction level changes logarithmically with amplitude of the wavelength. Another similar article with the flat plate is the work of Turner and Kim [65]. They compared them with the experimental data by making a numerical study instead of an experimental one. In the study of Mayer et al. [66], sinusoidal LE serration was added to the wing that has the NACA 0012 profile (leading edge serration add-ons). A total of five different LE plug-ins were used by varying the amplitudes and wavelengths. The study specifically references the stall condition of the baseline straight wing. While there was an increase in surface pressure fluctuations before the stall, a decrease was observed in the post-stall condition, and this decrease was found to be around 15dB, especially for the two serration designs. In addition, the boundary layer thickness was also examined, and for these two types of LE designs, the boundary layer increased before the stall and decreased after the stall compared to the reference straight wing. Based on these results, the researchers (Mayer et al.) hypothesized that LE serration should have a certain minimum amplitude in order to obtain more efficient results. Recent studies have focused on finding the optimum design parameters of the single wavelenght LE shape. The study of Kim et al. [67] is one of the examples of this situation. In the study, nine different serrated wings with NACA 65(12)-10 airfoil were examined experimentally and both aerodynamic and aeroacoustic data were obtained and these data were compared with the straight wing. In leading edge designs, amplitudes, h's are 3%, 6% and 12% of the chord length, and wavelengths, λ's are 10%, 20% and 30% of the chord length. Moreover, a grid was placed at the entrance of the test chamber of the wind tunnel in order to increase the turbulence intensity of the freestream and to provide a transition to turbulence even at the LE edge in the experiments. Looking at the results, the best result in terms of $C_{L_{max}}$ occurs when both the wavelength and the amplitude are the largest, on the contrary, the best result in terms of noise reduction is achieved in the case of small wavelength and large amplitude. The article of Lacagnina et al. [68] also provides similar content in terms of the design parameters used for the sinusoidal LE shape. It examines the wings in three different angles of attack that low, medium, and high, and provides a detailed example of pre-stall, stall, and post-stall situations. While noise reduction is observed for most cases at low and high angle of attack ranges, it has been observed that in the medium angle of attack range this is highly dependent on the wavelength of the LE design.That is, the effect is almost negligible in low wavelength situations, but can lead to noise increase in high wavelength situations. Also, in the study, it was stated that the noise reduction and aerodynamic performance due to λ and h act opposite each other, so it is necessary to investigate what the optimum values can be for this situation. In the study of Vemuri et al. [69], the NACA 65-710 airfoil was used and experiments formed in tandem configuration.In this way, it became an example to understand the effect of LE serration shape in uses such as contra-rotating open rotors. Article [70] is a detailed version of the study discussed in article [66]. Studies have focused on the case where the amplitude, h is 6% of the chord length and the wavelength, λ is 30% of the chord length, which is thought to be the optimum design for the sinusoidal leading edge shape. As studies on the efficiency of single wavelength shaped leading edge designs increase, it has been a matter of curiosity how the results will change with the combination of more than one sine waves, namely, whether the efficiency will increase more or decrease. The study of Narayanan and Singh [71] also exemplifies such a curiosity. In content of the study, multi-wavelength LE shapes in various design parameters are shown and compared with single wavelength design. In order to make comparisons, the maximum amplitude was taken equal to the amplitude of the single wavelength in all cases. Experimentally studied LE designs can be divided into three categories: single wavelength, dual wavelength and triple wavelength. Flat plate is used in the designs.The visuals of the flat plates with dual (double) and triple wavelenght designs used by the researchers in the experiments are shown in Figure 1.7. According to the results of the study, the highest noise reduction was observed in all designs of the flat plate with dual wavelength leading edge compared to both single wavelength and triple wavelength designs. It is also explained that the maximum amplitude for dual wavelength is the most important parameter for noise reduction. In other words, the dual wavelength shape is the most suitable control mechanism among the LE serrations compared to the others.

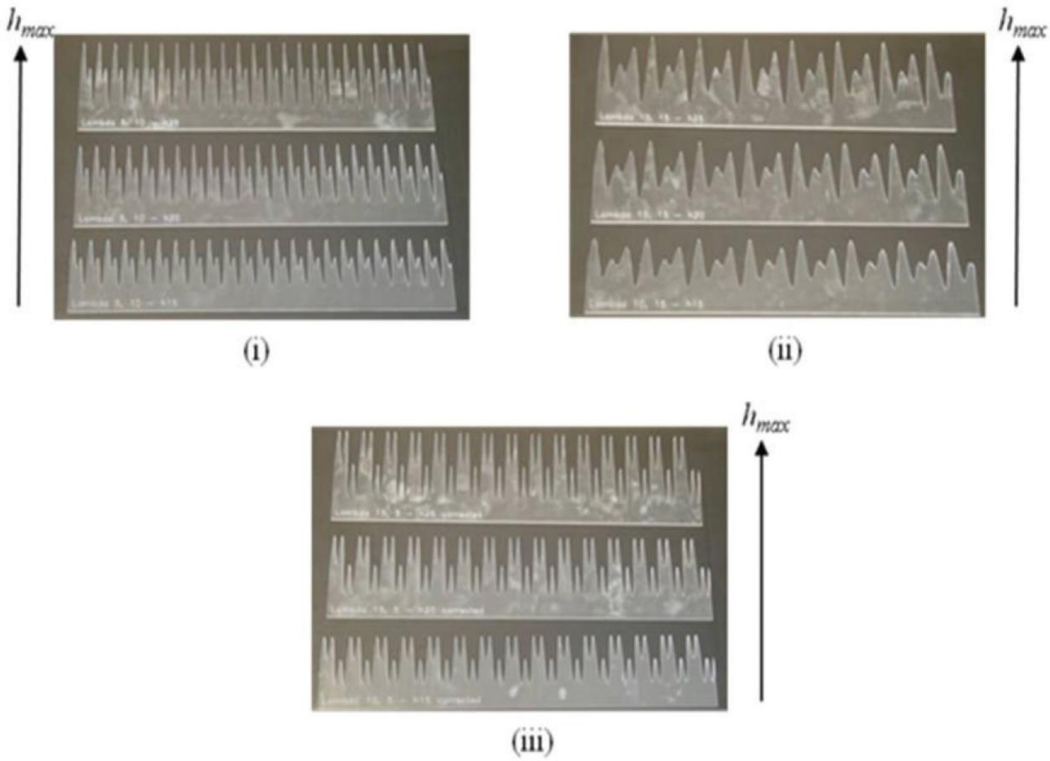

Figure 1.7 : Dual wavelength designs used in the study of Narayanan and Singh [71].

Another similar study is the study of Chaitanya et al. [72]. Within the scope of the study, twenty different double wavelength designs were experimentally investigated using flat plates and compared both with the single wavelength design and among themselves. The effect of the amplitude of these designs on noise is achieved by changing the phase difference as well as changing the total amplitude. The observed result for both cases is that there is a decrease in noise reduction with amplitude increase up to a certain frequency value, and after this frequency value there is an increase in noise reduction. When the effect of wavelength, which is expressed as dimensionless with the integral length scale of the incoming flow, on the noise level is examined, it is seen that the noise reduction decreases as the value of this dimensionless expression increases. One of these designs, which was examined as a flat plate, was also compared with a three-dimensional aerofoil produced using the NACA 65 airfoil, and as a result, it was seen that the flat plate values matched the real wing data. The image of the wing designed in three dimensions within the scope of the study is shown in Figure 1.8.

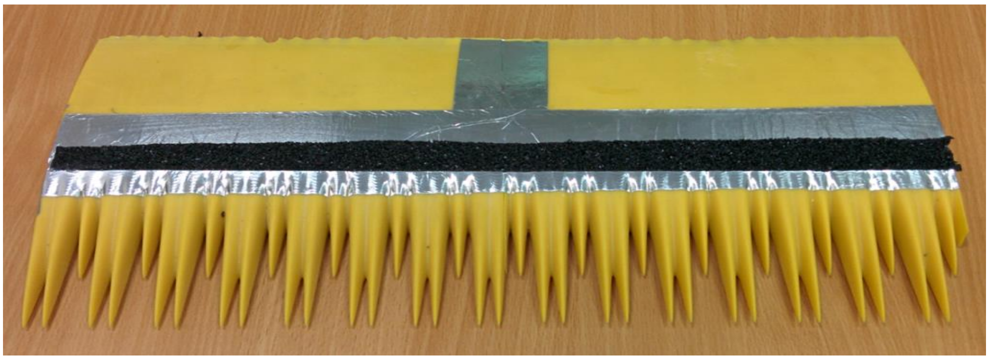

Figure 1.8 : 3D DW design used in the study of Chaitanya et al [72].

As a result of all these studies that especially focused on wavelenght shaped LE serrations,although waveform profiles are of two types in the form of single-wavelength and double-wavelength serrated edge structure, it has been observed by experiments that the use of double-wavelength structures is more efficient in terms of noise.

1.3 Reference Study

There is a comprehensive experimental study about leading edge that produced with double wavelength serration performed by Chaitanya et al. [73]. According to study , the amplitude of double wavelength indicates the distance between two roots in the streamwise direction, and the wavelength indicates the distance between two roots in the spanwise direction. This situation, whose expression is given, is more understandable with the sketch in Figure 1.9.

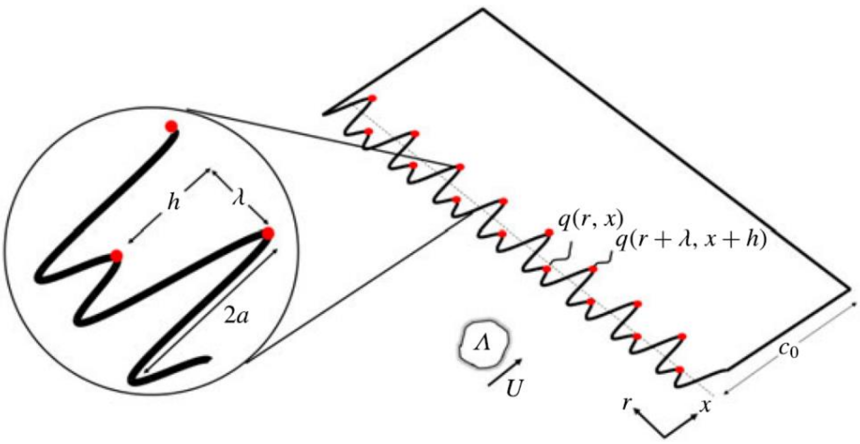

Figure 1.9 : Double wavelength serration on wing [73].

In the study, the designs were made using a flat plate in order to provide convenience in production and to make a clear observation without the effects of three-dimensionality. Within the scope of the experiments, firstly, two single wavelenght designs with equal amplitudes and different wavelengths (one adjusted to be twice the other) and a double wavelength design, which is the combination of these two single wavelengths, were compared. As a result of this comparison, it has been shown that the double wavelength design is visibly more effective. The graph created for the comparison within the study is given in Figure 1.10.

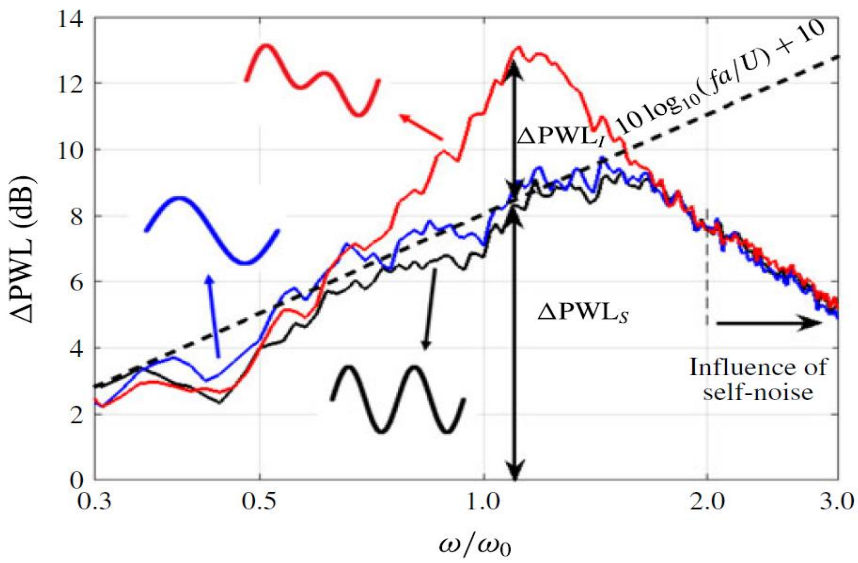

Figure 1.10 : Comparisons of SW and DW in the study of Chaitanya et al [73].

Then, the effect of amplitude, h and wavelength, λ on the noise reduction was investigated by experiments. For this, either the wavelength is kept constant and the amplitude is increased, or the amplitude is kept constant and the wavelength is increased. In these designs, the amplitude change is adjusted with the phase difference and these phase differences are ϕ =0, π/4 and π/2. As a result of the experiments according to change of amplitude, it was found that noise reduction decreased as amplitude, h increased up to a certain frequency, and noise reduction increased after that frequency. The graph of these obtained results is given in Figure 1.11.

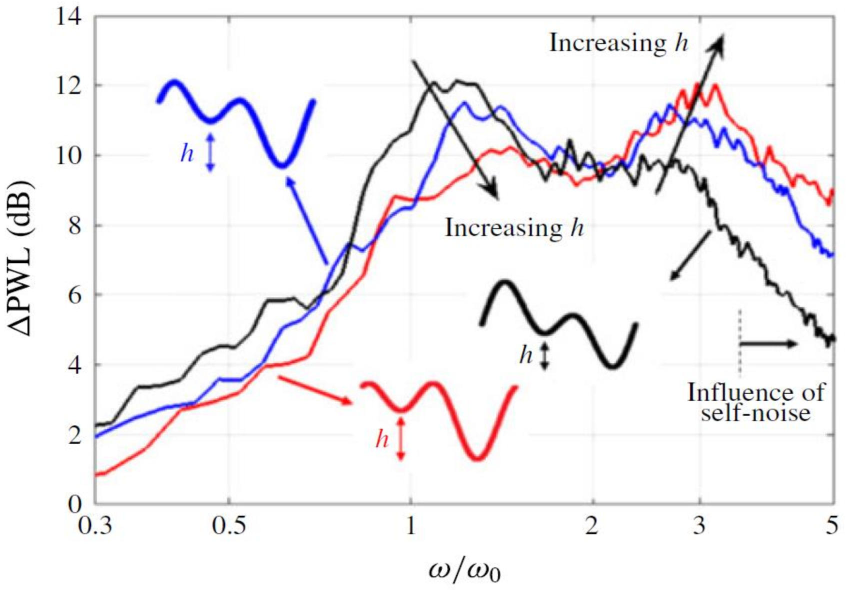

Figure 1.11 : NR levels due to h of DW in the study of Chaitanya et al [73].

The wavelength change in double wavelenght designs is achieved by changing λ_1, but the ratio between λ_1 and λ_2 is fixed and its value (λ_1/λ_2) is set to 0.5. In total, wings with six different wavelengths (as flat plates) were produced. As a result of the experiments according to change of wavelenght,which is expressed as dimensionless with the integral length scale of the incoming flow, it was found that noise reduction decreased as wavelenght, λ increased. However, noise reduction level achieved the its maximum value in situation where the dimensionless expressions nearly equals to 1. The graph created for these results is given in Figure 1.12.

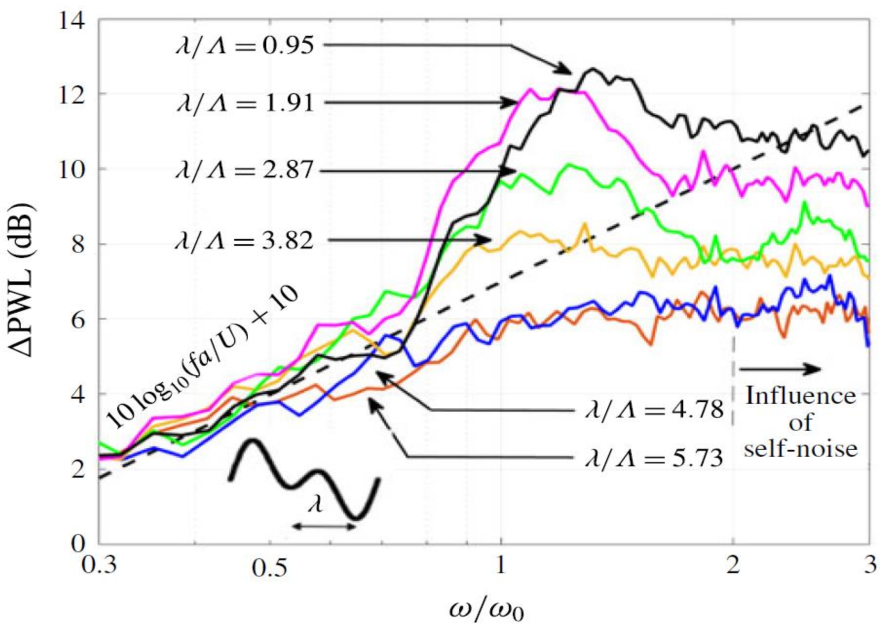

Figure 1.12 : NR levels due to λ of DW in the study of Chaitanya et al [73].

In addition, at the end of the study, the results of the three-dimensional wings produced using the NACA 65-(12)10 airfoil were compared with the flat plate values. Comparisons was made between both single wavelenght designs and double wavelength designs created by summing these single wavelengths. As a result of the comparisons, it was observed that flat plate and 3D aerofoils formed a similar trend and the graph about this is given in Figure 1.13.

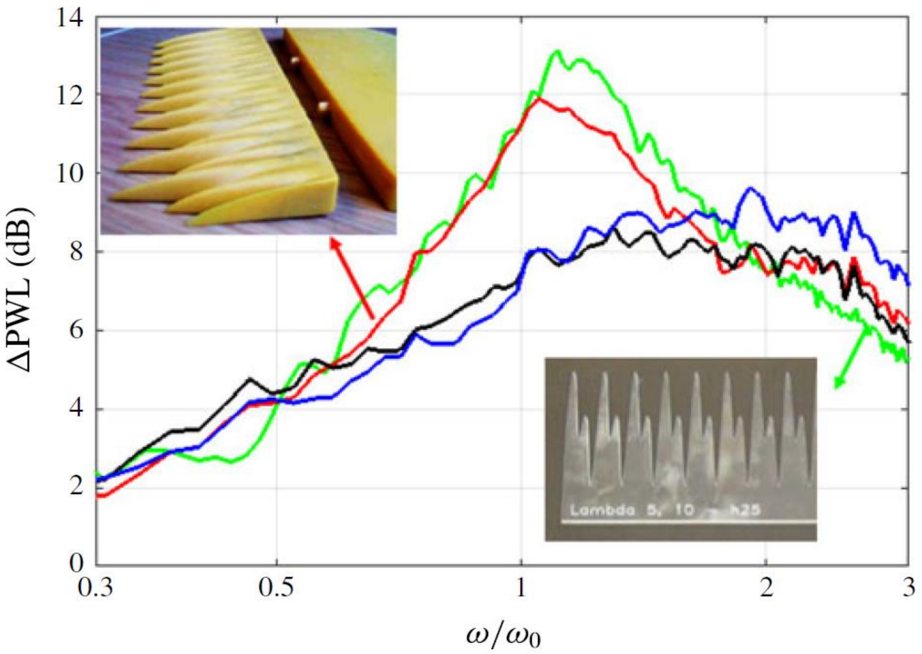

Figure 1.13 : NR levels of flat plate and 3D aerofoils with SW and DW in the study of Chaitanya et al [73].

In summary, it was shown in the study that the noise reduction would be maximum when the optimal values were selected for the distances in the streamwise and spanwise directions.

1.4 Motivation

Looking at the aforementioned studies about double wavelength LE serrations, it is seen that the experiments were carried out at a certain angle of attack, and this angle is relatively low. However, as it is known, as the angle of attack increases, flow separations can occur in the boundary layer, and as a result, losses in aerodynamic performance and significant increases in noise level may happen. Therefore, it is necessary to examine in high angles of attack and to clearly understand what the effects of using such an leading edge profile would be. Another conspicuous issue is that there are few studies on how aerodynamic performance is affected by this situation when noise reduction method is used. It is important to clarify the questions which are "is there a point where the optimum of both can be achieved" otherwise " is it to gain from one and lose from the other." In summary, with this study, it is aimed to investigate the aerodynamic performance experimentally, thought to be lacking in the literature, of the wings that noise situation was investigated and have double wavelength serration at leading edge, by considering an appropriate reference leading edge profiles. Double wavelength serration profiles, which are expected to be examined in the study, will be referenced from the study of Chaitanya et al. Accordingly, in this study, wings with different amplitudes will be used and the aerodynamic performance effect will be compared according to the amplitude change. Because it is a situation that has been mentioned in previous studies that especially the amplitude is more effective on the efficiency of these wings which have wave-shaped leading edge design. And also the straight wing structure (non-serrated wing) will be used for comparison of aerodynamic results.

2. WING DESIGN

2.1 Double-Wavelength Leading Edge Serration

Double wavelength can simply be explained as the superposition of single wavelengths that sine wave-shaped. In a sense, it is summing of the wave constituents which are the wavelengths, λ_1 , λ_2 and amplitudes, h_1, h_2 belong to each single wavelength. The length of the chord formed by the addition of these waves can be expressed as follows according to the position in any spanwise direction and c_0 is the mean chord [73].

$$c(r) = c_0 + h_1\, sin(2\pi r/\lambda_1) + h_2\, sin(2\pi r/\lambda_2 + \phi) \tag{2.1}$$

The ϕ in the formula refers to the phase difference and as shown in Figure 1.9, the ‘r’ direction represents the progress in the spanwise direction. As shown in the Figure 1.8, by adding the two sine waves to each other, distances h in the direction of streamwise and λ in the direction of spanwise are formed between adjacent roots. The total peak to root amplitude is expressed in 2a.

In this thesis, it is planned to examine the effect of amplitude change in double wavelength serration design on wing performance. In this context, two different amplitude designs were made. This amplitude change was achieved by taking the amplitude values of single wavelength, h_1 and h_2 equal to each other but different from each other in all two cases. In this way, the total amplitude, 2a of the designs is changed. Since only the amplitude change was examined, the wavelength values, λ_1 and λ_2 were kept constant. In addition, the phase difference, ϕ is the same in all cases and its value is taken as zero. The double wavelength design parameters of these wings are given in Table 2.1.

Table 2.1 : Design parameters of double wavelength LE

Parameters	DW 1	DW 2
c0	100	100
λ1	6.7	6.7
λ2	13.4	13.4
h1	9.4	5.4
h2	9.4	5.4
ϕ	0	0
2a	33	19
h	13	7.52
λ	5.9	5.9

Two-dimensional drawings of double wavelengths with these design parameters are shown in Figure 2.1 and Figure 2.2.

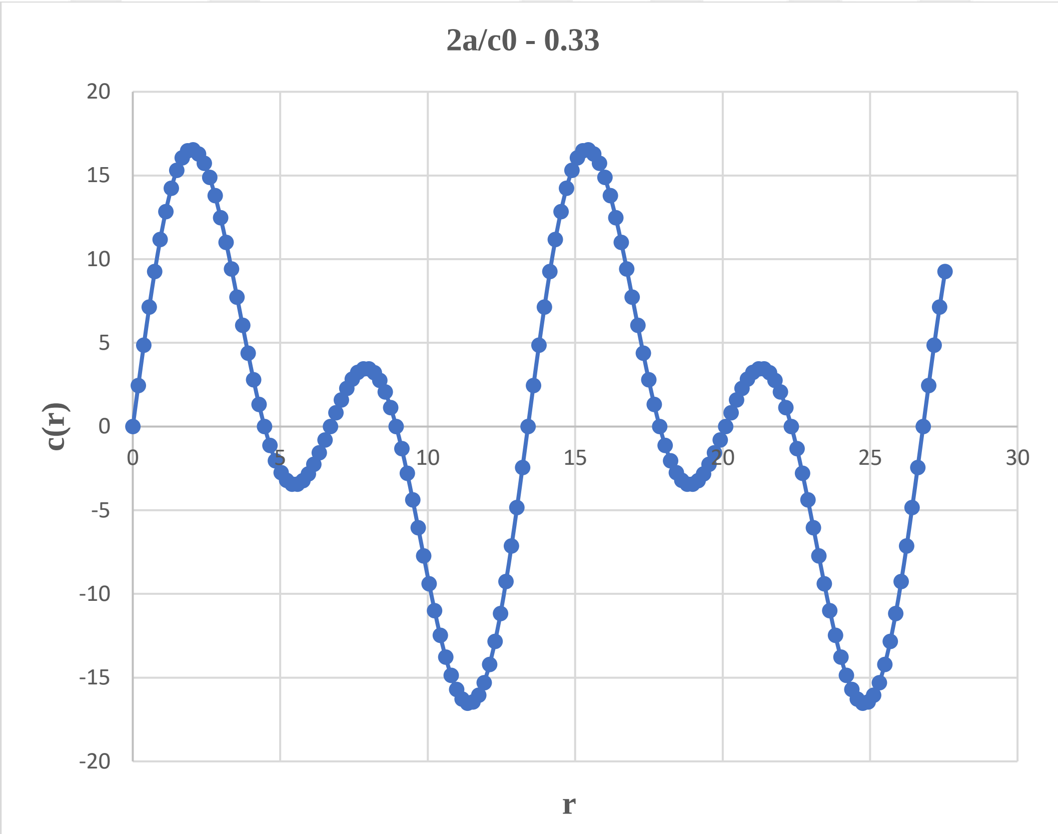

Figure 2.1 : DW 1 two dimensional sketch.

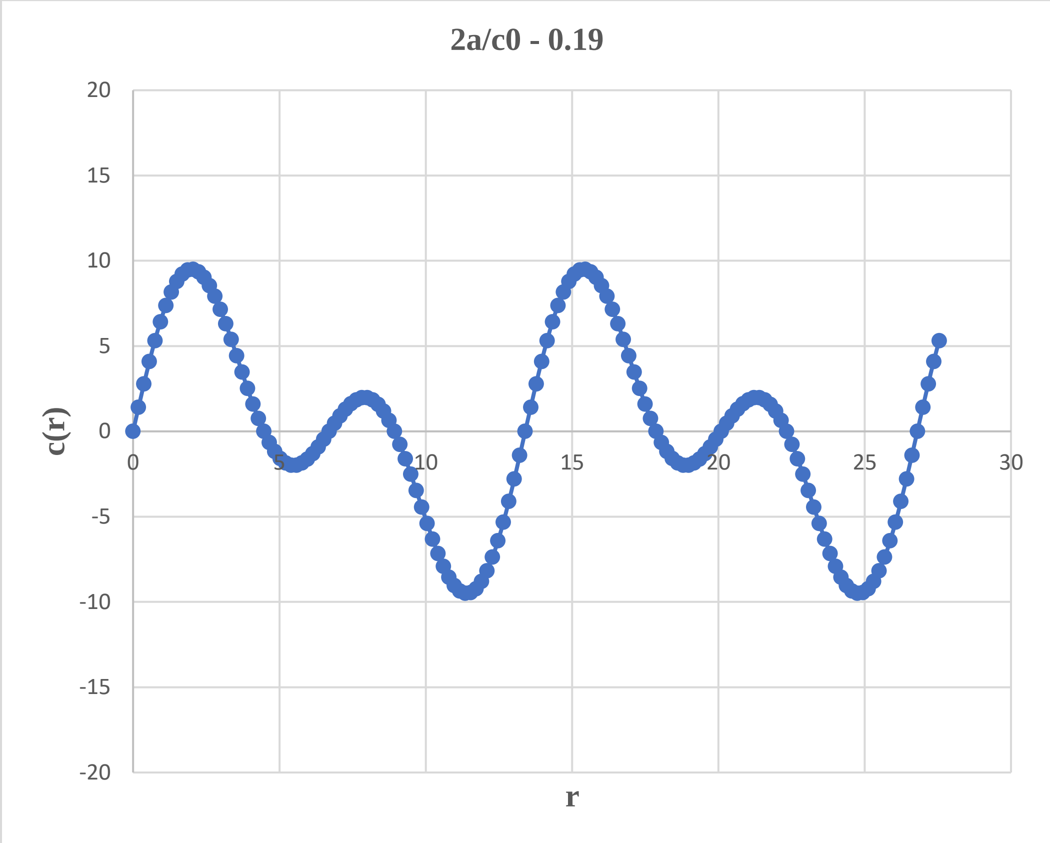

Figure 2.2 : DW 2 two dimensional sketch.

2.2 3D Aerofoil

The majority of the studies in the literature include the NACA 65 -(12)10 airfoil, which is also used in engine blades, so this airfoil profile is used in order to easily compare the results to be obtained in this study. Airfoil details required for 3D design are given in the article [74]. Airfoil shape sketched with indicated data is shown in Figure 2.3.

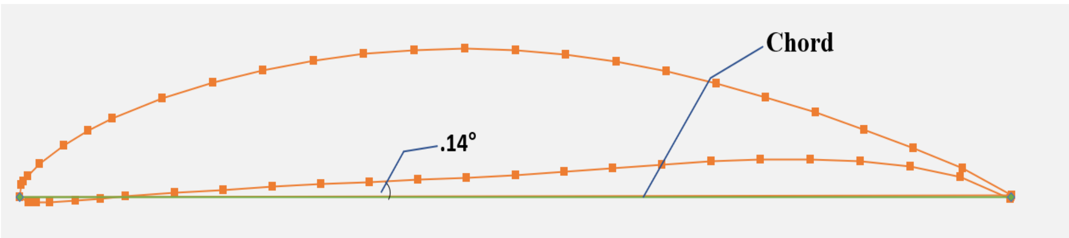

Figure 2.3 : NACA 65-(12)10 Airfoil.

The designed wings have a 100 mm mean chord and 500 mm span. In order to ensure the two dimensionality of the aerofoil, the span length was chosen in the size of the wind tunnel test section. Due to the size problem in production, the wing was produced by dividing it into equal parts in the span direction, that is, the wing was produced in five pieces totally. Besides, since the wings with different LE designs examined, for ease of production, the profile is separated from $c_0/3$, which corresponds to the approximate maximum thickness of airfoil, so that the wing is produced in two parts, rear and front. The separately produced rear and front parts are designed to be interlaced. That is, the rear part produced is always fixed and one, while the front part was produced in different numbers according to the design of double wavelength LE. These front parts of the wing are manufactured to examine two different h values corresponding to the same λ. Figure 2.4 shows the wing drawing designed in two parts.

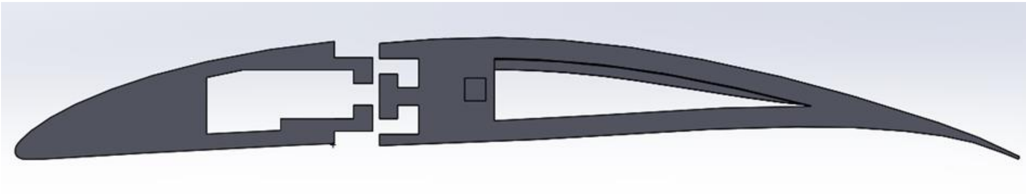

Figure 2.4 : Sketch of produced front and rear part of the wing.

By the way, the 3D design of the wings on the computer was made using the Solidworks program. The production of the wings is carried out with a 3D printer and unwanted roughness on the surface is eliminated. In addition, a non-serration flat model of the wing is also produced for comparisons. The visual of the straight baseline wing produced is also shown in Figure 2.5.

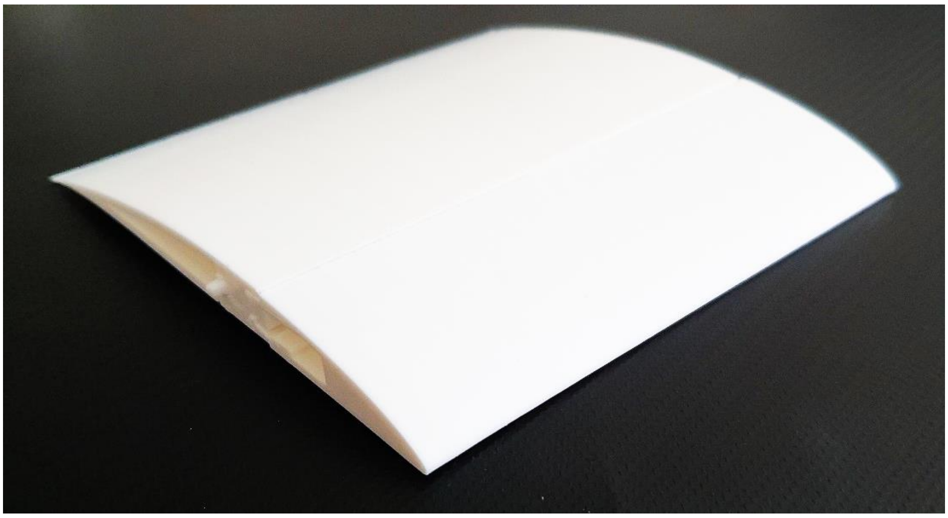

Figure 2.5 : Manufactured whole wing with baseline LE.

One of the front parts manufactured with a double wavelength serration is shown below in Figure 2.6. The whole wing with its rear and front parts assembled is shown in Figure 2.7.

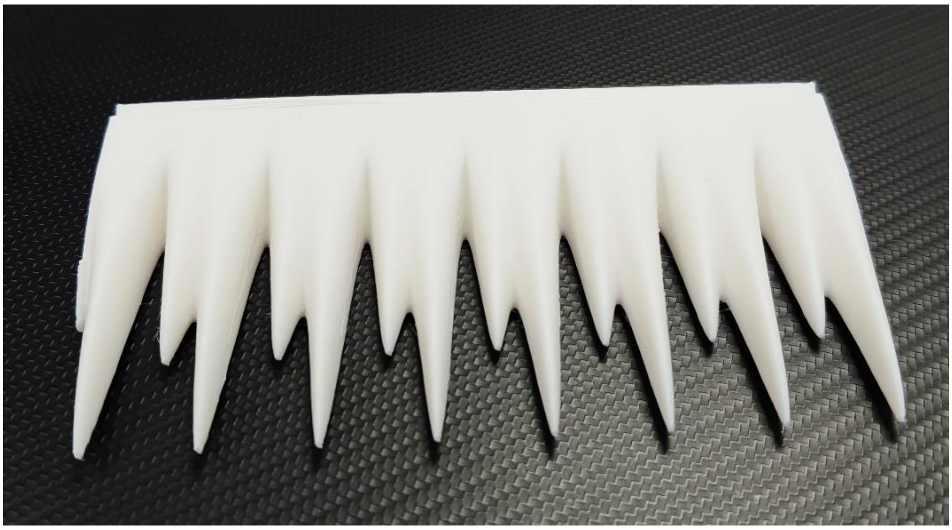

Figure 2.6 : Front part of of manufactured wing with DW1 LE.

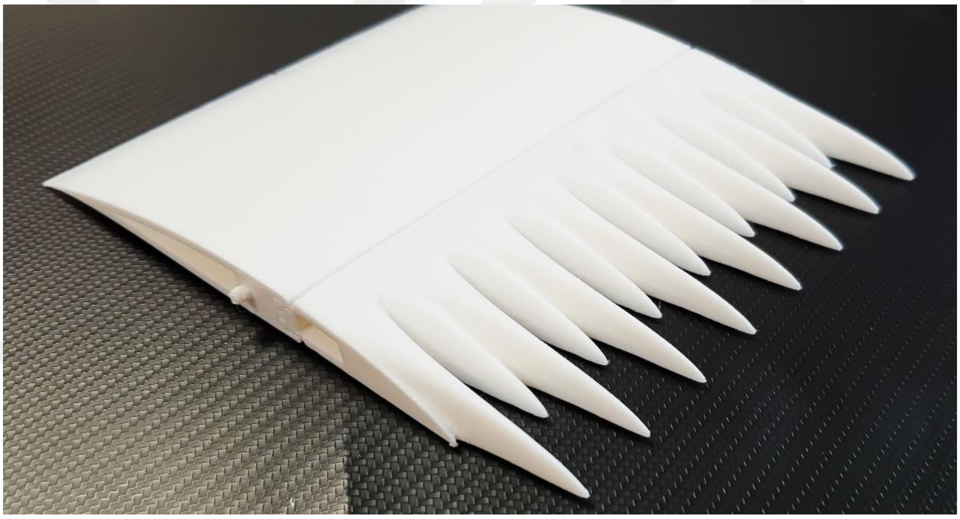

Figure 2.7 : Manufactured whole wing with DW1 LE.

Design parameters of this manufactured part are wavelengths are $\lambda_1/c_0 = 0.067$, $\lambda_2/c_0 = 0.13$ amplitudes are $h_1/c_0 = h_2/c_0 = 0.094$ and the phase difference is zero. All expressions are non-dimensionalized with mean chord. The total peak-to-root distance of the double wavelength formed by summing two waves with these values was $2a/c_0 = 0.33$, and the streamwise and spanwise distances between adjacent roots were $h/c_0 = 0.13$, $\lambda/c_0 = 0.059$ respectively. By the way, the photograph of the front part produced for the wing with the other leading edge design is shown in Figure 2.8.

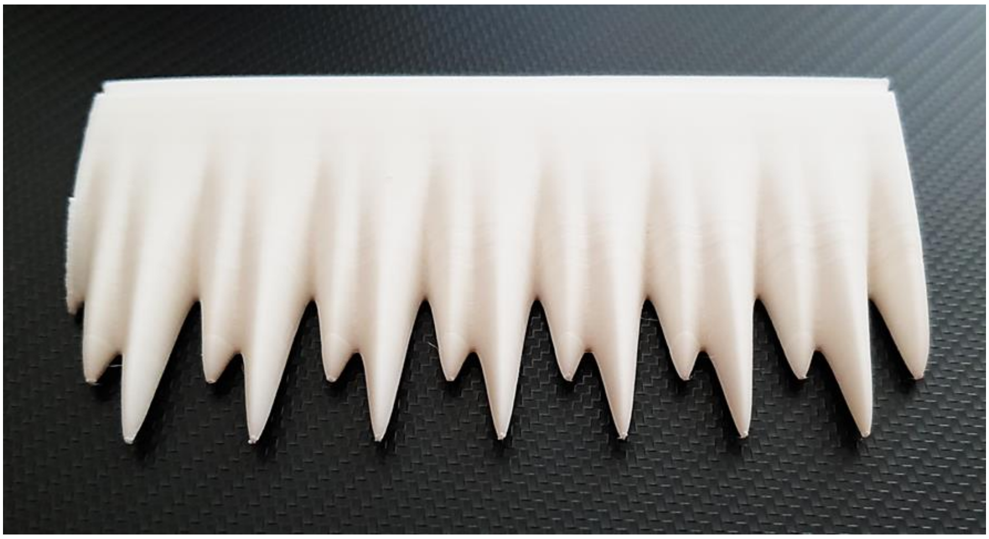

Figure 2.8 : Front part of of manufactured wing with DW2 LE.

Design parameters of this manufactured part are wavelengths are $\lambda_1/c_0 = 0.067$, $\lambda_2/c_0 = 0.13$ amplitudes are $h_1/c_0 = h_2/c_0 = 0.054$ and the phase difference is zero. All expressions are non-dimensionalized with mean chord. The total peak-to-root distance of the double wavelength formed by summing two waves with these values was $2a/c_0 = 0.19$, and the streamwise and spanwise distances between adjacent roots were $h/c_0 = 0.0752$, $\lambda/c_0 = 0.059$ respectively.

3. EXPERIMENTAL SETUP

3.1 Wind Tunnel

For aerodynamic performance measurements, a subsonic, open circuit wind tunnel with in ITU Trisonic Research Laboratory is used and it shown in Figure 3.1. It has an open test section and this test chamber entrance of this wind tunnel has dimensions of 50cm x 50cm and its operating speed range is 0 - 30 m/s. In the experiments carried out here, freestream velocity is 20m/s (Re =137563) .

Figure 3.1 : Open circuit, subsonic, 50 x 50 cm wind tunnel.

Before the wing was placed in the tunnel, the rear and front parts were fitted together, and these five wing parts in total were glued together with a putty-like substance. This wing, placed vertically in the experimental test section, is shown in Figure 3.2a. Figure 3.2b shows the application of the angle of attack given to the wing in the experimental setup. This process is done by the circle on which there are lines with one degree intervals. Since the chord line is close to the connection point of the wing to the tunnel and it creates diffuculties in the placement of this circle, this circle is rotated from a lower center that parallel to the chord line.

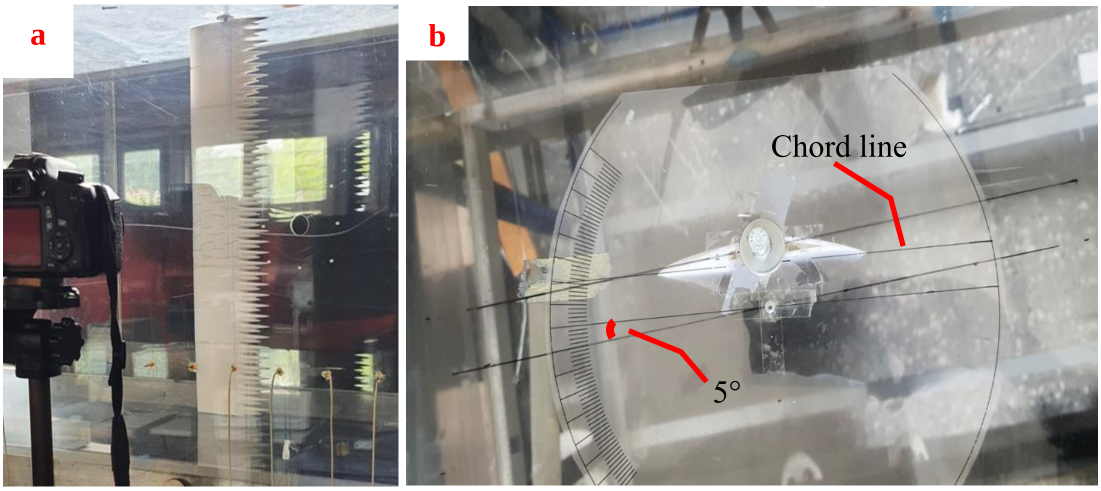

Figure 3.2 : Wing placement (a), AoA adjustment (b).

3.2 Pressure Measurement

Pressure taps were installed on the surfaces of the aerofoil models and these pressure taps were placed at different airfoil sections along the spanwise direction in order to three-dimensional effects will be taken into account. Figure 3.3 shows the placement of these pressure taps. Since the flow in the middle part of the wing is more decisive, measurement process was adjusted according to this part.

Figure 3.3 : Pressure taps on wing .

Pressure taps for the rear part of wing formed on a cover. The hoses placed for pressure measurement and this cover located on the rear part of the wing are shown in detail Figure 3.4.

Figure 3.4 : Inserted hoses and cover of rear part of the wing.

A 32 channel ESP pressure scanner was used for measurements. ESP Pressure Scanners are electronic differential pressure measuring element consisting of a series of silicon piezoresistive pressure sensors, one for each pressure port [75]. The outputs of the sensors in the device are electronically reproduced at a rate of up to 70.000 Hz through only one amplifier in the built-in state, through the use of dual addressing. This multiplexed amplified analog output data is capable of being transmitted even to a long-distance A/D converter. The operating ambient temperature range of these ESP pressure scanners is -25 to 80 °C. A technical drawing of an ESP pressure scanner is given in Figure 3.2. Data retrieval from the pressure scanner is carried out via the Aeroprobe program.

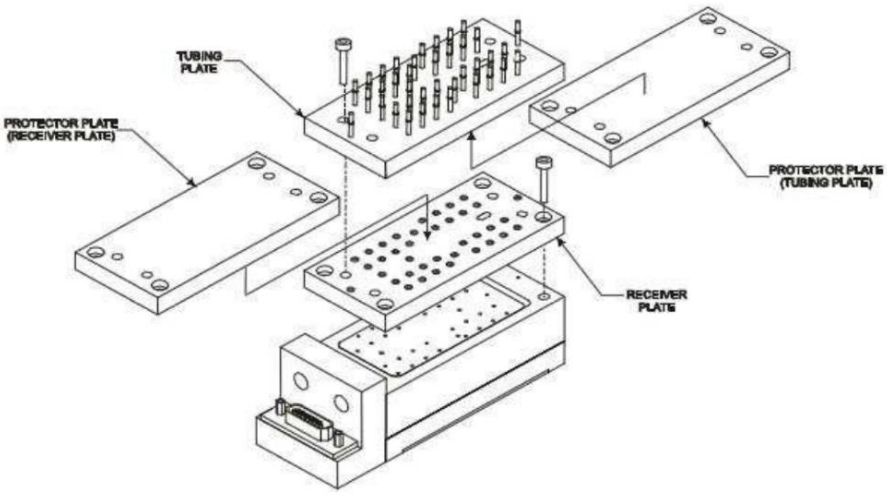

Figure 3.5 : ESP Pressure Scanner [75].

At the same time, measurements were made at the values of the angle of attack ranging from 0° to 28° and how the wings were affected by this situation was examined.

The main reason why the angle ends at 28° is the blocking rate, which is one of the experimental constraints. Stall angles were also determined.

3.3 Flow Visualization

In order to flow visualization of the wings, tufts visualization technique was used in this study. A wing prepared for flow visualization is shown in Figure 3.6. This method is a fairly old and common method used during wind tunnel tests because it is cost-effective although it is time-consuming to be placed in the parts to be examined. The materials used in the method can be monofilament nylon, polyester or cotton [76]. These tufts are attached to the surface with the help of an adhesive that does not damage the model. As air is blown over the model, the tufts move according to the flow [77]. When applied to the entire model, many details such as flow separations, reverse flow can be determined by the orientation of these tufts. However, they must be cut and glued to the appropriate length and weight so that the tufts can move with this incoming flow. In addition, the tuft method only provides information about the lower parts of the boundary layer formed on the model surface.

Figure 3.6 : Tufted baseline wing.

Cotton thread was chosen in the experiments. As mentioned in pressure measurement, since the flow in the middle part of the wing is more decisive, photographing process was adjusted according to this part. Figure 3.2 is also a visual showing this photography process. For flow visualization, tuft sizes were set to 2cm and they were placed on the wing with a distance of 2cm between them. Since the LE design of the wing has changed, the tufts locations have not remained constant, but the tufts have been placed in positions that are suitable for the design and expected to provide the most accurate visual. At the same time, measurements were made at the values of the angle of attack ranging from 6° to 28° and how the wings were affected by this situation was examined. Stall angles were also determined.

4. RESULTS OF EXPERIMENTS

In this section, the data obtained as a result of flow visualization (FV) and pressure measurement experiments are detailed.

4.1 Flow Visualization

Flow visualization experiments were carried out for a total of three different wings: Baseline, DW1 and DW2. Since approximately the same visuals would be obtained at low angles of attack where the flow is likely to be laminar, the experiments were started from an 6°. And since there was a laminar flow situation on all three wings at an angle of attack of 6°, there was no return to lower angles of attack. Meanwhile, for photographs obtained in flow visualization, the direction of flow is from right to left.

4.1.1 Baseline wing

According to the Figure 4.1 taken at 6° angle of attack for the baseline wing, it can be seen that tufts are completely smooth,so there is a fully laminar flow on the wing.

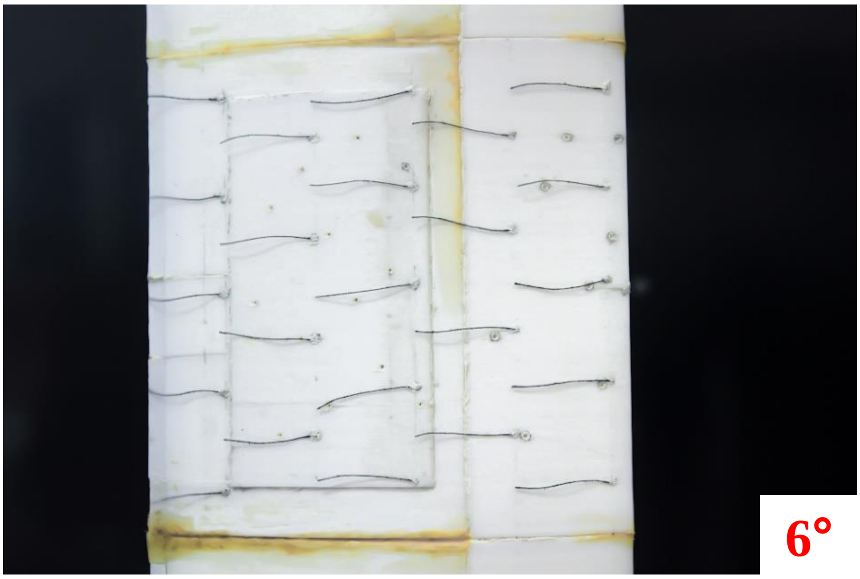

Figure 4.1 : FV of baseline wing at 6°AoA.

When an angle of attack of 8° was given, the flow started to become partially turbulent within approximately 20% from trailing edge of the wing. This is shown in Figure 4.2.

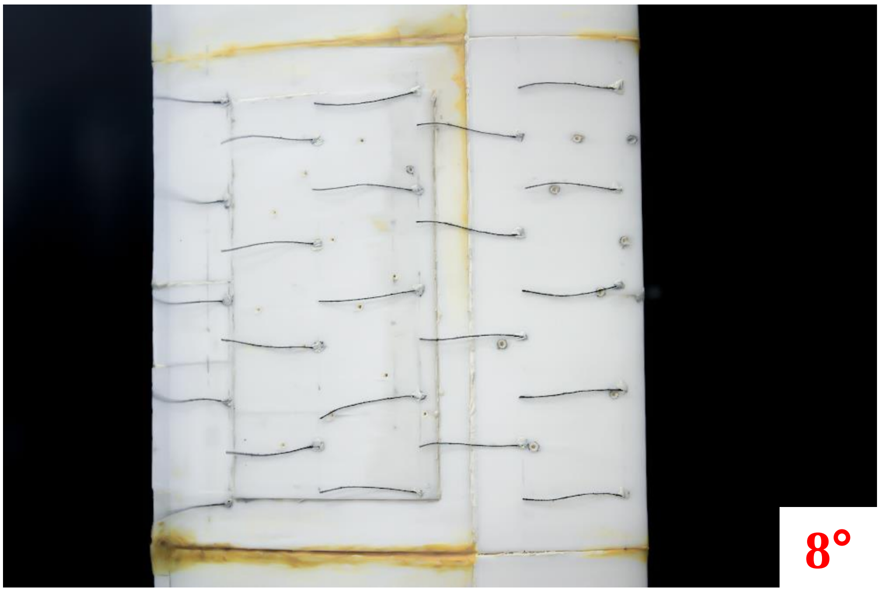

Figure 4.2 : FV of baseline wing at 8°AoA.

As seen in Figure 4.3, when the angle of attack of 10° was reached, the turbulent flow that started to be seen on the wing, this time advanced by about 40% from the trailing edge.

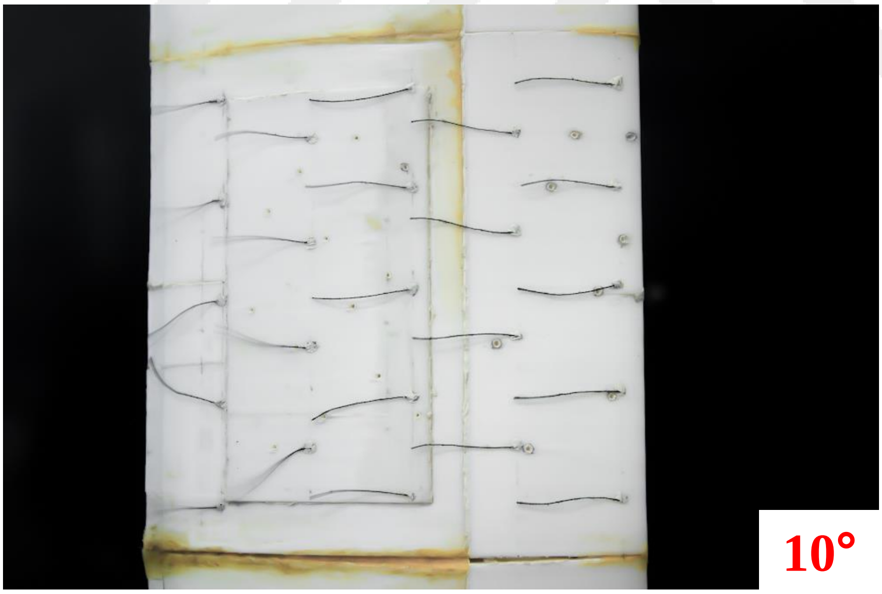

Figure 4.3 : FV of baseline wing at 10°AoA.

When the angle of attack was 12°, an image similar to the situation at 10° was obtained. This is shown in Figure 4.4. However, at this angle value, the tufts in the third row move slightly instead of remaining completely flat.

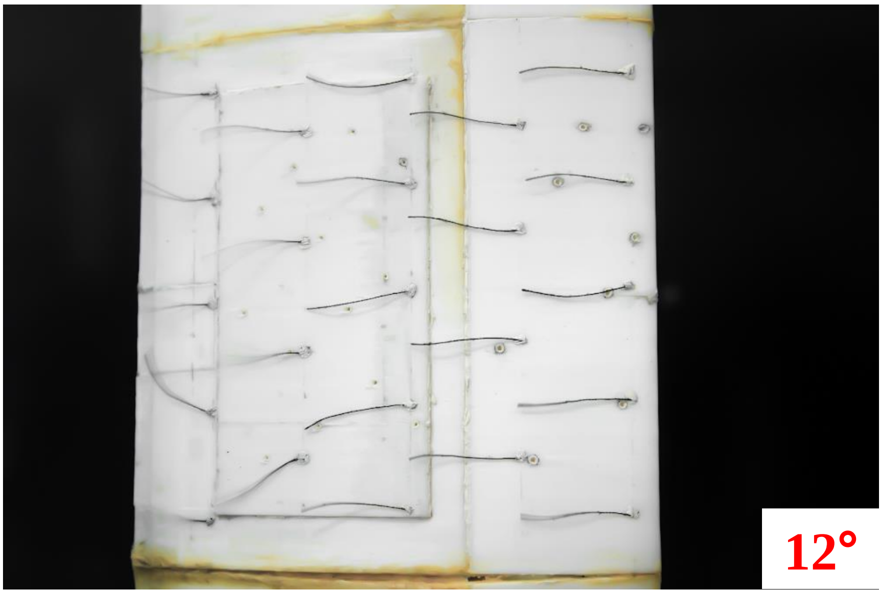

Figure 4.4 : FV of baseline wing at 12°AoA.

At the 14° angle of attack shown in Figure 4.5, the flow on the wing became completely turbulent within the 60% range from the trailing edge. However, the tufts in the first two rows starting from the leading edge also started to move, that is, to become turbulent.

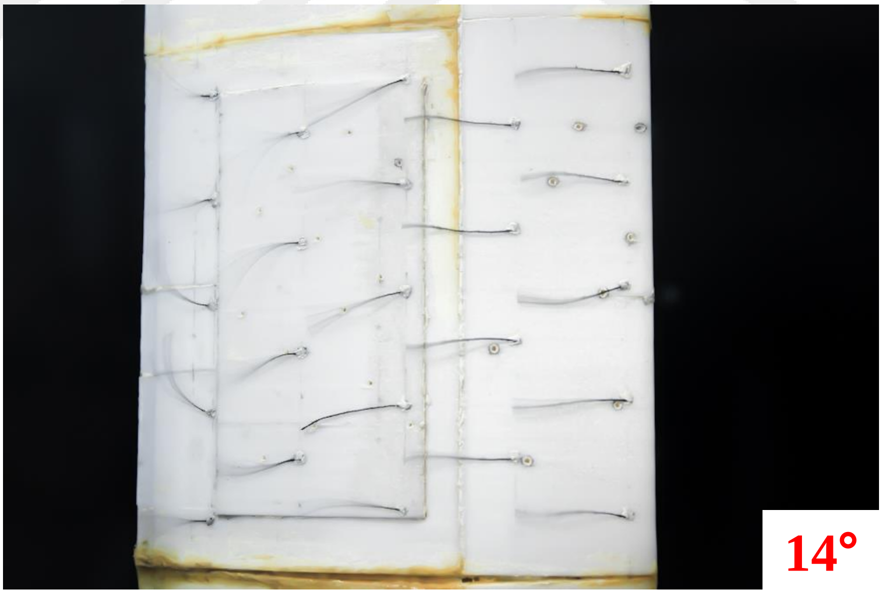

Figure 4.5 : FV of baseline wing at 14°AoA.

When the angle of attack was 15°, the image completely changed. The flow on the wing has become complicated. Especially in the tufts in the back three rows, it is clearly seen that there is a direction from the trailing edge to the leading edge, that is, the flow is separated. This situation is shown in Figure 4.6.

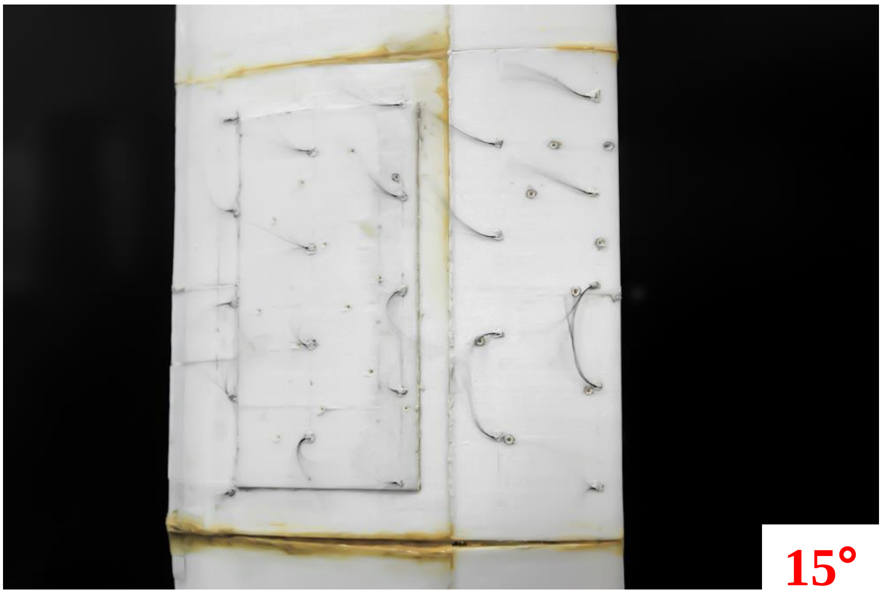

Figure 4.6 : FV of baseline wing at 15°AoA.

In order to be sure of the transition at 15°, the flow visual was checked when the angle of attack was 16°. The visual of this angle is given in Figure 4.7. When the figure is examined, it is clearly seen that the flow on the wing is separated, and cannot re-attach to the wing in the back tufts. The data obtained from the pressure measurements, consistent with the flow images, show that the flow is completely separated, especially after 18 degrees, and couldn't reattach on to the wing again.

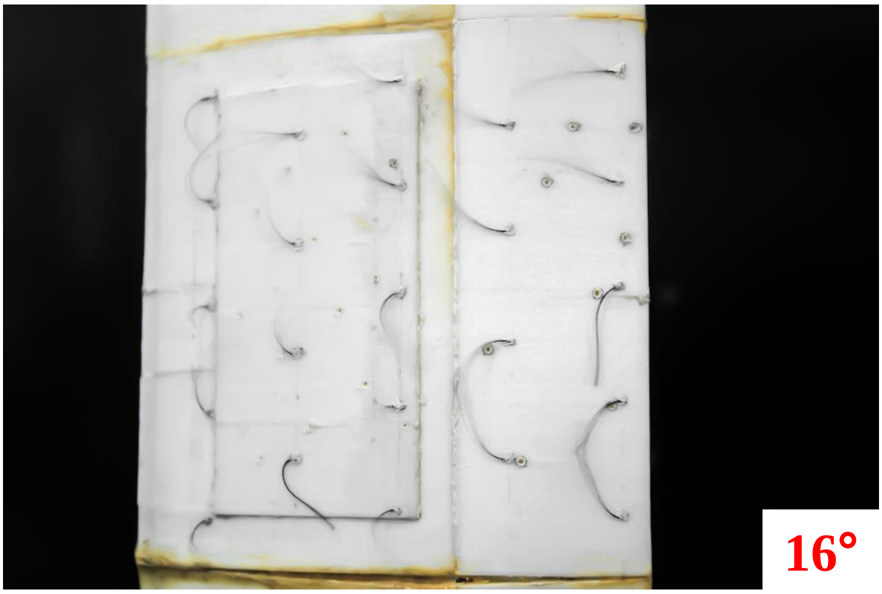

Figure 4.7 : FV of baseline wing at 16°AoA.

4.1.2 DW1 wing

In this wing, the tufts are placed further away from the LE compared to the baseline wing due to the LE design. In other words, there are tufts in approximately 70% of the wing, starting from the TE. Looking at Figure 4.8, it can be seen that the flow on this wing with double wavelenght LE at a 6° angle of attack is laminar. However, there was a very small amount of fluctuation in the tuft's tip located close to the trailing edge.

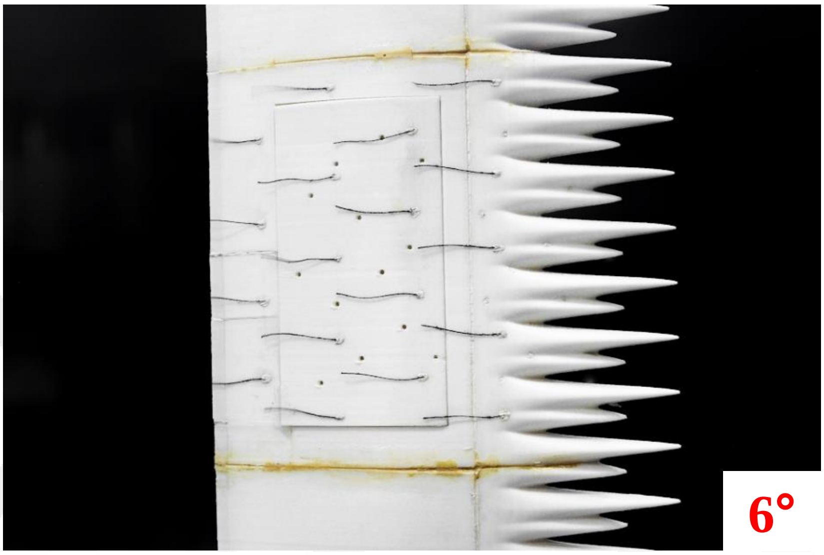

Figure 4.8 : FV of DW1 wing at 6°AoA.

When an angle of attack of 8° was given, the turbulence intensity of the flow increased in tufts located in approximately 30% from trailing edge of the wing. This is shown in Figure 4.9.

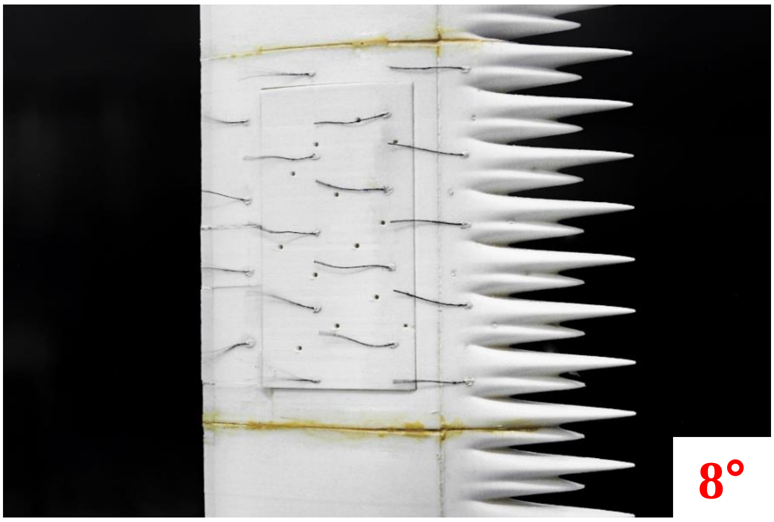

Figure 4.9 : FV of DW1 wing at 8°AoA.

As seen in Figure 4.10, when the angle of attack of 10° was reached, the turbulent behaviour began to be observed even in the tufts located at nearly %55 from the TE. The tufts in the back two rows have started to rise outward from the wing surface. In addition, as seen in the photo, it was also observed that the flow was directed upward, from bottom to top relative to the photograph plane. It is thought that this orientation stems from its roots in LE design.

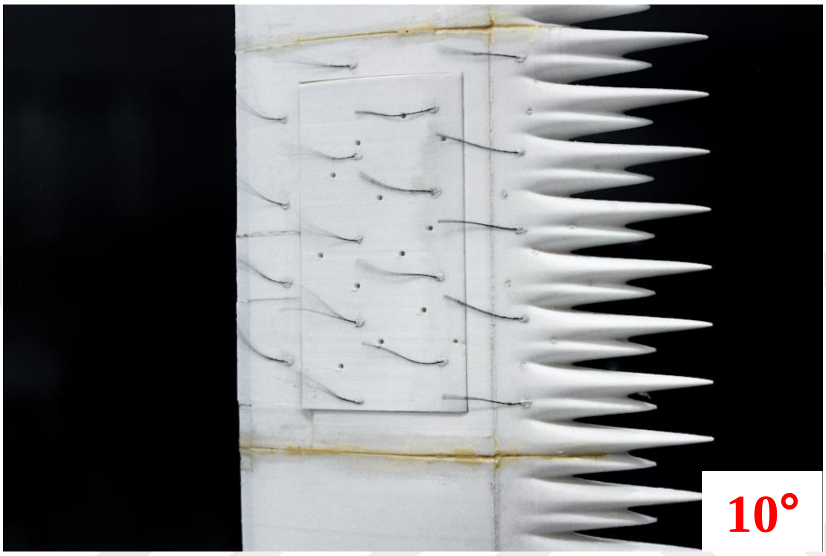

Figure 4.10 : FV of DW1 wing at 10°AoA.

When the angle of attack was 12°, an image similar to the situation at 10° was obtained. This is shown in Figure 4.11. However, at this angle value, the turbulence intensity of the flow increased in the tufts in the second row and these have also started to high outward from the wing surface.

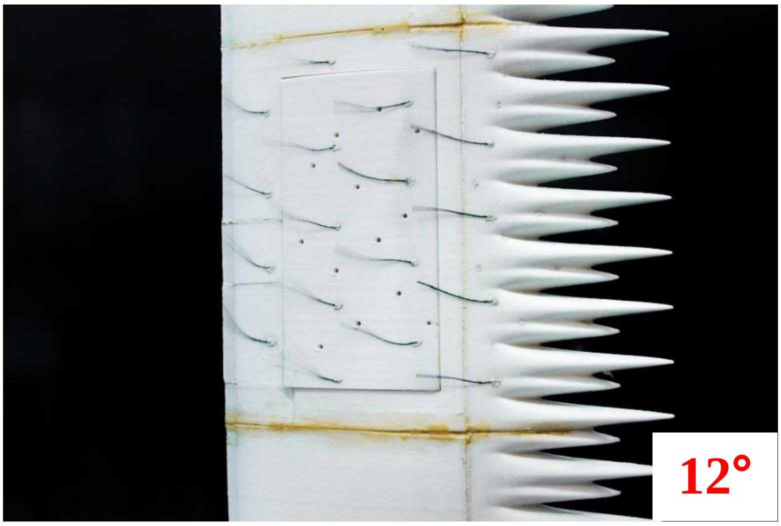

Figure 4.11 : FV of DW1 wing at 12°AoA.

At the 14° angle of attack shown in Figure 4.12, the flow on the wing behaves fully turbulently on tufts located in almost 50% from the TE. At the same time, the tufts especially at the back row have tended to return.

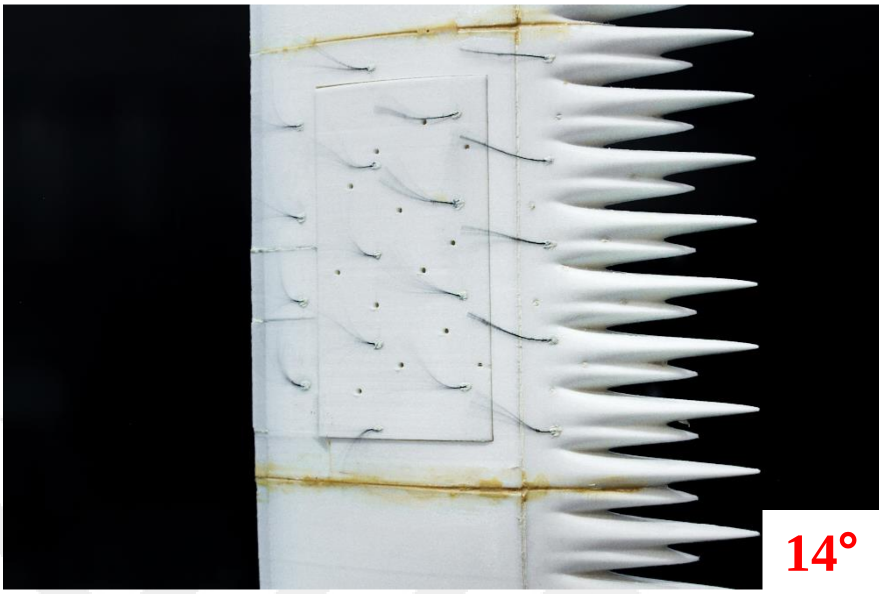

Figure 4.12 : FV of DW1 wing at 14°AoA.

When the angle of attack was 16°, the flow behaves similarly to 14°. Besides, at this angle value, almost all tufts have been rise outward from the wing surface. At the same time, the tufts, especially in the back two rows, tended to return more than the situation at 14 degrees.This situation is shown in Figure 4.13. Even if there is a tendency to return, there is still no complete seperation in the flow.

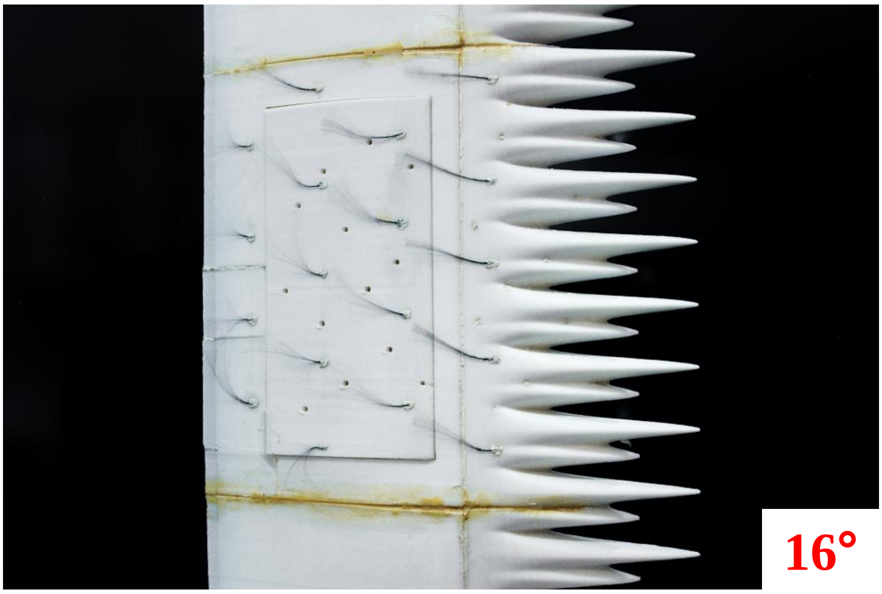

Figure 4.13 : FV of DW1 wing at 16°AoA.

As seen in Figure 4.14, when the angle of attack of 18° was reached , it is clearly seen that the flow on the wing became more complex to previous angles of attack. When looking at the tufts, it is seen that the flow is extremely turbulent and tufts have risen out of the wing surface, but a complete return of the tufts were not observed. In addition, the tufts in the first row tend to remain smooth in the parts close to the attachment point. Therefore, just by looking at the visual, a clear statement cannot be made that 'the flow has completely separated and the wing has fallen into a stall state'.

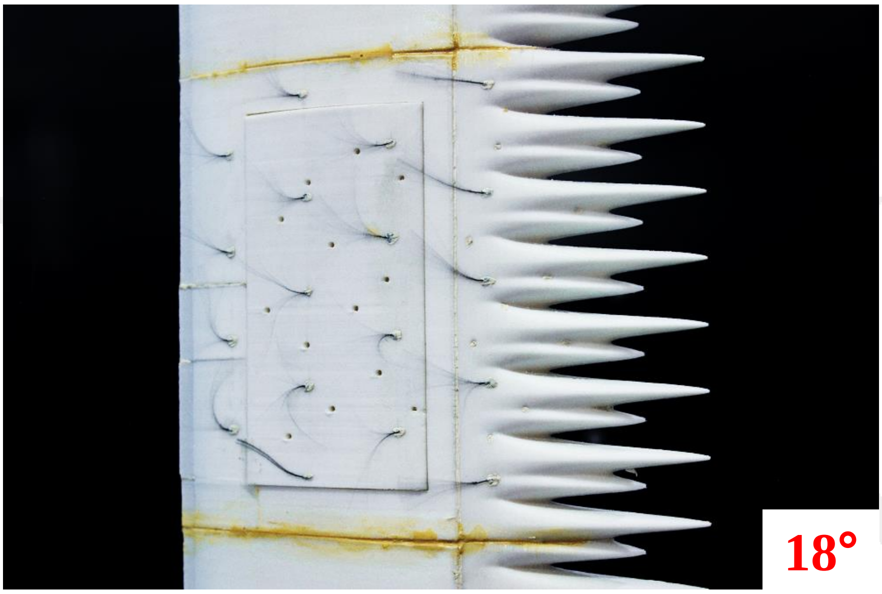

Figure 4.14 : FV of DW1 wing at 18°AoA.

After 18° angle of attack, flow visualization experiments were also carried out for 20°, 22°, 24°, 26° and 28°, respectively. Nevertheless, when the images obtained in these experiments were examined, it was seen that the flow on the wing was approximately the same as that observed at 18°. In other words, although the flow is not stable, the statement 'the wing has fallen into stall' cannot be said clearly as in the previous angle. Unlike the baseline wing, in this wing design it couldn't possible to observe the angle at which the tufts return completely, that is, the flow is completely separated, just from the flow visualization images. According to these images supported by pressure measurements, it can be said that for 20° and beyond, the flow is completely separated and couldn't hold on to the wing again. The images obtained when the angle of attack is 20°,22°,24°,26° and 28° are given in Figure 4.15,.16,.17,.18 and Figure 4.19, respectively.

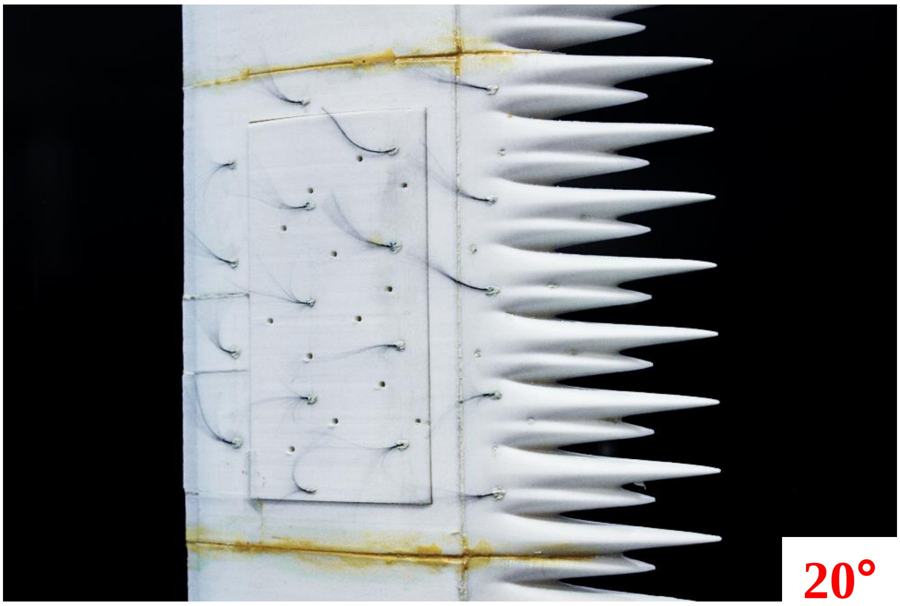

Figure 4.15 : FV of DW1 wing at 20°AoA.

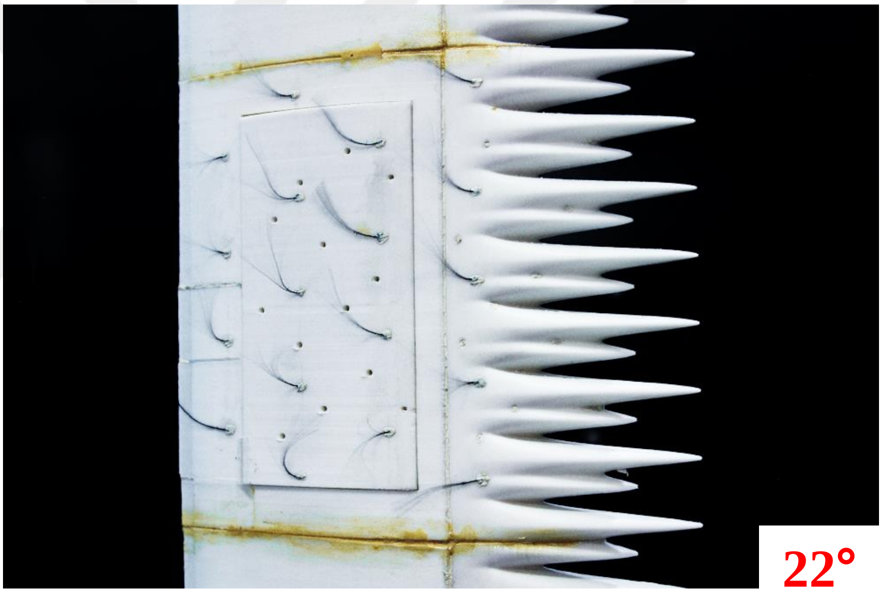

Figure 4.16 : FV of DW1 wing at 22°AoA.

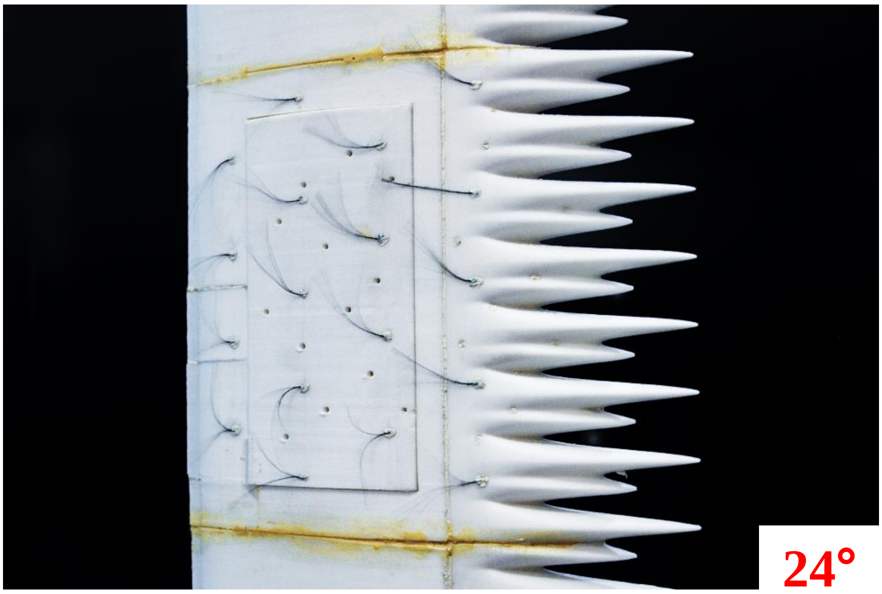

Figure 4.17 : FV of DW1 wing at 24°AoA.

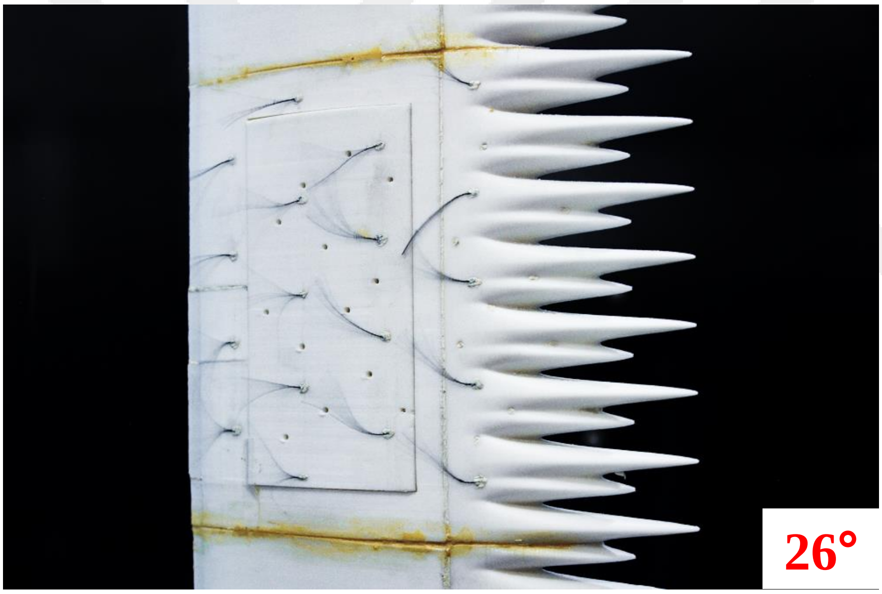

Figure 4.18 : FV of DW1 wing at 26°AoA.

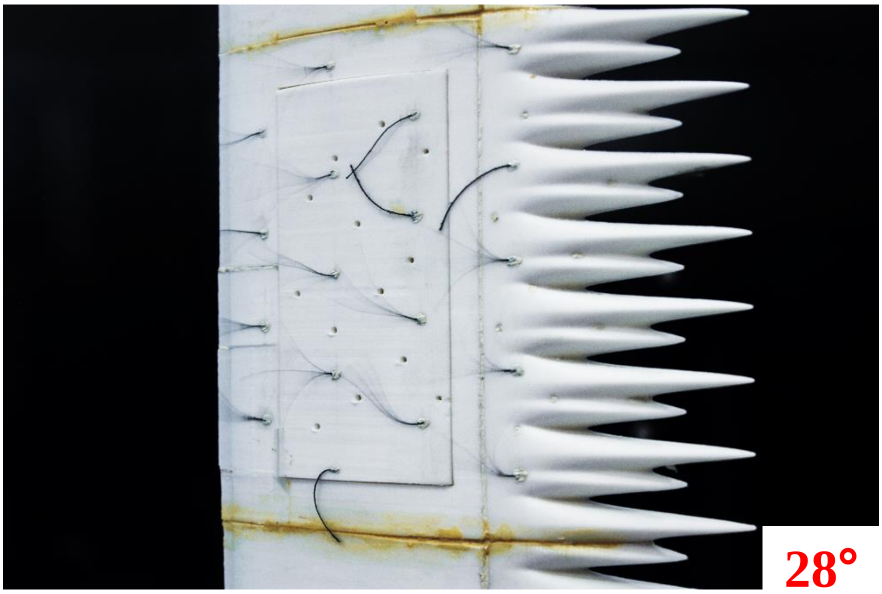

Figure 4.19 : FV of DW1 wing at 28°AoA.

4.1.3 DW2 wing

In this wing, the tufts are also placed further away from the LE likewise in the DW1 wing due to the LE design. In other words, there are tufts in approximately 75% of the wing, starting from the TE. Experiments were also started on this wing with an angle of attack of 6°. Looking at Figure 4.20, it can be seen that the flow is laminar throughout almost the entire wing, but a slight fluctuation in the tuft’s tip in the last row at the back.

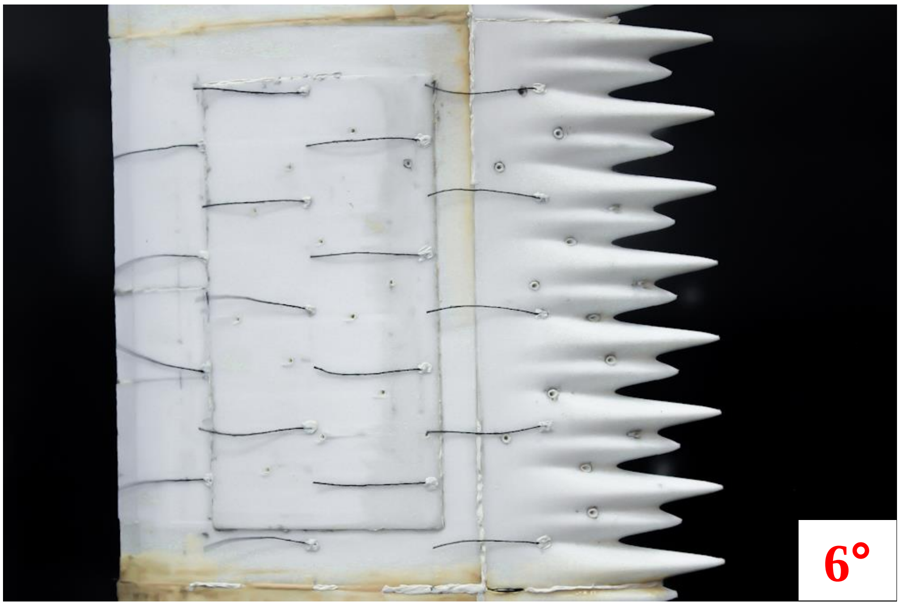

Figure 4.20 : FV of DW2 wing at 6°AoA.

When an angle of attack of 8° was given, it was observed that the flow remained laminar except for the tufts located in 20% from the TE. Besides, the turbulence intensity of the flow increased in the tufts at last row. This is shown in Figure 4.21.

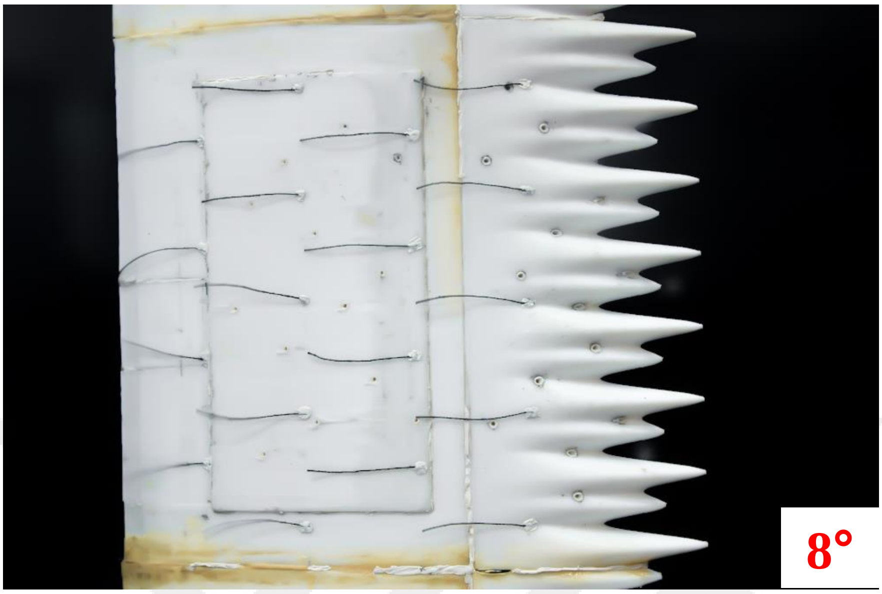

Figure 4.21 : FV of DW2 wing at 8°AoA.

As seen in Figure 4.22, when the angle of attack of 10° was reached, it was observed that the flow remained still laminar in the tufts at first two row. However the turbulent flow that started to be seen on the wing, this time advanced by about 35% from the trailing edge.

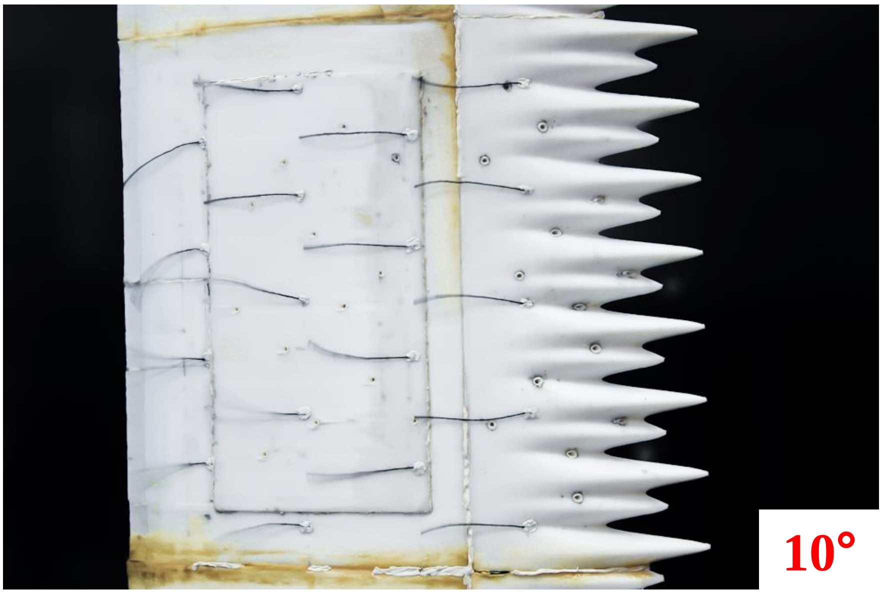

Figure 4.22 : FV of DW2 wing at 10°AoA.

When the angle of attack was 12°, it was observed that there was not much change in the flow over the wing. In other words, an image similar to the situation at 10° was obtained. But, at this angle value, it can be seen that a slight fluctuation in the tuft's tip at the second row. This situation is shown in Figure 4.23.

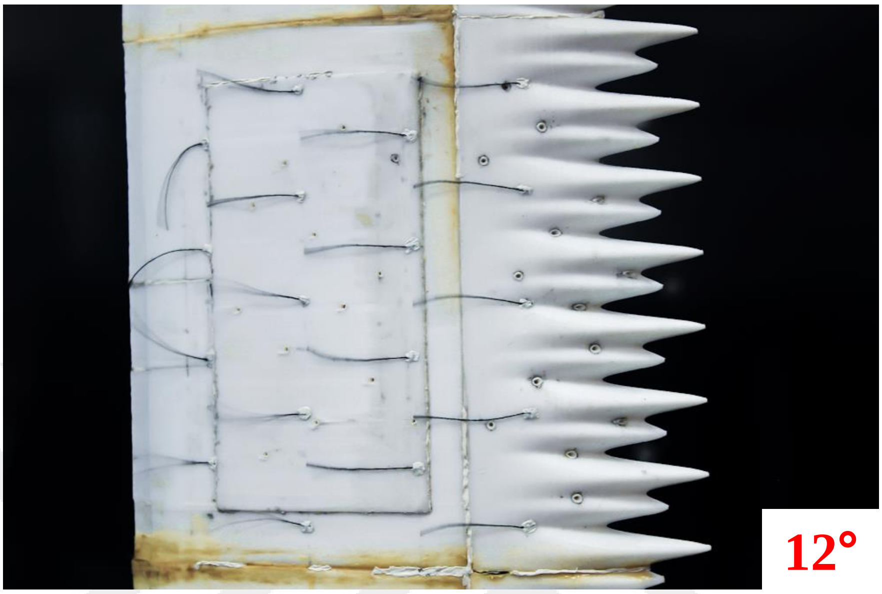

Figure 4.23 : FV of DW2 wing at 12°AoA.

At the 14° angle of attack shown in Figure 4.24, the turbulent behaviour began to be observed even in the tufts located at nearly %60 from the TE. In addition, the tufts in the back two rows have started to rise outward from the wing surface.

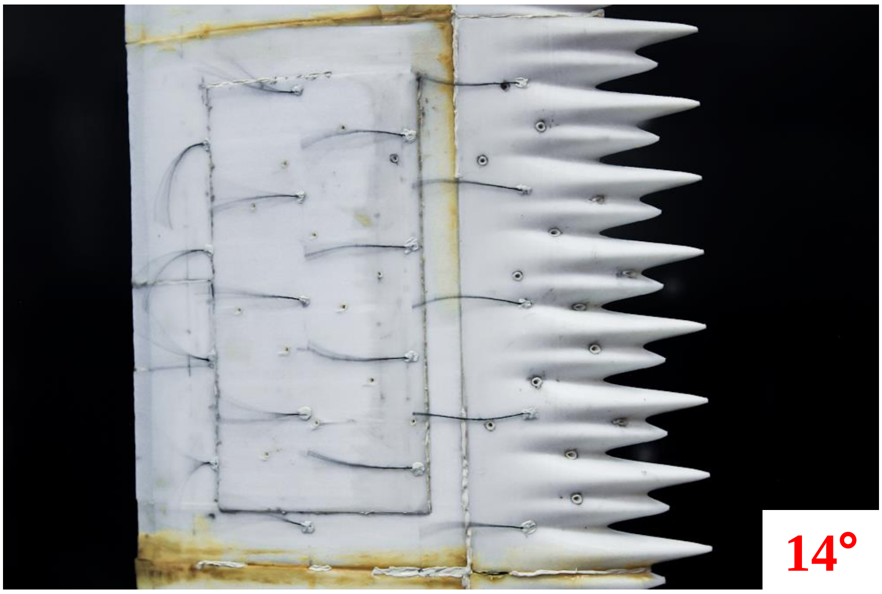

Figure 4.24 : FV of DW2 wing at 14°AoA.

When the angle of attack was 15°,the turbulent intensity increased also in second row of tufts from the LE. In addition, the tufts in the back two rows have rise much more outward from the wing surface in regard to 14°. This situation is shown in Figure 4.25.

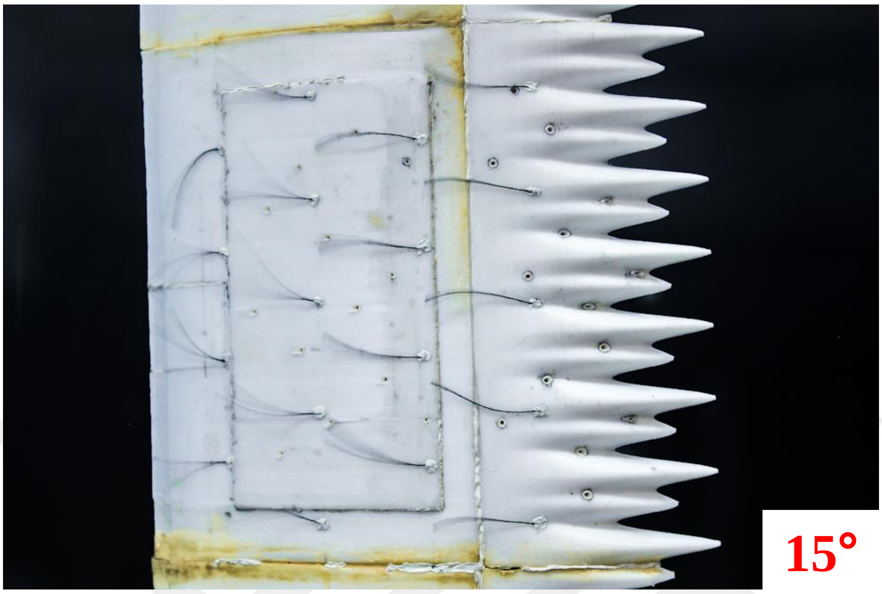

Figure 4.25 : FV of DW2 wing at 15°AoA.

When the angle of attack was 16°, the flow behaves similarly to 15°. Besides, at this angle value, the tufs in the first row have started to become turbulent at tip. At the same time, the tufts, especially in the back row have tended to return. This situation is shown in Figure 4.26.

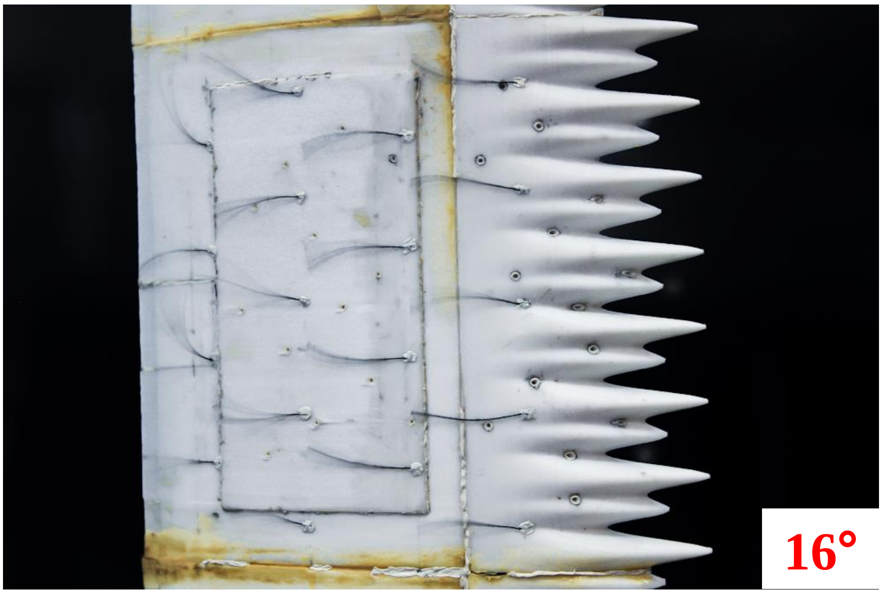

Figure 4.26 : FV of DW2 wing at 16°AoA.

As seen in Figure 4.27, when the angle of attack is 17°, the flow is nearly turbulent everywhere on the wing. In addition, the tufts in the first row tend to remain smooth in the parts close to the attachment point. The tufts in the back three rows have started to rise outward from the wing surface. Even refluctuation in the tufts are observed located approximately 20% of the wing from the TE.

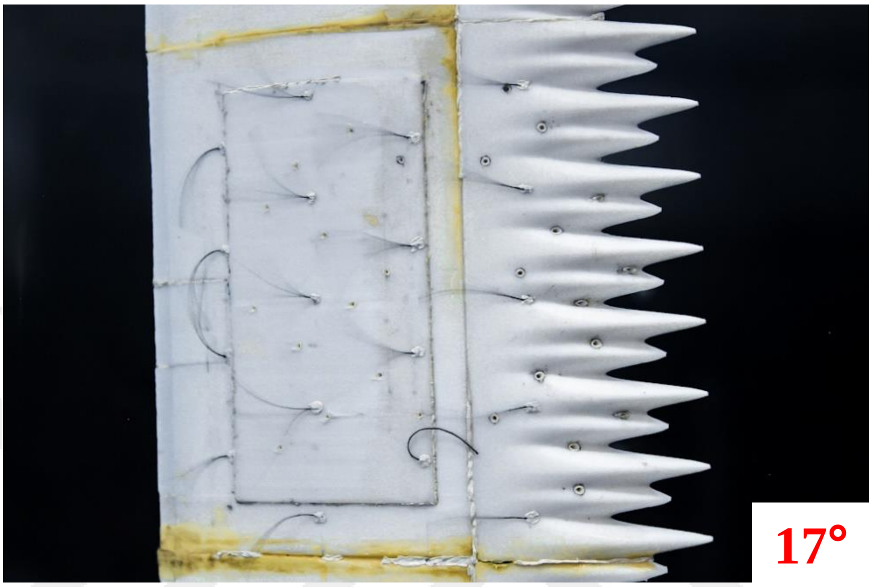

Figure 4.27 : FV of DW2 wing at 17°AoA.

When the angle of attack was 18°, the flow looked similar to 17°, but the instability of the flow within nearly 55% of the wing from the TE and the tuft's return increased. In addition, almost all tufts have rise much more outward from the wing surface as regard to previous angles.This situation is shown in Figure 4.28.

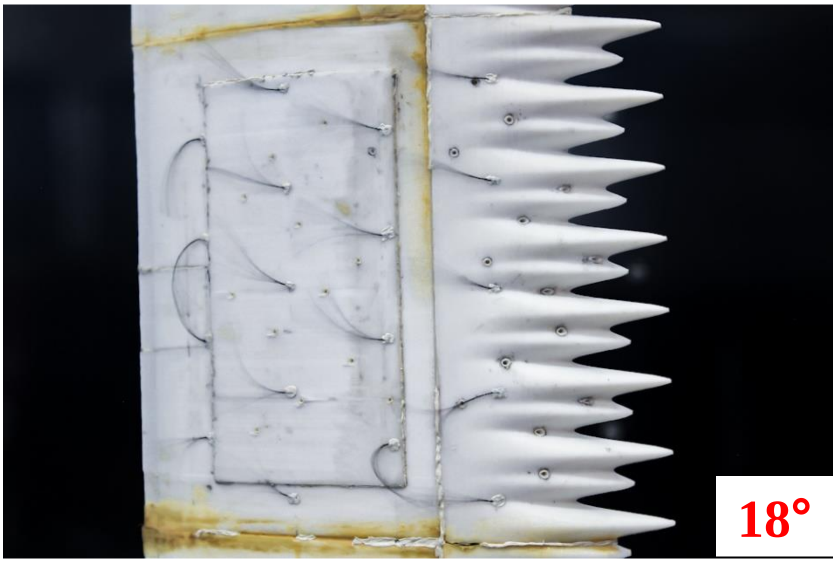

Figure 4.28 : FV of DW2 wing at 18°AoA.

According to the Figure 4.29 taken at 19° angle of attack, it can be said that the flow behaves completely unstable compared to the previous angles. Almost all tufts on the wing tend to return back and rise outward from the wing surface.

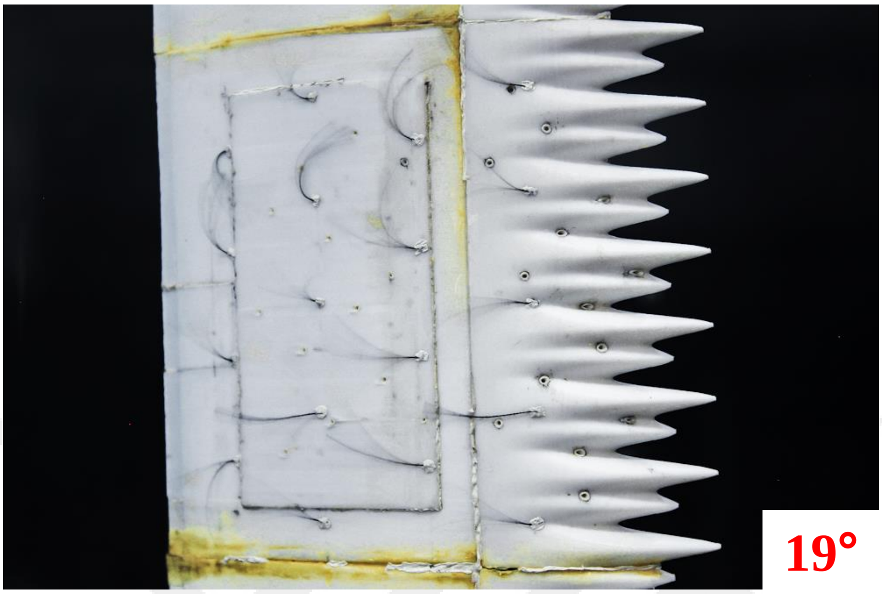

Figure 4.29 : FV of DW2 wing at 19°AoA.

After 19° angle of attack, flow visualization experiments were also carried out for 20°, 22°, 24°, 26° and 28°, respectively. However, when the images obtained in these experiments were examined, it was seen that the flow on the wing was approximately the same as that observed at 19°. In other words, flow behaves completely unstable also for these angles of attack. And, almost all tufts on the wing tend to return back, in fact many of these exactly return and rise outward from the wing surface. For this wing, it can be said that there is a possibility that the wing may have fallen into a stall state, especially after 20°, but this cannot be clearly understood just from the images. According to these images supported by pressure measurements, it can be said that for 24° and beyond, the flow is completely separated and couldn't hold on to the wing again. The images obtained when the angle of attack is 20°,22°,24°,26° and 28° are given in Figure 4.30,.31,.32,.33 and Figure 4.34, respectively.

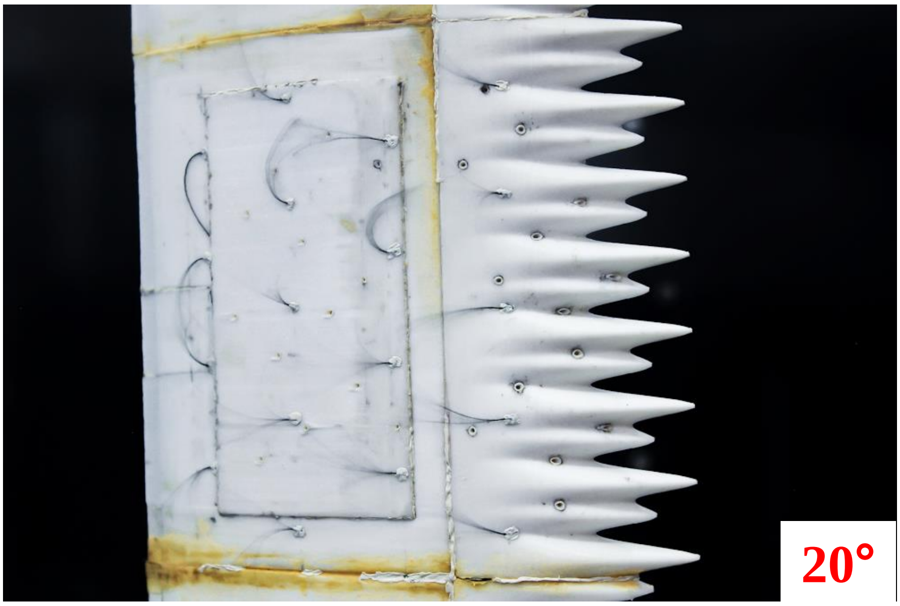

Figure 4.30 : FV of DW2 wing at 20°AoA.

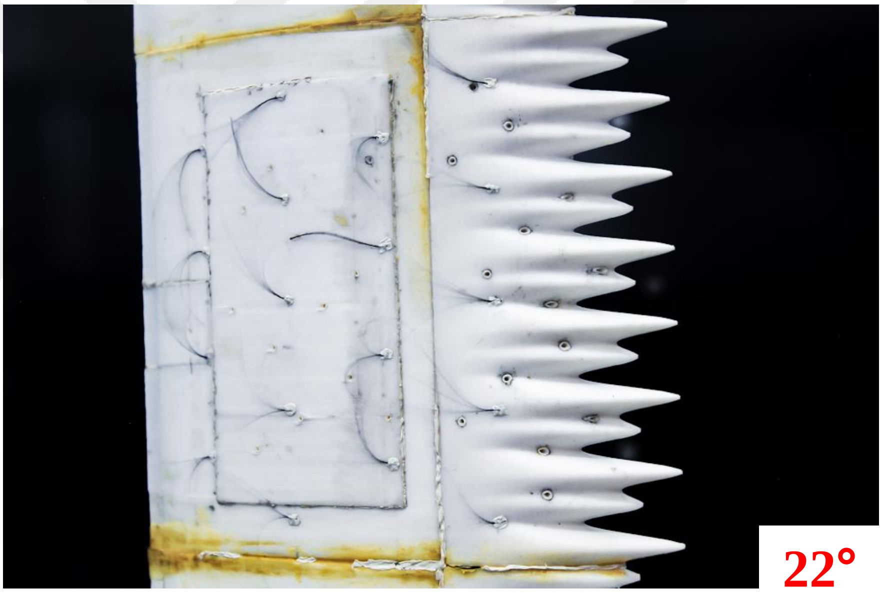

Figure 4.31 : FV of DW2 wing at 22°AoA.

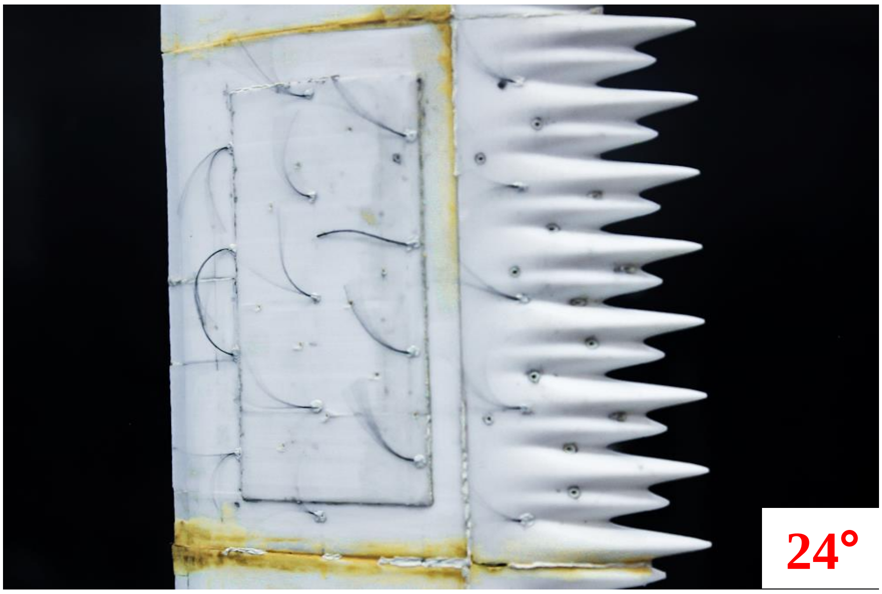

Figure 4.32 : FV of DW2 wing at 24°AoA.

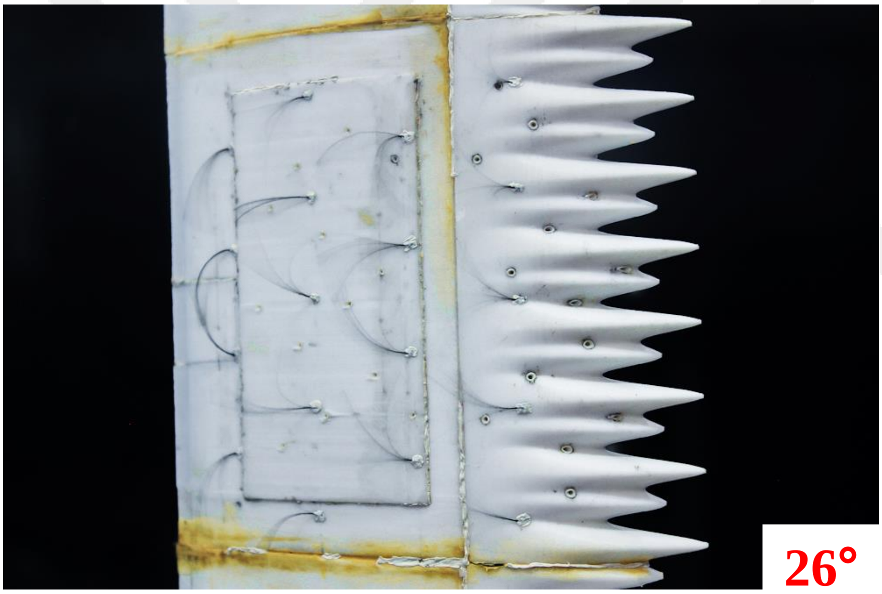

Figure 4.33 : FV of DW2 wing at 26°AoA.

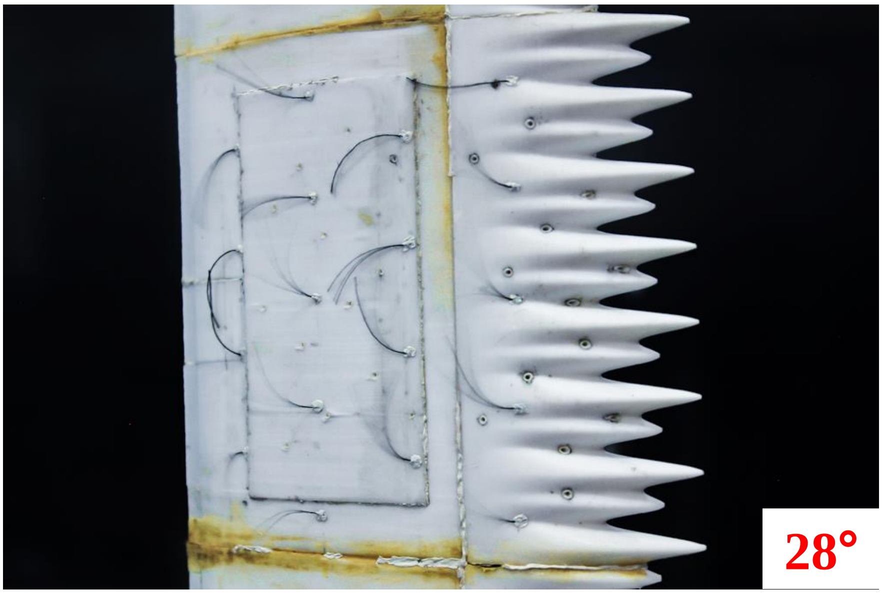

Figure 4.34 : FV of DW2 wing at 28°AoA.

4.2 Pressure Measurements

Pressure measurements were also carried out for a total of three different wings: Baseline, DW1 and DW2. Meanwhile, while there is no different cross-section on the baseline wing, there are two different cross-sections where the pressure taps are placed on the other two double wavelenght wings due to the LE design. In this thesis, these two sections are named A and B. The sketch of the location of the sections is given in Figure 4.35.

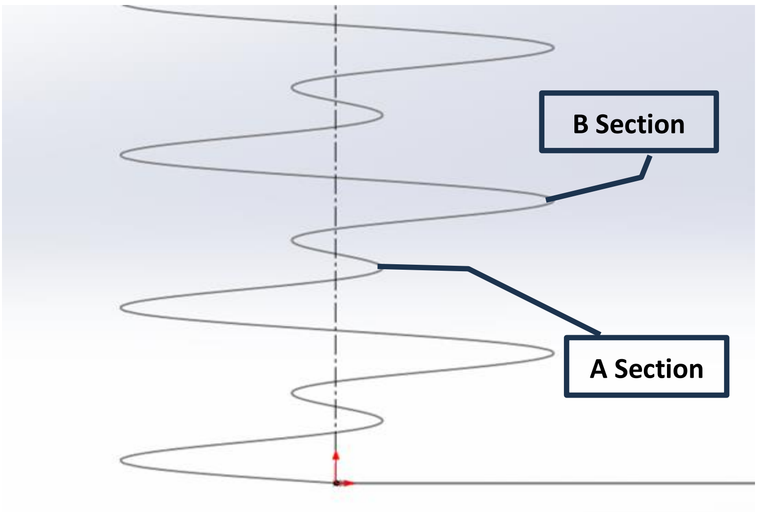

Figure 4.35 : Pressure taps section on DW wing.

The pressure taps placed on the cover on the rear part of the wing remain constant, there are a total of 6 pressure taps for section A and 7 pressure taps for section B. Since there is no section in the baseline wing, any of the values measured in the sections in the rear part of the wing were used, and there are a total of 9 pressure taps in the front part of the wing. For the DW1 wing, there are a total of 8 pressure taps for section A and 3 pressure taps for section B in the front part. On the DW2 wing, there are a total of 9 pressure taps for section A and 7 pressure taps for section B in the front part. In addition to the pressure values measured from the wing, total and static pressure were also measured from the wind tunnel. In this way, the measured pressure values were non-dimensionalized and pressure coefficient was obtained.

$$C_P = \frac{P - P_\infty}{P_0 - P_\infty} \tag{4.1}$$

The P value in equation 4.1 expresses the pressure at the measured point. In addition, P_0 refers to the total pressure measured from the tunnel, while P_∞ refers to the static pressure measured from the tunnel.

In order to compare the experimentally measured data for the baseline wing, the Cp distribution of the NACA65-(12)10 airfoil was derived from the article of Lacagnina et al. [68]. This graph is shown in Figure 4.36.

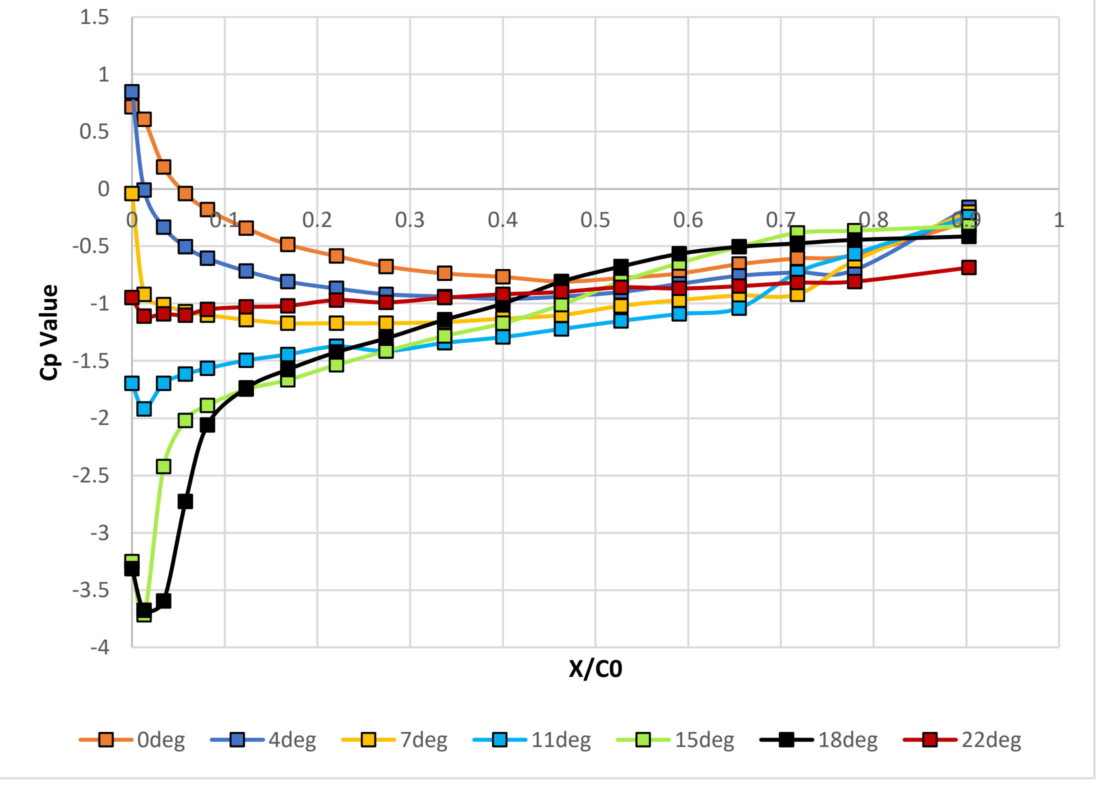

Figure 4.36 : Pressure coeffient of NACA65-(12)10.

4.2.1 Baseline wing

Pressure measurements for the baseline wing were made at 2° intervals from 0° to 20° angles of attack. However, due to the flow visualization results, measurements were also made for the 15°. The Cp distribution graph of the baseline wing is given in Figure 4.37. Looking at the graph , at the leading edge, Cp has a positive value for all angles of attack. While the negative pressure area increased as the angle increased until the angle of attack 15°, it started to decrease as the angle increased after 15°.When the angle is 16 degrees, the area where the negative pressure zone peaks has expanded and its value has decreased compared to the previous angles. If looking at the curves obtained especially at 18° and 20°, it is seen that the Cp value remains almost constant around -1 as moving to towards the rear of the wing. This situation shows that the flow has separated from the wing in those parts and cannot hold on again.

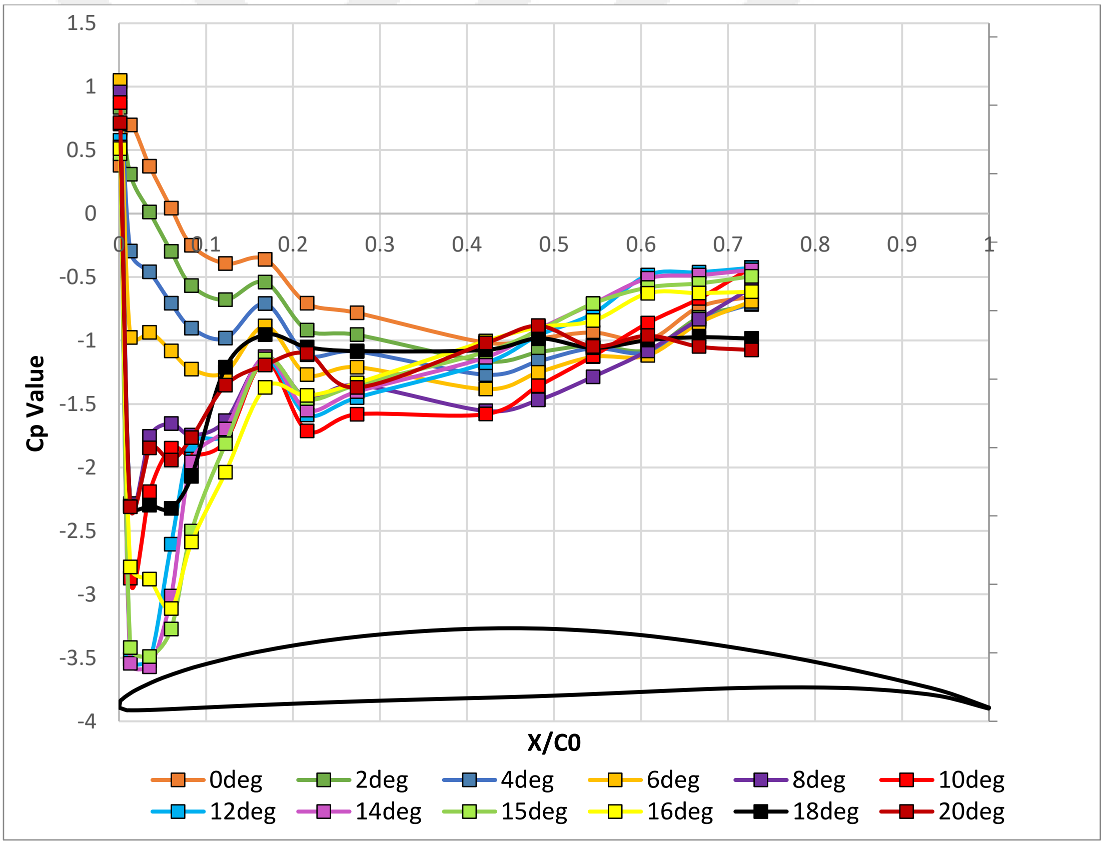

Figure 4.37 : Measured pressure coeffient of baseline wing.

These data obtained from the experiments were compared with the data derived from the article. When comparing, curves with the same or close angle values from both graphs were used. The graph of this comparison is given in Figure 4.38. The data obtained in the experiments at 0°, 4° and 15° angles of attack are similar to the data in the article. In addition, angle values of 6° in the experiments and 7° in the article, which are close to each other, gave similar and close results. However, as mentioned above, Cp values were always measured as positive at the leading edge in the experiments while the values derived from the article started to become negative values after 7° at the leading edge. In addition, the difference between the Cp values, especially in the parts close to the leading edge, is high for the 10 degrees in the experiments and the 11 degrees in the article, which are close to each other in terms of angle. A similar situation exists at values of 18°. According to the values derived from the article, the negative pressure zone reaches its maximum value at 15°. However, while in the experiments there was a decrease in this value after 15°, in the article data it remained around the average maximum value even at 18°.

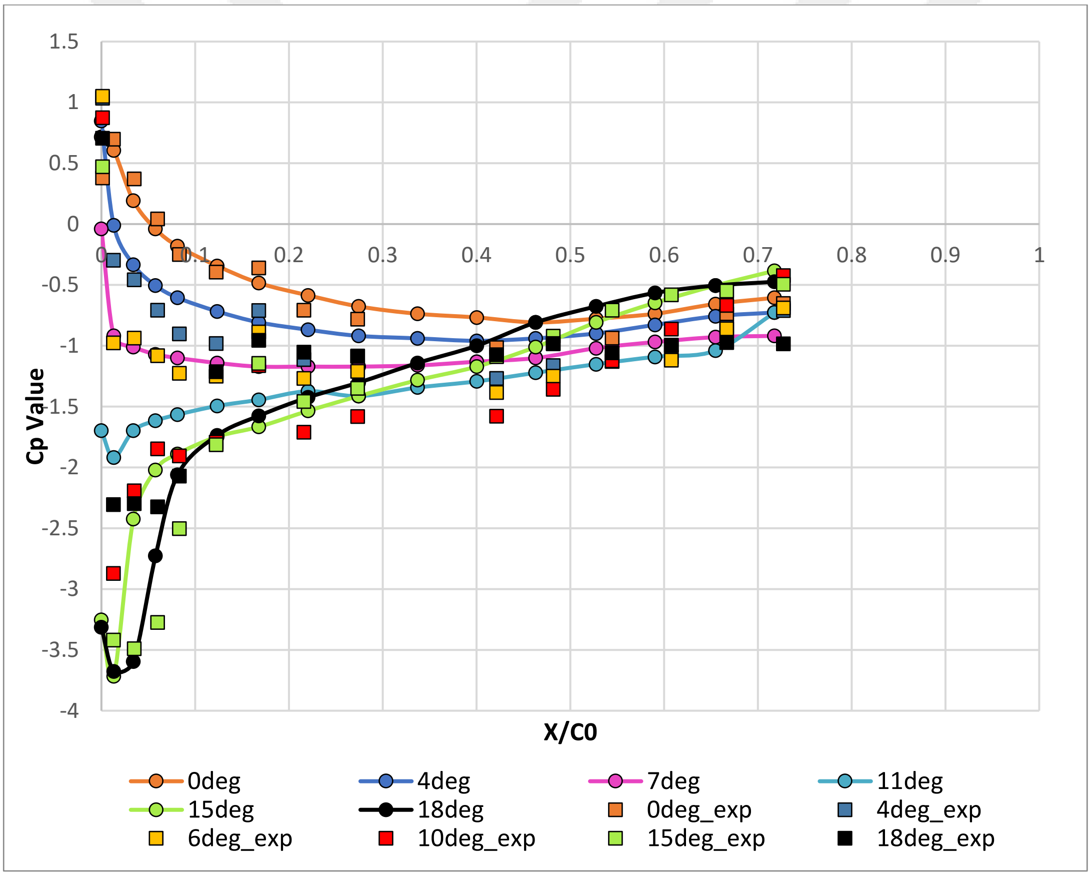

Figure 4.38 : Comparisons of pressure coeffient for baseline wing.

Besides, according to the referred article, it is mentioned that the separation on the wing reaches 90% distance from the TE between 11° and 15° of attack angle go by Cp graph. Therefore, using the pressure measurements and flow visualization results, it can be said that for the baseline wing, the separations in the flow shifted towards the

LE as of 15°, and especially as of 18°, the flow was completely separated and could not re-attach to the wing.

4.2.2 DW1 wing

Pressure measurements for the baseline wing were made at 2° intervals from 0° to 28° angles of attack. It has been mentioned before that there are two sections on this wing due to the double wavelength design at the leading edge. Figure 4.39 shows the measurements in section A, which has less amplitude. When looking at the Cp graph obtained for section A, the first situation that attract the attention is that the curves, especially in the area up to 18°, show that firstly decreases and then increases again in the range of 0.1 to 0.3 of X/C0.

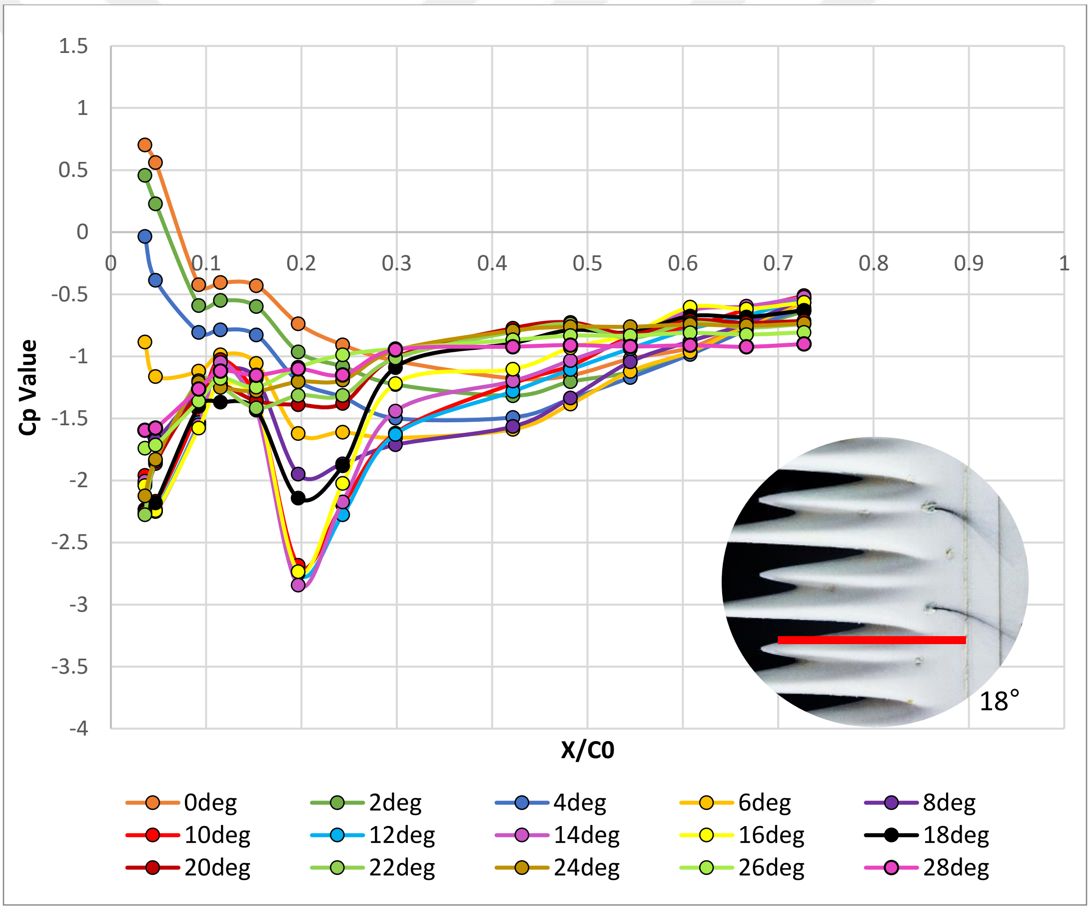

Figure 4.39 : Measured pressure coeffient of DW1 wing at Asection.

Considering the flow visualization results, it can be said that the flow in this section starts laminar and continues turbulent. A zoomed image to LE for 18° has been added in the lower right corner of the graph and the red line shows the range from 0.1 to 0.3. Therefore, it is thought that this second peak observed in the graphs may be caused by the separation bubble. Because it is similar to the Cp distribution graphs in the separation bubble situation that have been researched in the literature. As an example, Figure 4.40 shows the graph of the separation bubble situation taken from the study of Li et al. [78].

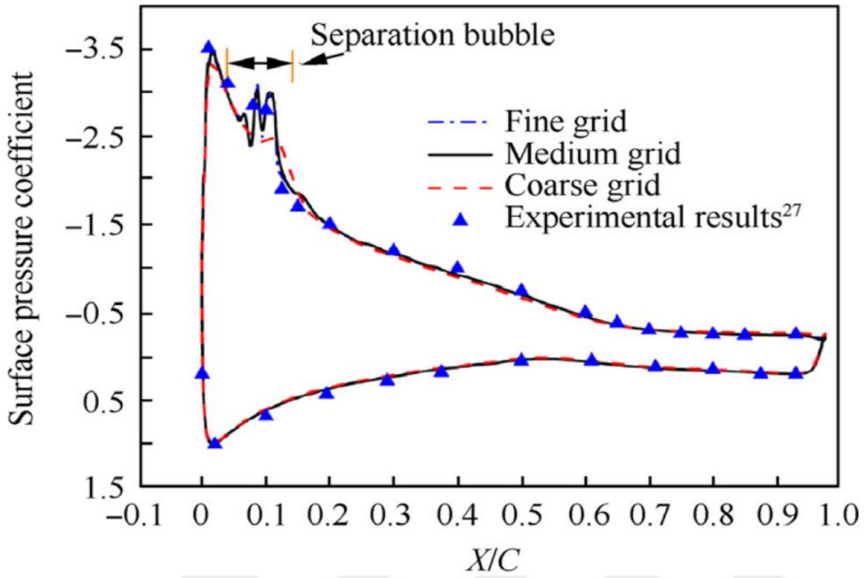

Figure 4.40 : Pressure coefficient at a situation of seperation bubble [78].

For this part of the A section Cp graph, which is thought to be caused by the separation bubble situation, it can be said that the flow separates from the wing, attach to the wing again and then continues in a turbulently. However, with an angle of attack of 20°, it is clearly seen that the Cp value remains almost constant, that is, the curve started to become flat and around -1 as moving forward from the LE. This is a sign that the flow in the wing has completely separated and could not be reattach to the wing.

Figure 4.41 shows the measurements in section B. The separation bubble condition could not observed in the pressure measurements obtained for section B. Because, due to design problems, pressure measurements could not start from the leading edge, especially for the B section. But, the other cases mentioned for section A, these were also observed for section B. In other words, also for section B, especially after the 20° angle of attack, the Cp curves started to become flat, that is, to take a constant value around -1.

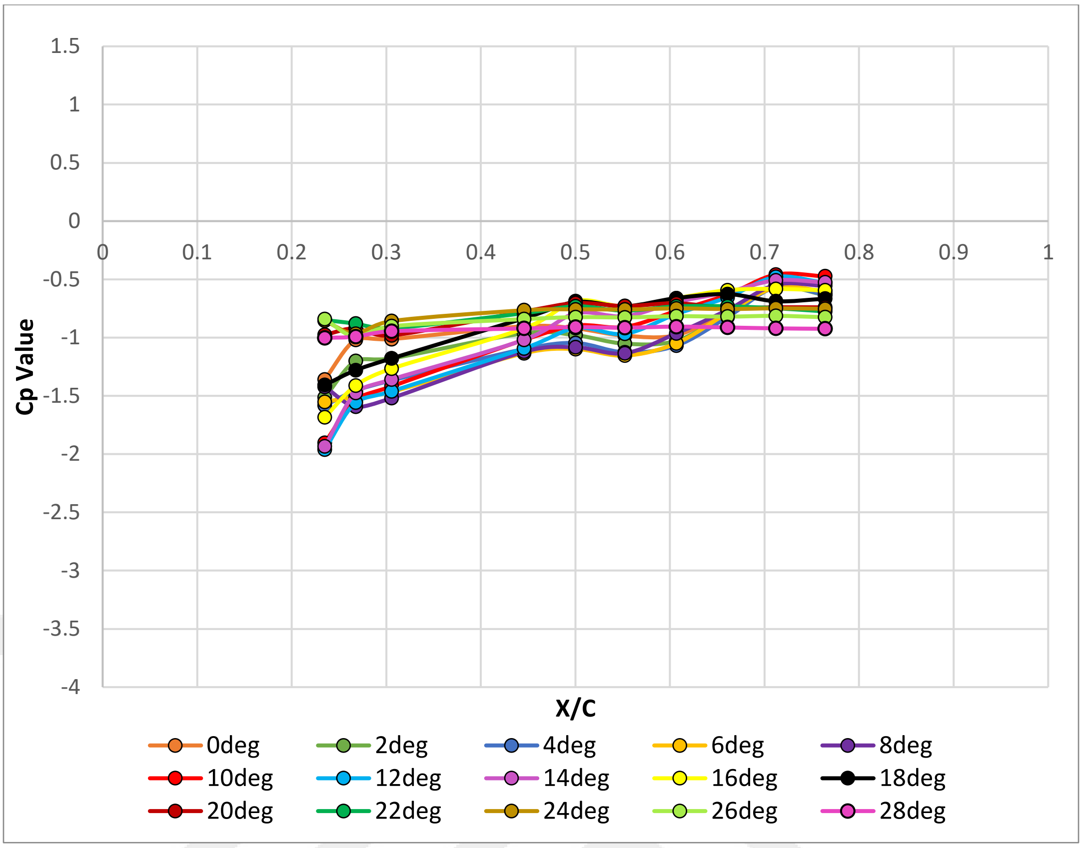

Figure 4.41 : Measured pressure coeffient of DW1 wing at B section.

In addition, the maximum negative pressure value at 14° for both A and B sections, therefore, for the entire DW1 wing. To summarize, using the pressure measurements and flow visualization results, it can be said that for the DW1 wing, the separations in the flow shifted towards the LE as of 18°, and especially as of 20°, the flow was completely separated and could not re-attach to the wing.

4.2.3 DW2 wing

Pressure measurements for the baseline wing were made at 2° intervals from 0° to 28° angles of attack. However, due to the flow visualization results, measurements were also made for the angles 15°,17° and 19°. As in DW1 wing, Cp graph for this wing were obtained according to two different sections, A and B. The graph obtained for section A is given in Figure 4.42. When the graph is examined,the first situation that stand out in this wing is that there is a second peak at negative Cp values again. Looking at the flow visualization results, until the angle of attack of 18°, it can be said that the flow in this section starts laminar and continues turbulent. Therefore, it is again thought that there is a separation bubble situation for the area up to this angle value.

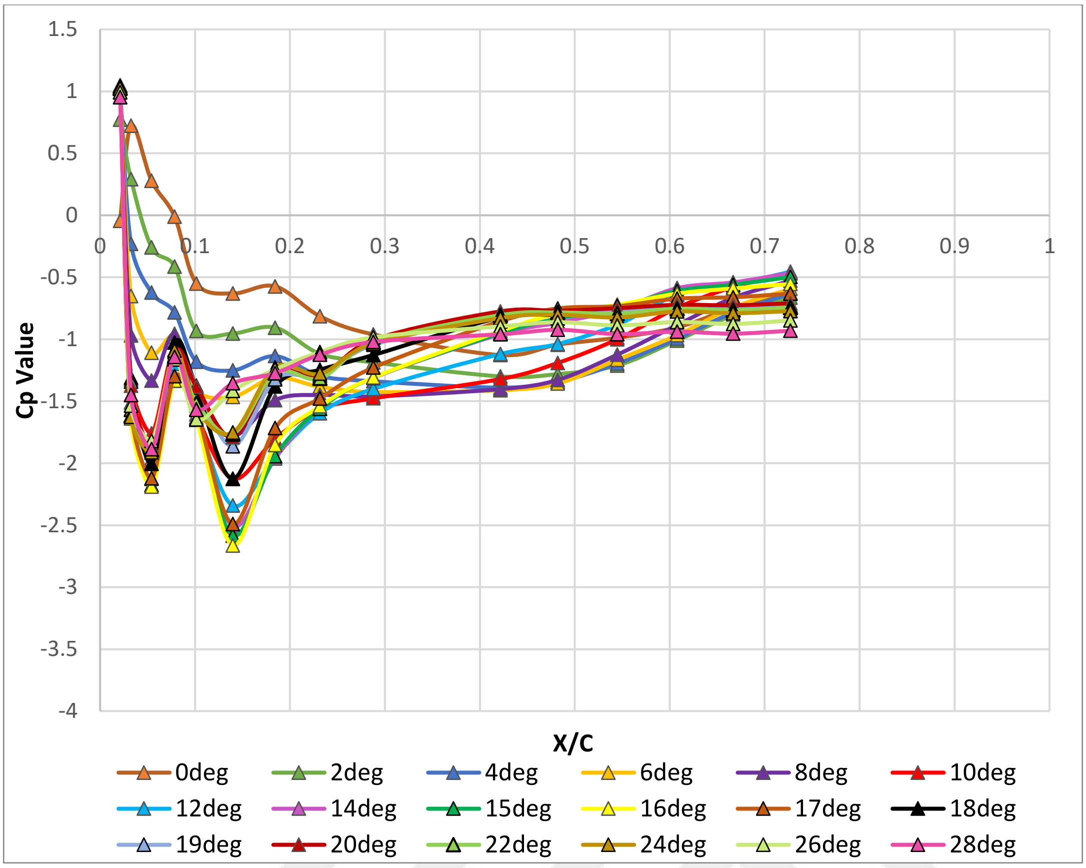

Figure 4.42 : Measured pressure coeffient of DW2 wing at A section.

For this part of the A section Cp graph, which is thought to be caused by the separation bubble situation, it can be said that the flow separates from the wing, attach to the wing again and then continues in a turbulently. In addition, the maximum negative pressure value at 16° for A section. As can be clearly seen in the graph, this value have started to decrease after that degree. Besides, with an angle of attack of 24°, it is clearly seen that the Cp value remains almost constant and around -1 as moving forward from the LE. This is a sign that after the 24° the flow in the wing has completely separated and could not be reattach to the wing.

Figure 4.43 shows the measurements in section B. The separation bubble condition could not observed in the pressure measurements obtained for section B. In addition to this, the maximum negative pressure value at 12° for B section. However, the maximum value of negative pressure, until the 16°, remained around this maximum value on average. By the way, the other case mentioned for section A, these were also observed for section B. In other words, also for section B, especially after the 24° angle of attack, the Cp curves started to become flat, that is, to take a constant value around -1.

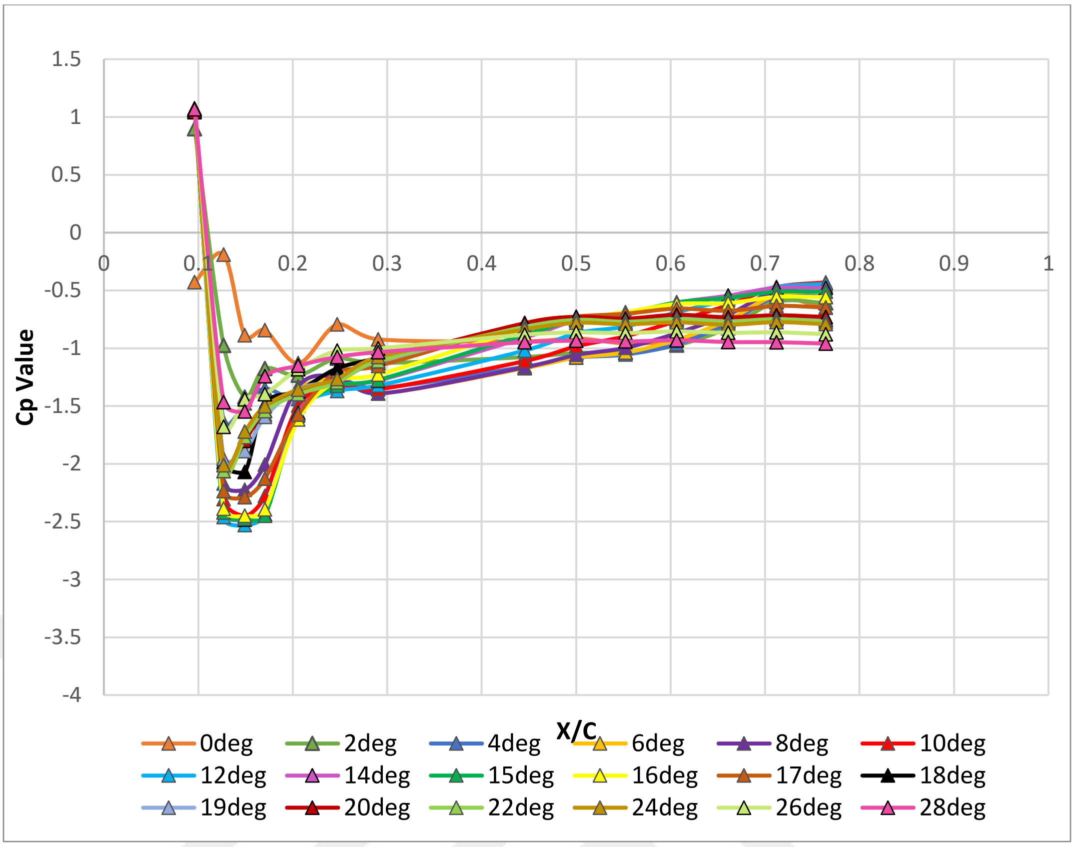

Figure 4.43 : Measured pressure coeffient of DW2 wing at B section.

To summarize, using the pressure measurements and flow visualization results, it can be said that for the DW2 wing, the separations in the flow shifted towards the LE as of 18°, and especially as of 24°, the flow was completely separated and could not re-attach to the wing.

4.3 Comparisons

As a result of the flow visualization and pressure measurement experiments performed for each wing, comments can be made about the aerodynamic performance of the wings within themselves and against to each other. In the pressure measurement section, each wing was examined separately. To better compare the wings each other, forces perpendicular to the flow and parallel to the flow were calculated using the pressure coefficients obtained as a result of the experiments carried out within a certain angle of attack range. In this way, the contribution of the pressure coefficient to the lift and drag forces was found. However, due to the double wavelenght LE design, these graphics are also divided into A section and B section. Since there is no A and B section in the baseline wing, the same values are valid in all cases. Cpl and Cpd graphs from Figure 4.44 to Figure 4.54 are the graphs obtained for section A. In addition, in these graphs, instead of using all the angle values observed in the experiments, angles that provide more comparable information for the wings were selected.

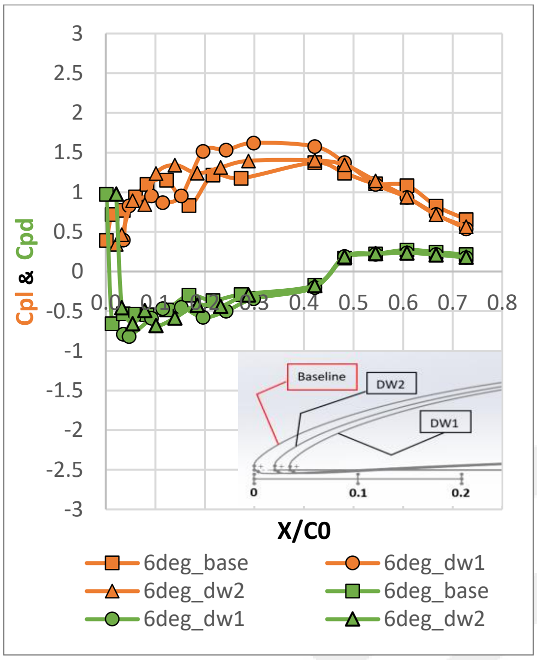

Figure 4.44 : Calculated *Cpl* and *Cpd* at A section for 6°AoA.

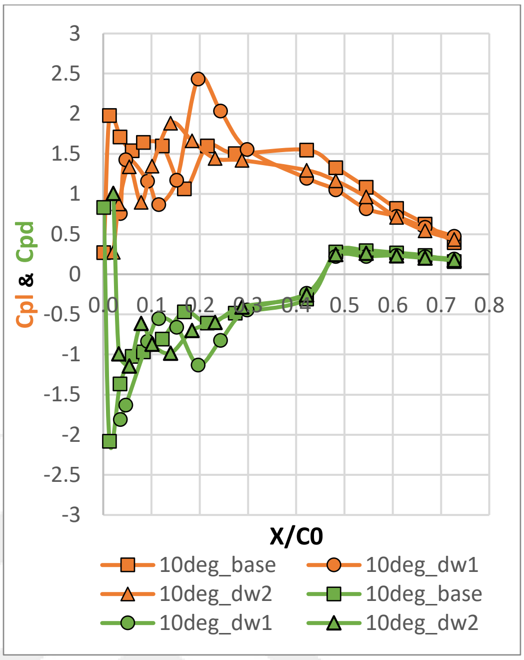

Figure 4.46 : Calculated *Cpl* and *Cpd* at A section for 10°AoA.

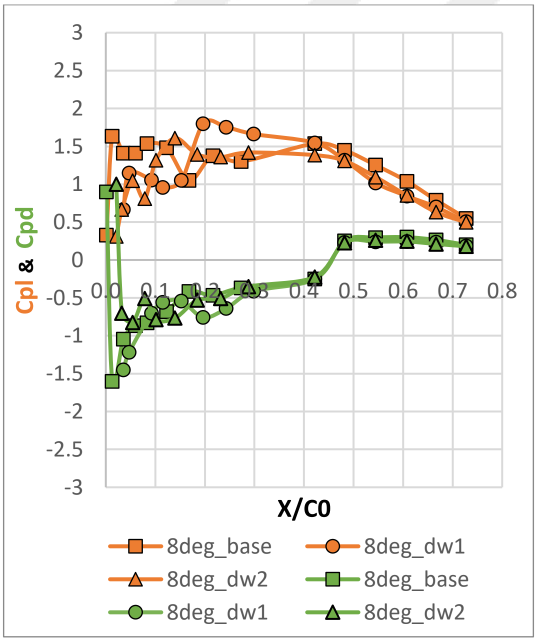

Figure 4.45 : Calculated *Cpl* and *Cpd* at A section for 8°AoA.

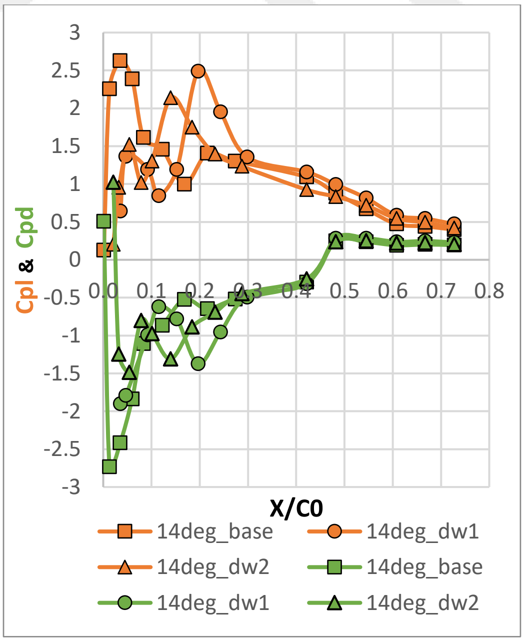

Figure 4.47 : Calculated *Cpl* and *Cpd* at A section for 14°AoA.

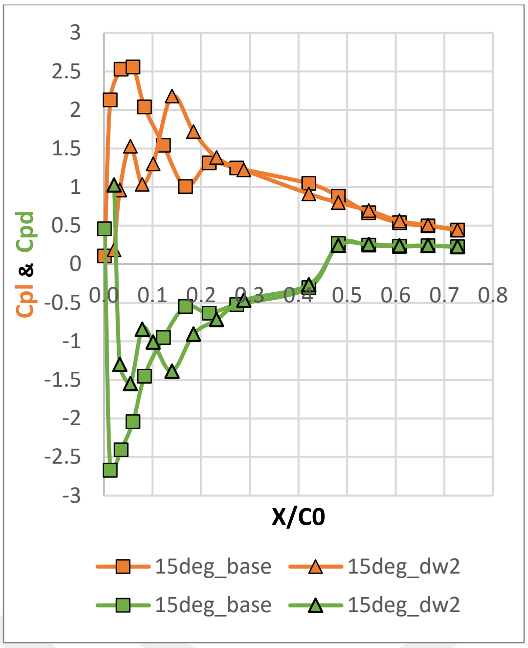

Figure 4.48 : Calculated *Cpl* and *Cpd* at A section for 15°AoA.

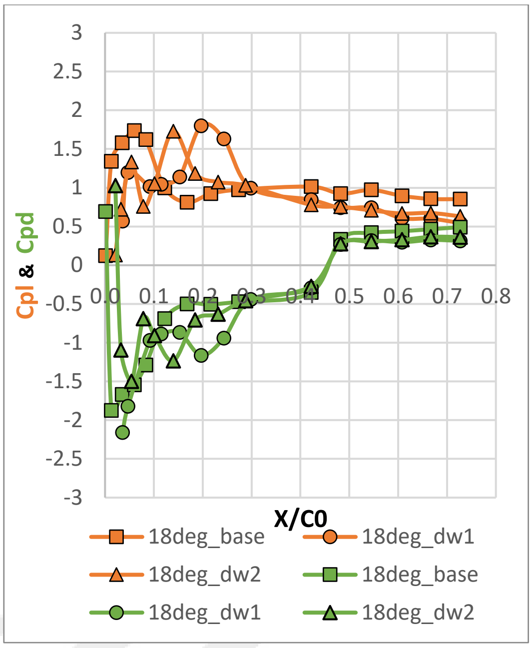

Figure 4.50 : Calculated *Cpl* and *Cpd* at A section for 18°AoA.

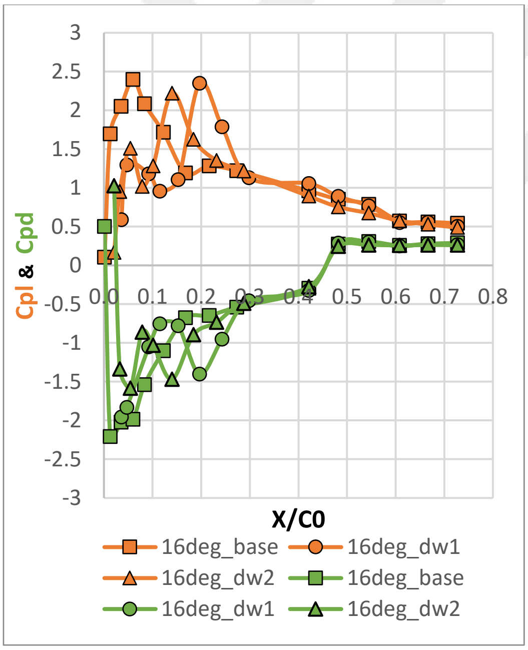

Figure 4.49 : Calculated *Cpl* and *Cpd* at A section for 16°AoA.

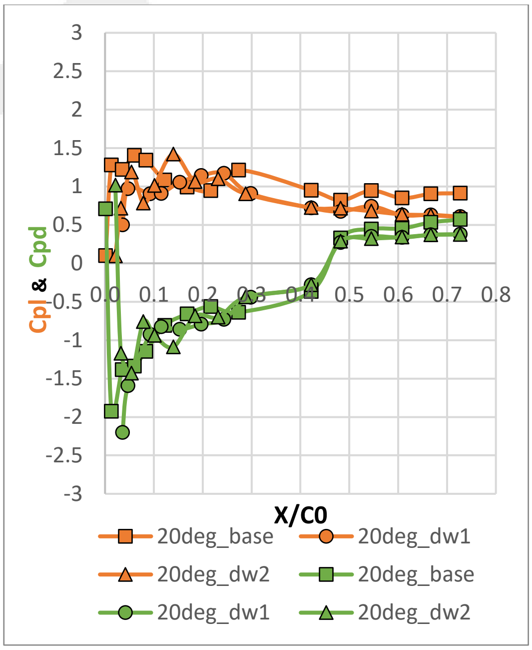

Figure 4.51 : Calculated *Cpl* and *Cpd* at A section for 20°AoA.

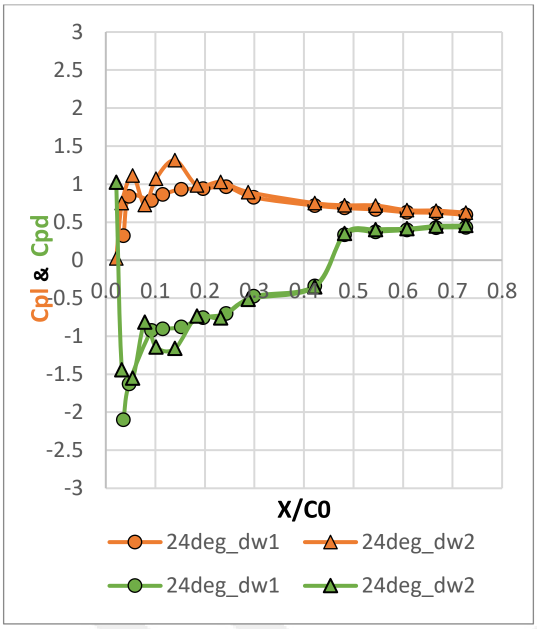

Figure 4.52 : Calculated Cpl and Cpd at A section for 24°AoA.

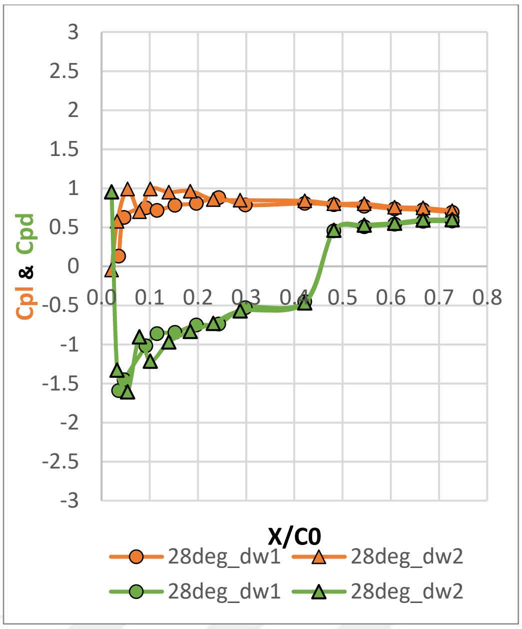

Figure 4.54 : Calculated Cpl and Cpd at A section for 28°AoA.

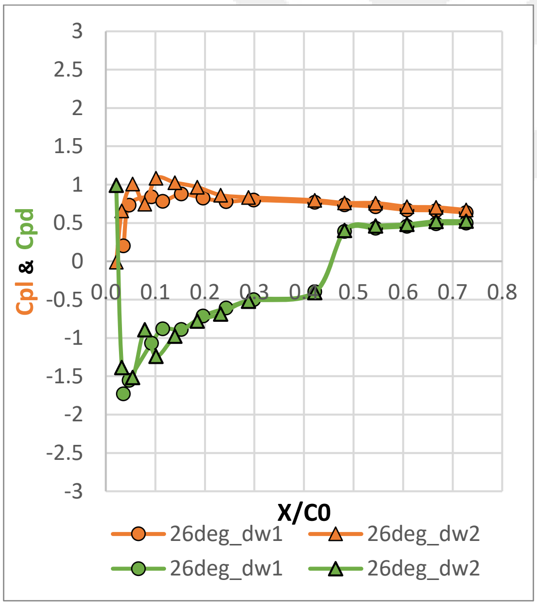

Figure 4.53 : Calculated Cpl and Cpd at A section for 26°AoA.

When the graphs given for section A are examined, as the angle of attack increases up to 15° on all wings, both the Cpl and Cpd values increase. Cpl increases positively and Cpd increases negatively. After 15°, it starts to decrease. However, it was observed that the decrease in Cpd values was lower rate than the decrease in Cpl values. The appearance of peaks in the graphs begins especially after 10° of angle of attack. While the maximum values of Cpl for the baseline wing are much closer to the LE, these maximum values for the DW1 and DW2 wings are slightly behind the LE. It approximately corresponds to the range of 0-0.1 of X/C0 for baseline, the range of 0.2-0.3 of X/C0 for DW1, and the range of 0.1-0.2 of X/C0 for DW2. In addition, as moving towards the back of the wing, especially after the maximum thickness of the wing, that is, from the value of 0.4 of X/C0, the value of the curves have almost the same in all wings. After 20° angle of attack, there was almost no change in the Cpl and Cpd curves for the DW1 wing. Additionally, the peaks in the curves have disappeared. It was observed that this situation occurred later in the DW2 wing. In this wing, after 24°, the change in the curves was almost negligible and the peak points of the curves disappeared.

Cpl and Cpd graphs from Figure 4.55 to Figure 4.65 are the graphs obtained for section B.

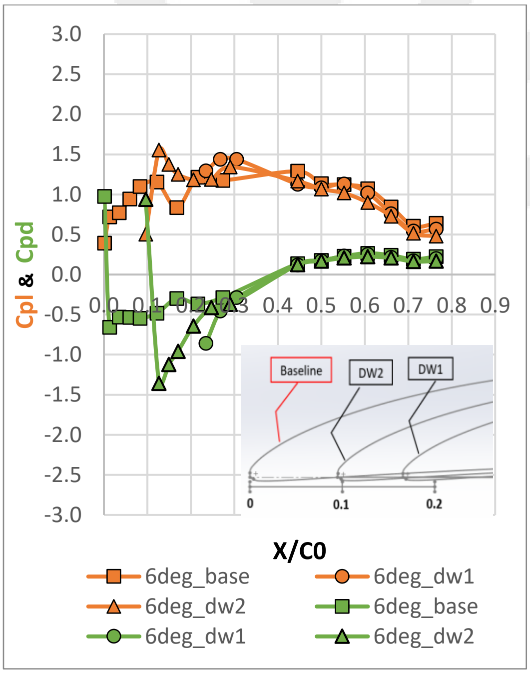

Figure 4.55 : Calculated Cpl and Cpd at B section for 6°AoA.

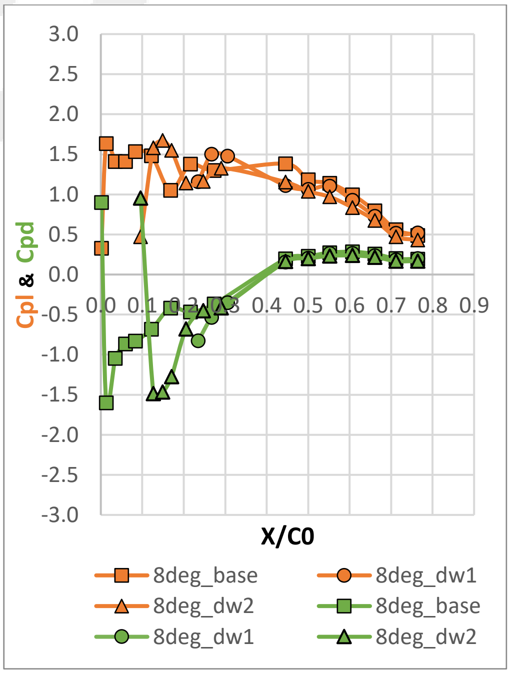

Figure 4.56 : Calculated Cpl and Cpd at B section for 8°AoA.

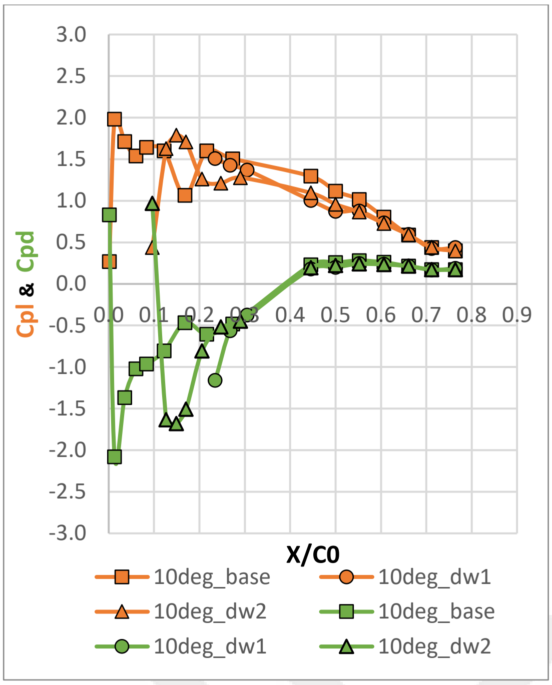

Figure 4.57 : Calculated *Cpl* and *Cpd* at B section for 10°AoA.

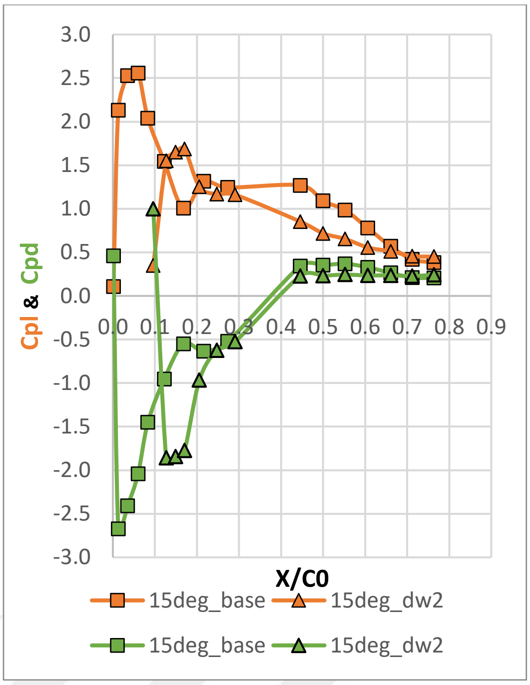

Figure 4.59 : Calculated *Cpl* and *Cpd* at B section for 15°AoA.

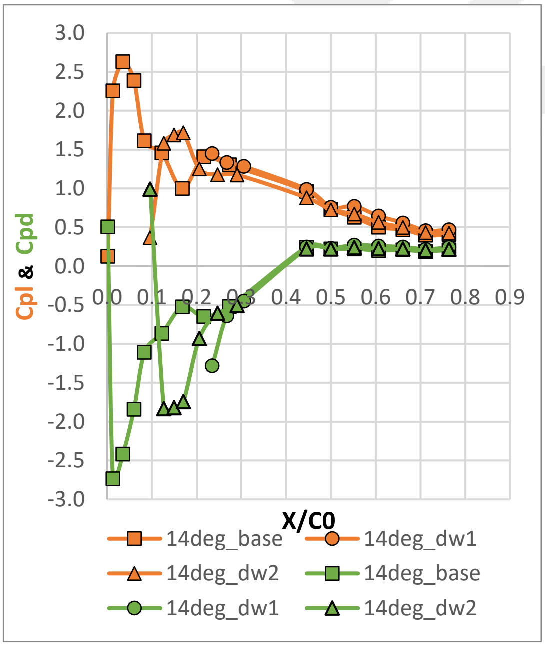

Figure 4.58 : Calculated *Cpl* and *Cpd* at B section for 14°AoA.

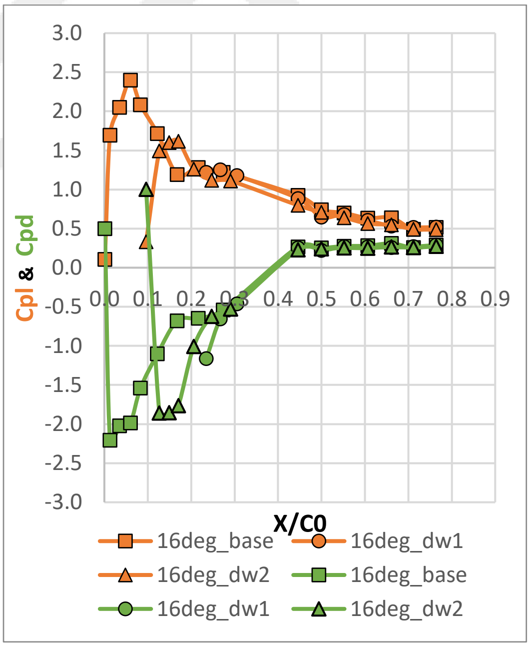

Figure 4.60 : Calculated *Cpl* and *Cpd* at B section for 16°AoA.

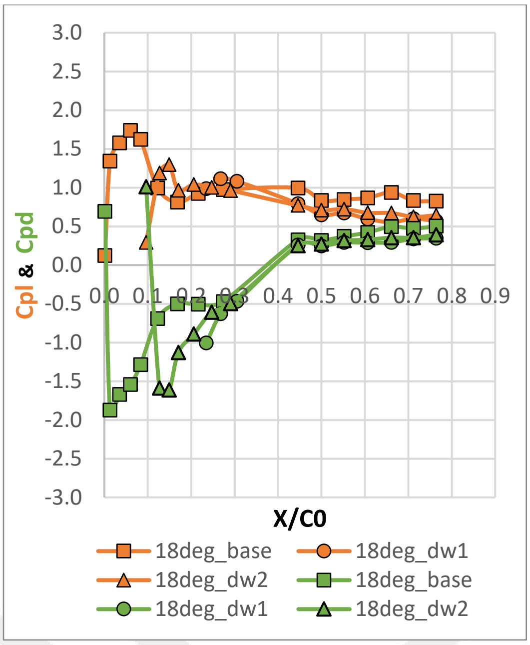

Figure 4.61 : Calculated Cpl and Cpd at B section for 18°AoA.

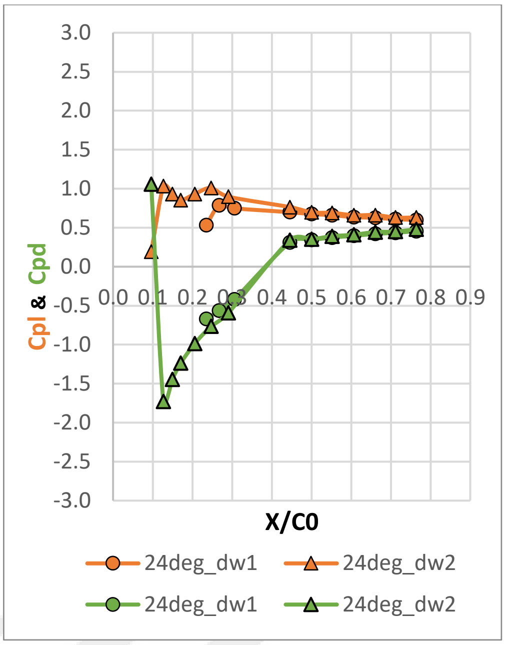

Figure 4.63 : Calculated Cpl and Cpd at B section for 24°AoA.

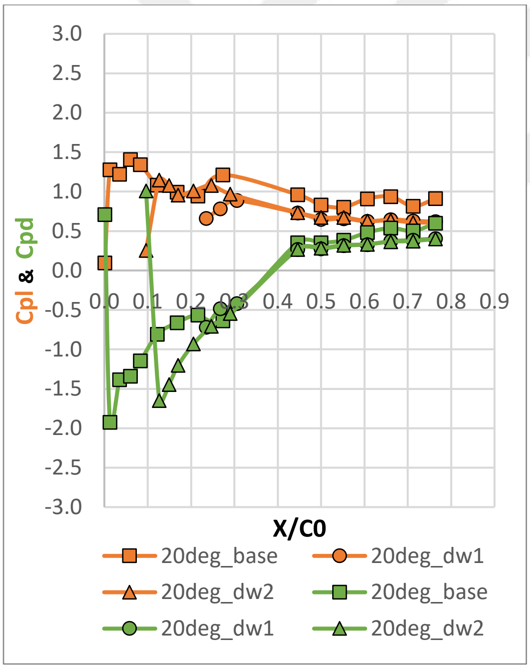

Figure 4.62 : Calculated Cpl and Cpd at B section for 20°AoA.

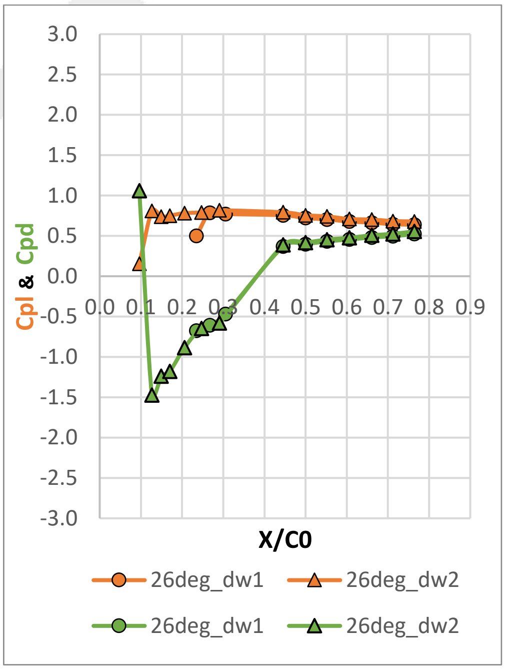

Figure 4.64 : Calculated Cpl and Cpd at B section for 26°AoA.

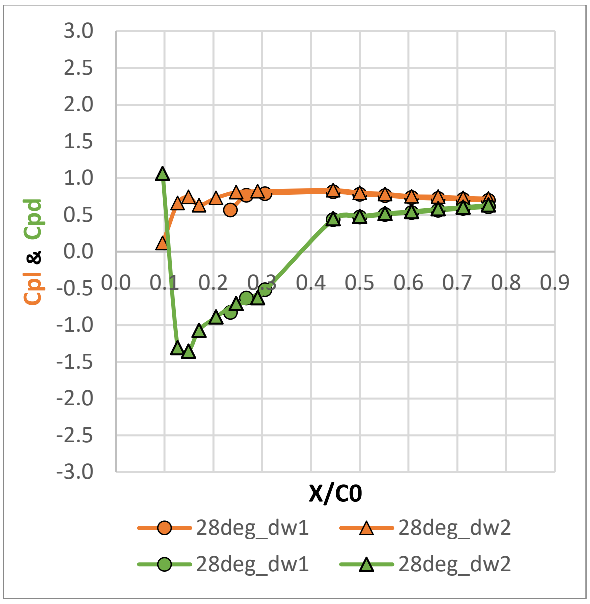

Figure 4.65 : Calculated Cpl and Cpd at B section for 28°AoA.

There is no obvious difference between the graphs of sections A and B. However, due to the LE design, the position of the pressure values measured in the B section is further behind than those in the baseline wing, so it is not possible to talk clearly about the peak points in this section. Although there is no change in the baseline wing in terms of peak point, the peak point is observed in the same position for DW2 and this value is lower than in section A. But in general, as in section A, Cpl and Cpd values in section B increased until the angle of attack of 15° and started to decrease after this degree. The decrease in Cpl values is slightly higher than the Cpd value. Same as A section, after 20° angle of attack, there was almost no change in the Cpl and Cpd curves for the DW1 wing. Additionally, the Cpl curve was almost flat in the horizontal position. It was observed that this situation occurred later in the DW2 wing. In this wing, after 24°, the change in the curves was almost negligible and the peak points of the curves disappeared especially for Cpl curve.

As a result of all these, it can be interpreted that DW1 and DW2 wings can resist higher angles of attack than the baseline wing. Among the wings with double wavelenght leading edge, it can be said that the resistance of the DW2 wing to the angle of attack may be slightly higher than that of the DW1 wing. In this case, it is inferred that the one with less amplitude in terms of $2a$ value may have better resistance to high angles of attack.

5. CONCLUSIONS AND RECOMMENDATIONS

In this study, focused on wings with double wavelenght design at the leading edge, which is one of the passive methods of noise reduction in wings. Since only noise studies have been done in the literature on wings with this design, it was planned to contribute to the aerodynamic deficiency within the scope of this thesis. For this, the study of Chaitanya et al., which is an example of noise study, was taken as a reference and the wing designs were made in this. In total, two wings with different amplitudes were produced. Only the amplitudes of these wings and the 2a values that vary depending on the amplitude are different from each other. Same design parameters of these manufactured parts are wavelengths are $\lambda_1/c_0 = 0.067,\ \lambda_2/c_0 = 0.13$ and the phase difference is zero. All expressions are non-dimensionalized with mean chord. The spanwise distance between adjacent roots was, $\lambda/c_0 = 0.059$. The different design parameters of these manufactured parts are amplitudes are $h_1/c_0 = h_2/c_0 = 0.094$ for DW1 wing and $h_1/c_0 = h_2/c_0 = 0.054$ for DW2 wing. The total peak-to-root distance of the double wavelength formed by summing two waves with these values were $2a/c_0 = 0.33$, $2a/c_0 = 0.19$, and the streamwise distances between adjacent roots were $h/c_0 = 0.13$, $h/c_0 = 0.0752$, for DW1 and DW2 wings, respectively. In addition, in order to understand the effect of the design on the wings, a baseline wing was also produced.

During the experiments carried out within the scope of the thesis, a subsonic, open circuit wind tunnel located in the ITU Trisonic Research Laboratory was used. Experiments were performed for flow visualization and pressure measurement separately for each wing. All experiments were effected at a speed of 20m/s. In addition, flow visualization experiments were performed from 6 to 28° angle of attack, and pressure measurements were made from 0 to 28°angle of attack.

In line with the results obtained from both flow visualization and pressure measurements, the angles at which the wings fall into a stall state were determined and information about their aerodynamic performance was obtained. Accordingly, for the baseline wing, as of the 15° angle of attack, the flow separation on the wing spreads almost to the entire wing. Considering the graphics and photographs, it is possible to say that, especially from 18° , the flow on the wing completely separated and could not attach to the wing again. Since there are two different roots in wings with a double wavelength leading edge design, there are two different sections where pressure measurements are made.These are expressed as section A and section B. Considering the results obtained, the difference between the two sections is not much, but the peak values in the graphs are lower in section B than in section A. According to the pressure and photograph results obtained for the DW1 wing, it was observed that the flow on the wing, as of the 18° angle of attack, the flow separation on the wing spreads almost to the entire wing and it was completely separated from the 20° angle of attack and could not hold on to the wing again. When looking at the DW2 wing, it is observed that the angle of attack value is 24°, situation where the flow on the wing completely separates from the wing and cannot reattach to the wing. In addition, components perpendicular to the flow and parallel to the flow were calculated using pressure coefficients. The component perpendicular to the flow is called Cpl, and the component parallel to the flow is called Cpd. The graphs drawn according to these calculated data show the situations mentioned above for each wing more clearly.

If we summarize the results of the studies carried out within the scope of the thesis, DW1 and DW2 wings, which have a double wavelenght shaped LE design, were resisted higher angles of attack better than the baseline wing. This is an indication that such a change in the leading edge design may have had an effect on increasing the aerodynamic performance of the wing. When looking at the situation between DW1 and DW2 wings, it can be said that the DW2 wing endures better than DW1 at high angle of attack. In other words, it can be deduced that the aerodynamic performance of the wing with a smaller value in terms of total amplitude $2a$ may be better.

Within the scope of this thesis, experiments were carried out considering the upper surface of the wing. If pressure is measured on the lower surface of the wing, the total lift and drag forces acting on the wing can be calculated. These measurements can be made to improve the study carried out here. In this way, the aerodynamic performance criterion can be seen more clearly between wings with double wavelength leading edge design. If necessary after these are done, experiments can be carried out for a design that will either fall between the $2a$ values of these two wings or have a lower value than these values.

REFERENCES

[1] **European Environment Agency** (2020). Environmental noise in Europe, *EEA Report*.

[2] **European Commission** (2011). Flightpath 2050 Europe's Vision for Aviation, *Report of the High Level Group on Aviation Research*.

[3] **Deshmukh, S., Bhattacharya, S., Jain, A. and Paul, A. R.** (2018).Wind Turbine Noise and its Mitigation Techniques : A Review, *2nd International Conference on Energy and Power (ICEP2018)*, 13-15 December, Sydney, Australia

[4] **Zamponi, R., Suresh, T., Teruna, C. and Bampanis, G.** (2020). Aerodynamic Noise Reduction with Flow Control Devices, *SA Public Workshop*, 26 November.

[5] **Brooks, T. F., Pope, D. S. and Marcolini, M. A.** (1989). Airfoil Self-Noise and Prediction, *NASA*, July.

[6] **Krusz, W.** (2017). Passive methods for airfoil noise reduction, 13 January.

[7] **Dassen, T., Parchen R., Guidati, G. And Wagner, S.** (1997). Comparison of measured and predicted airfoil self-noise with application to wind turbine noise reduction, *the European Wind Energy Conference & Exhibition*, 6-9 October, Dublin.

[8] **Yang, S. J.** (2019). Drag and Noise Reduction of Flatback Airfoil by Span-Wise Wavy Trailing Edge (Doctoral dissertation)

[9] **Bushnell, D. M. and Wygnanski, I.** (2020). Flow Control Applications, *National Aeronautics and Space Administration (NASA)*, January.

[10] **Ashill, P. R., Fulker, J. L. and Hackett, H. C.** (2005). A review of recent developments in flow control, *The Aeronautical Journal*, May.

[11] **Szoke, M., Elsahhar, W. and Azarpeyvand, M.** (2016). Aerodynamic Noise Reduction Using Active Flow Control Techniques, October.

[12] **Szoke, M. and Azarpeyvand, M.** (2017). Active Flow Control Methods for the Reduction of Trailing Edge Noise, *In 23rd AIAA/CEAS Aeroacoustics Conference [AIAA 2017-3004]* American Institute of Aeronautics and Astronautics Inc. (AIAA).

[13] **Akkermans, R. A. D., Stuermer, A. and Delfs, J. W.** (2016). Active Flow Control for Interaction Noise Reduction of Contra-Rotating Open Rotors, *American Institute of Aeronautics and Astronautics, Inc.* (AIAA), 5 January.

[14] **Atkin, C. and Wahlich, M.** (2016). Active Flow Loads & Noise Control on Next Generation Wing, *ICAS,* September, Daejon, South Korea.

[15] **DLR – Institute of Propulsion Technology.** (2021). Flow Control and Noise Reduction. https://www.dlr.de/at/en/desktopdefault.aspx/tabid-9004/15550_read-38383/

[16] **European Commission** (2016). FLOCON : Adaptive and Passive Flow Control for Fan Broadband Noise Reduction, http://cordis.europa.eu/result/rcn/55824_en.html

[17] **Wolf, A., Lutz, T., Würz, W., Stalnov, O. and Seifert, A.** (2014). Trailing edge noise reduction of wind turbine blades by active flow control, *Wind Energy*, 18 February.

[18] **Cesar, L. M., Jawahar, H. K., Azarpeyvand, M.** (2018). Airfoil Trailing-edge Noise Reduction using Flow Suction. In 2018 24th AIAA/CEAS Aeroacoustics Conference [AIAA 2018-2814] American Institute of Aeronautics and Astronautics Inc. (AIAA).

[19] **Gerhard, T., Erbslöh, S. and Carolus, T.** (2014). Reduction of airfoil trailing edge noise by trailing edge blowing, *Journal of Physics: Conference Series 524 (2014) 012123.*

[20] **Szoke, M., Fiscaletti, D. and Azarpeyvand, M.** (2020). Uniform flow injection into a turbulent boundary layer for trailing edge noise reduction, *Physics of Fluids 32, 085104 (2020).*

[21] **Sutliff, D. L.** (2005). Broadband Noise Reduction of a Low-Speed Fan Noise Using Trailing Edge Blowing, *NASA*, June.

[22] **Szoke, M. and Azarpeyvand, M.** (2017). On the Use of Active Flow Control for Aerofoil Noise Reduction, *24th International Congress on Sound and Vibration*, 23-27 July, London.

[23] **Abdessemed, C., Bouferrouk, A. And Yao, Y.** (2021). Aerodynamic and Aeroacoustic Analysis of a Harmonically Morphing Airfoil Using Dynamic Meshing, *Acoustics 2021, 3, 177–199.*

[24] **Ai, Q., Azarpeyvand, M., Lachenal, X. and Weaver, P. M.** (2015). Aerodynamic and aeroacoustic performance of airfoils with morphing structures, *Wind Energy*, 31 July.

[25] **Yadegari, M., Ommi, F. and Saboohi, Z.** (2020). Synergy between Noise Reduction Techniques Applied in Different Industries: A Review, *Int. Jnl. of Multiphysics Volume 14 · Number 2.*

[26] **Zamponi, R., Ragni D., Van de Wyer, N. and Schram, C.** (2019). Experimental Investigation of Airfoil Turbulence-Impingement Noise Reduction Using Porous Treatment, *25th AIAA/CEAS Aeroacoustics Conferences*, 20-23 May, Delft, The Netherlands

[27] **Ayton, L. J., Colbrook, M. J., Geyer, T. F., Chaitanya, P. and Sarradj, E.** (2020). Reducing aerofoil–turbulence interaction noise through chordwise-varying porosity, *J. Fluid Mech. vol. 906, Cambridge University Press*, 3 September.

[28] **Geyer, T., Sarradj, E. and Fritsche, C.** (2010). Porous airfoils: noise reduction and boundary layer effects, International Journal of Aeroacoustics vol.9 number 6, 3 June.

[29] **Geyer, T. F., Wasala, S. H. And Sarradj, S. H.** (2020). Experimental Study of Airfoil Leading Edge Combs for Turbulence Interaction Noise Reduction, 1 April.

[30] **Finez, A., Jondeau, E., Roger, M. and Jacob, M. C.** (2010). Broadband Noise Reduction With Trailing Edge Brushes, *16th AIAA/CEAS Aeroacoustics Conference*.

[31] **Wang, Y., Tang, D. F., Zhao, K., Li, W. J. and Huang, B.** (2007). Experimental Study on Noise Reduction using Brush-Serrated Trailing Edges, May.

[32] **Lyu, B. and Ayton, L. J.** (2019). Serrated leading-edge and trailing-edge noise prediction models for realistic wavenumber frequency spectra, *AIAA*, May.

[33] **Lyu, B., Ayton, L. J. and Chaitanya, P.** (2019). Leading and trailing edge noise reduction using serrations of new geometry, *23rd International Congress on Acoustics*, 9-13 September.

[34] **Wang, Y., Zhao, K., Lu, X-Y., Song, Y.-B. and Bennett, G. J.** (2019). Bio-Inspired Aerodynamic Noise Control: A Bibliographic Review, *Applied Science*, 30 May.

[35] **Gruber, M.** (2012). Airfoil noise reduction by edge treatments (Doctoral dissertation)

[36] **Oerlemans, S., Schepers, J. G., Guidati, G. and Wagner, S.** (2001). Experimental demonstration of wind türbine noise reduction through optimized airfoil shape and trailing-edge serrations, *National Aerospace Laboratory NLR*, 10 July.

[37] **Wang, J., Zhang, C., Wu, Z., Wharton, J. and Ren, L.** (2016). Numerical study on reduction of aerodynamic noise around an airfoil with biomimetic structures, *Journal of Sound and Vibration*, 14 November.

[38] **Bodling, A. and Sharma, A.** (2019). Numerical investigation of noise reduction mechanisms in a bio-inspired airfoil, *Journal of Sound and Vibration*, 12 February.

[39] **Liorente, E. and Ragni, D.** (2019). Serrations effect on the aerodynamic performance of wind turbine airfoils, *IOP Conf. Series: Journal of Physics: Conf. Series 1222*.

[40] **Liu, X., Theunissen, R. and Jahawar, H. K.** (2015). Aerodynamic and Aeroacoustic Performance of Serrated Airfoils, *American Institute of Aeronautics and Astronautics*, June.

[41] **Chong, T. P., Joseph, P. F. and Gruber, M.** (2012). Airfoil self noise reduction by non-flat plate type trailing edge serrations, *Applied Acoustics*, 6 November.

[42] **Lyu, B. and Ayton, L. J.** (2019). Rapid noise prediction models for serrated leading and trailing edges, *Journal of Sound and Vibration*, 4 December.

[43] **Chong, T. P. and Joseph, P. F.** (2013). An experimental study of airfoil instability tonal noise with trailing edge serrations, *Journal of Sound and Vibration*, 26 June.

[44] **Liu, X., Jawahar, H. K., Azarpeyvand, M. and Theunissen, R.** (2015). Aerodynamic and Aeroacoustic Performance of Serrated Airfoils, *21st AIAA/CEAS Aeroacoustics Conference [AIAA 2015-2201].*

[45] **Singh, S. K., Garg, M., Narayanan, S., Ayton, L. J. and Chaitanya, P.** (2022). On the Reductions of Airfoil Broadband Noise through Sinusoidal Trailing-Edge Serrations, *Journal of Aerospace Engineering*, January.

[46] **Gruber, M., Joseph, P. F. and Chong, T. P.** (2011). On the mechanisms of serrated airfoil trailing edge noise reduction, *17th AIAA/CEAS Aeroacoustics Conference,* 5-8 June, Portland, Oregon.

[47] **Ji, L., Qiao, W., Wang, L., Tong, F. and Chen, W.** (2014). Experimental and Numerical Study on Noise Reduction Mechanisms of an Airfoil with Serrated trailing edge, *20th AIAA/CEAS Aeroacoustics Conference*, 16-20 June, Atlanta, GA

[48] **Moreau, D. J., Brooks, L. A. and Doolan, C. J.** (2012). Experimental investigation of flat plate self-noise reduction using trailing edge serrations, *28th International Congress of the Aeronautical Science*, September.

[49] **Afshari, A., Azarpeyvand, M., Dehghan, A. A. and Szoke, M.** (2016). Trailing Edge Noise Reduction Using Novel Surface Treatments, *22nd AIAA/CEAS Aeroacoustics Conference*, 30 May-1 June, Lyon, France.

[50] **Liu, X., Jawahar, H. K., and Azarpeyvand, M.** (2016). Wake Development of Airfoils with Serrated Trailing Edges, *22nd AIAA CEAS Aeroacoustics Conference [AIAA 2016-2817]*.

[51] **Tang, H., Lei, Y. and Fu, Y.** (2019). Noise Reduction Mechanisms of an Airfoil with Trailing Edge Serrations at Low Mach Number, *Applied Science*, 10 September.

[52] **Ayton, L. J., and Chaitanya, P.** (2019). An analytical and experimental investigation of aerofoil-turbulence interaction noise for plates with spanwise-varying leading edges, *Journal of Fluid Mechanics*, 18 January.

[53] **Chaitanya, P., Joseph, P. and Ayton, L. J.** (2018). Leading-Edge Profiles for the Reduction of Airfoil Interaction Noise, *AIAA/CEAS Aeroacoustics Conference*, 25–29 June, Atlanta, GA.

[54] **Bampanis, G., Roger, M., Ragni, D., Avallone, F. and Teruna, C.** (2019). Airfoil-Turbulence Interaction Noise Source Identification and Reduction by Leading-Edge Serrations, *25th AIAA/CEAS Aeroacoustics Conference*, 20-23 May, Delft, The Netherlands.

[55] **Ayton, L. J. and Kim, J. W.** (2018). An analytic solution for the noise generated by gust-aerofoil interaction for plates with serrated leading edges, *Journal of Fluid Mechanics*, 23 July.

[56] **Lyu, B. J. and Azarpeyvand, M.** (2017). On the noise prediction for serrated leading edges, *Journal of Fluid Mechanics*, 15 June.

[57] **Cannard, M., Joseph, P., Chaitanya, P., Turner, J. and Kim, J. W.** (2019). Slitted leading-edge profiles for the reduction of broadband interaction noise; physical mechanisms and performance, *25th AIAA/CEAS Aeroacoustics Conference*, 20-23 May, Delft, The Netherlands.

[58] **Cannard, M., Joseph, P., Turner, J., Kim, J. W. and Chaitanya, P.** (2020). Physical mechanisms and performance of slitted leading-edge profiles for the reduction of broadband aerofoil interaction noise, *Journal of Sound and Vibration*, 27 January.

[59] **Paul, R.** (2013) Design Inspiration from Nature-Biomimicry for a Better Planet, 2013 from https://inhabitat.com/finding-design-inspiration-in-nature-biomimicry-for-a-better-planet/whale/

[60] **Johari, H., Henoch, C., Custodio, D. and Levshin, A.** (2007). Effects of Leading-Edge Protuberances on Airfoil Performance, *36th AIAA Fluid Dynamics Conference and Exhibit*, 2 July, San Francisco.

[61] **Hansen, K., Kelso, R. M. and Doolan, C. J.** (2010). Reduction of Flow Induced Tonal Noise through Leading Edge Tubercle Modifications, *16th AIAA/CEAS Aeroacoustics Conference*, June.

[62] **Clair, V., Polacsek, C., Reboul, G., Gruber, M. and Joseph, P.** (2013). Experimental and Numerical Investigation of Turbulence-Airfoil Noise Reduction Using Wavy Edges, *18th AIAA/CEAS Aeroacoustics Conference (33rd AIAA Aeroacoustics Conference)*, 23 April.

[63] **Skillen, A., Revell, A., Pinelli, A., Piomelli, U. and Favier, J.** (2014). Flow over a Wing with Leading-Edge Undulations, *American Institute of Aeronautics and Astronautics*, 29 June.

[64] **Narayanan, S., Chaitanya, P., Haeri, S., Joseph, P., Kim, J. W. and Polacsek, C.** (2015). Airfoil noise reductions through leading edge serrations, *PHYSICS OF FLUIDS*, 23 January.

[65] **Turner, J. M. and Kim, J. W.** (2019). On the universal trends in the noise reduction due to wavy leading edges in aerofoil-vortex interaction, *Journal of Fluid Mechanics*, 17 May.

[66] **Mayer, Y. D., Zang, B. and Azarpeyvand, M.** (2019). On the effects of leading edge serrations on aeroacoustic properties during stall, *23rd International Congress on Acoustics*, 9-13 September, Aachen, Germany.

[67] **Kim, J. H., Choi, K. S., Chaitanya, P., Joseph, P., Hasheminejad S. M. and Pinelli, A.** (2019). Optimization of Leading Edge Undulation of a NACA 65(12)-10 Aerofoil for Noise Reduction and Aerodynamic Enhancement, *23rd International Congress on Acoustics*, 9-13 September, Aachen, Germany.

[68] **Lacagnina, G., Chaitanya, P., Kim, J. H., Joseph, P., Stalnov O. and Omidyeganeh, M.** (2020). Leading edge serrations for the reduction of aerofoil selfnoise at low angle of attack, pre-stall and post-stall conditions, *International Journal of Aeroacoustics*, 31 May.

[69] **Vemuri, SH. S., Liu, X., Zang, B. and Azarpeyvand, M.** (2020). On the use of leading-edge serrations for noise control in a tandem airfoil configuration, *Physics of Fluids*, 10 June.

[70] **Kim, J. H., Choi, K. S., Chaitanya, P., Joseph, P., Hasheminejad S. M. and Pinelli, A.** (2021). Aerodynamic and Aeroacoustic Optimization of Leading-Edge Undulation of a NACA 65(12)-10 Airfoil, *AIAA Journal*,12 October.

[71] **Narayanan, S. and Singh, S. K.** (2020). On the reductions of aerofoil-turbulence interaction noise through multiwavelength leading edge serrations, *Journal of Aerospace Engineering*, 10 September.

[72] **Chaitanya, P., Narayanan, S., Joseph, P. and Kim, J. W.** (2016). Leading edge serration geometries for signicantly enhanced leading edge noise reductions, *22nd AIAA/CEAS Aeroacoustics Conference*, 30 May-1 June, Lyon, France.

[73] **Chaitanya, P., Joseph, P., Narayanan, S. and Kim, J. W.** (2018). Aerofoil broadband noise reductions through double-wavelength leading-edge serrations: a new control concept, *Journal of Fluid Mechanics*, 29 July.

[74] **Bogdonoff, S. M. and Bogdonoff, H. E.** (1945). Blade Design Data for Axial Flow Fans and Compressors, *National Advisory Committee for Aeronautics*, *Advanced Confidental Report*, July.

[75] **TE Connectivity Company** (2021). Miniature Electronic Pressure Scanners. https://marmatek.com/wp-content/uploads/2021/06/ENG_DS_DS-AR-ESP-DATASHEET_B.pdf

[76] **NASA.** Smoke and Tufts. https://www.grc.nasa.gov/www/k-12/airplane/tunvsmoke.html

[77] **Ristic, S.** (2007). Flow Visualisation Techniques in Wind Tunnels Part I – Non optical Methods, Scientific Technical Review, Vol.LVII, p.44-45.

[78] **Li, Z., Zhang, P., Pan, T., Li, Q. and Zhang, J.** (2020). Study on effects of thickness on airfoil-stall at low Reynolds numbers by cusp-catastrophic model based on GA(W)-1 airfoil, Chinese Journal of Aeronautics, March.

CURRICULUM VITAE

Name Surname **:** Zehra Nur KAPLAN

EDUCATION

- **B.Sc. :** 2020, Necmettin Erbakan University, Faculty of Aeronautics and Astronautics, Aeronautical Engineering
- **M.Sc. :** 2023, Istanbul Technical University, Faculty of Aeronautics and Astronautics, Aeronautical Engineering